HAL open science

Many body dynamics in nuclear spin diffusion

Jean-Nicolas Dumez

▶ To cite this version:

Jean-Nicolas Dumez. Many body dynamics in nuclear spin diffusion. Other. Ecole normale supérieure de lyon - ENS LYON, 2011. English. NNT : 2011ENSL0625 . tel-00657067

HAL Id: tel-00657067

https://theses.hal.science/tel-00657067v1

Submitted on 5 Jan 2012

HAL is a multi-disciplinary open access archive for the deposit and dissemination of scientific research documents, whether they are published or not. The documents may come from teaching and research institutions in France or abroad, or from public or private research centers.

L'archive ouverte pluridisciplinaire **HAL**, est destinée au dépôt et à la diffusion de documents scientifiques de niveau recherche, publiés ou non, émanant des établissements d'enseignement et de recherche français ou étrangers, des laboratoires publics ou privés.

N° d'ordre : 625

N° attribué par la bibliothèque : 2011ENSL0625

THÈSE

en vue d'obtenir le grade de

Docteur de l'Ecole Normale Supérieure de Lyon - Université de Lyon

Discipline : Chimie

Centre de RMN à très hauts champs

Ecole Doctorale de Chimie de Lyon

présentée et soutenue publiquement le 4 juillet 2011

par Monsieur Jean-Nicolas DUMEZ

Many-body dynamics in nuclear spin diffusion

Directeur de thèse : Monsieur Lyndon EMSLEY

Devant la commission d'examen formée de :

Monsieur Lyndon EMSLEY, Membre

Monsieur Malcom H. LEVITT, Rapporteur

Monsieur Dominique MASSIOT, Membre

Monsieur Beat H. MEIER, Membre

Monsieur Dieter SUTER, Rapporteur

Many-body dynamics in nuclear spin diffusion

Jean-Nicolas Dumez
Centre de RMN à très hauts champs
Ecole Normale Supérieure de Lyon

A thesis submitted for the degree of
Doctor of Chemistry of the Ecole Normale Supérieure de Lyon

4 July 2011

Supervised by Prof. Lyndon Emsley

Examined by a Jury composed of:
Prof. Malcolm H. Levitt
Prof. Dieter Suter
Prof. Beat H. Meier
Dr. Dominique Massiot
Prof. Lyndon Emsley

Remerciements

Au cours de cette thèse m'a été donnée la chance d'interagir avec de nombreuses personnes, que je souhaite désormais remercier, bien qu'il s'agisse pour la plupart de marquer une étape plutôt qu'un accomplissement.

Je souhaiterais remercier les Professeurs Malcolm Levitt et Dieter Suter pour avoir accepté d'évaluer ce manuscrit, ainsi que le Professeur Beat Meier et le Docteur Dominique Massiot pour avoir accepté de participer à la soutenance.

Je tiens principalement à remercier le Professeur Lyndon Emsley pour les projets auxquels il m'a permis de participer, l'atmosphère exceptionnelle qu'il contribue à maintenir, ainsi que pour son soutien et sa confiance tout au long de cette thèse. Nombre des idées explorées dans cette thèse ont émergé, parfois péniblement et parfois spontanément, de nos longues discussions sur la dynamique de spin. Lyndon est par ailleurs toujours resté présent et disponible, tout en m'offrant un savant mélange de liberté réelle et de subtiles ficelles. Il m'a souvent éclairé, sur de nombreux aspects de la résonance magnétique bien sûr, mais également sur les rouages de la recherche et les façons enthousiasmantes dont elle pouvait être conduite. Et si les conséquences ne transparaissent pas dans ce manuscrit, de nombreux moments ont participé à l'atmosphère dans laquelle s'est déroulée cette thèse, qu'il s'agisse d'enseigner la relaxation, de dévaler les pistes, ou d'explorer les coulisses de mes premières conférences.

De nombreuses heures ont également été passées avec Mark et Meghan, qui dans des styles radicalement différents m'ont beaucoup appris. Merci à Mark pour ses conseils, ainsi que pour sa volonté de propager son enthousiasme et de partager sa vision de la dynamique de spin. Merci à Meghan également, dont la perspicacité, la patience et la bonne humeur ont rendu nos heures de recherches en commun à la fois intéressantes et agréables.

Merci à Elodie pour tout ce que nous avons partagé, de nos tentatives variées pour manipuler les déplacements chimiques à l'apprentissage de la conduite d'une barque. Son expertise en RMN, sa persévérance et parfois simplement son sourire ont largement enrichi les années où nous avons été voisins. Merci à Bénédicte également, pour ce qu'elle m'a enseigné et ses nombreux conseils avisés. Ce fût par ailleurs un plaisir de partager brièvement l'animation d'un enseignement, et de tenter de faire face ensemble à des difficultés logistique ou quantique.

Au cours de ces trois années de nombreuses occasions se sont présentées pour explorer

d'autres sujets, avec un degré de profondeur variable, et ces opportunités ont bien sûr toutes été le résultat d'une interaction avec les membres du CRMN. Józef a fait le choix saugrenu de me demander de l'assister et j'espère avoir été un acolyte honorable ; je le remercie en tout cas pour ses conseils et sa patience pendant les heures que nous avons passées à acquérir et analyser des données. Nous n'aurons pas complètement avec Maria résolu l'énigme qui nous a été confiée, mais les progrès que nous avons fait l'ont été dans une atmosphère toujours excellente et colorée pour laquelle je la remercie. Et bien que nous ne sachions pas si ce en quoi elles ont résulté a un sens, les conversations que nous avons eues avec Andrew, Amy et Guido furent très intéressantes, et je les remercie de m'avoir donné un aperçu de leurs aventures.

Bien qu'il agisse la plupart du temps dans l'ombre, je ne pourrais pas oublier de remercier Hervé Gilquin, dont la compétence et l'implication ont permis aux calculs effectués pendant cette thèse de toujours paraître simples et efficaces.

Nous n'avons que rarement eu l'occasion de nous voir, mais je souhaite également remercier le Professeur Chris Pickard, qui m'a en seulement six mois enseigné de nombreux concepts, et permis déjà d'envisager une recherche qui valait la peine d'être menée et qu'on prenait plaisir à mener. Je remercie également les Professeurs Jonathan Yates et Sharon Ashbrook, que j'ai eu le plaisir de revoir pendant une trop courte semaine britannique.

Je souhaite remercier les personnes avec qui la place du CRMN dans un réseau européen m'a conduit à collaborer. Les projets menés avec les Professeurs Robin Harris et Paul Hodgkinson, le Professeur Norbert Müller et le Docteur Judith Schlagnitweit, furent intéressants et fructueux.

Et bien que la densité de personnes passionnées par la dynamique de spin dans des espaces de Liouville réduits ne soient pas particulièrement élevée, les conférences et visites leur permettent de se retrouver, et je remercie tout particulièrement le Professeur Shimon Vega et le Docteur Ilya Kuprov, dont les paroles, parfois tard le soir ou au petit déjeuner, ont contribué au dynamisme de cette thèse. D'autres ont eu l'occasion d'exprimer leur point de vue lors d'un passage à Lyon, et je remercie notamment le Docteur Dimitris Sakellariou, le Professeur Walter Kockenberger et le Professeur Matthias Ernst.

Je remercie l'ensemble des personnes que j'ai côtoyées au centre de RMN pendant plusieurs années, et qui ont contribué à la façon dont cette thèse s'est déroulée. Pierre, Anne, Torsten et Moreno ont contribué avec Lyndon, Bénédicte et Guido, par leur talent et leur bienveillance, à l'atmosphère de simplicité et d'efficacité dans laquelle j'ai eu le sentiment d'évoluer. Et même si nos conversations furent moins denses en spectroscopie, ce fut toujours un plaisir d'interagir avec Valérie, Emmanuel et Audrey. Nombreux sont les membres du CRMN passés, Elodie, Mark, Ségolène, Julien, Gwendal, Sylvian, Robin, Laetitia, Marc, Céline, Vincent, présents, Clément, Benjamin, Meghan, Józef, Amy, Andrew, Maria, Emeline, Alessandro, Elodie, Michael, Paul, Mathilde, Andrei, Aaron, Alexandre, Stefan, avec qui j'ai pu partager quelques mots ou de longues conversations, et que j'espère croiser à nouveau à d'autres occasions. Je remercie partic-

ulièrement Anne, tout en n'étant cependant pas certain d'être le plus sociable des voisins de bureau.

Je suis également redevable à mes étudiants de TD, qui m'ont poussé à maintenir un certain degré de rigueur. A défaut d'autre chose, nous aurons ensemble contribué à modifier la définition officielle de la grandeur la plus employée en spectroscopie de RMN. Avec les stagiaires du CRMN, Sirena et Sophie, ils m'ont permis de souhaiter être à la hauteur d'une autre manière, et m'ont apporté plus ou moins délibérément de nombreux bons moments.

Les enseignants qui m'ont formé ont tous influencé mon parcours, mais je tiens à remercier plus particulièrement mon professeur de mathématiques de lycée, M. Grégoire Cadot, qui m'a le premier exposé la perspective d'une trajectoire académique et parlé de cette mystérieuse normale sup', ainsi que le dynamique duo de sciences physiques de classes préparatoires, MM. Rémi Barbet-Massin et Jean-Pierre Foulon, avec qui j'ai même eu le plaisir de parler un peu de RMN.

Je souhaite remercier mes parents, qui sont restés pendant (presque) toute la durée de cette thèse présents à mes côtés. Le fait de pouvoir en permanence compter sur eux et profiter d'excellents moments avec eux est bien sûr une des raisons de ma reconnaissance. Mais c'est aussi la manière dont ils ont, chacun à leur façon, cherché et partiellement réussi à comprendre ce qu'étaient ma recherche et les raisons pour laquelle j'y consacrais du temps qui me touche beaucoup. Mes frères et sœurs ont également exprimé de la curiosité vis à vis de mes activités et fait preuve de patience, et je les en remercie. Merci également à mes oncles et tantes, ainsi qu'à mes cousins, qui m'ont entouré à divers moments de ma thèse, et en particulier à mon oncle Bruno qui m'a fréquemment accueilli à Lyon.

La proximité fortuite de nos appartements et de nos bureaux m'a permis de passer avec Clément un temps conséquent, compte tenu de ses multiples vies. Cette chance aura dans une certaine mesure participé à l'établissement et au maintien du rythme et de l'équilibre de ces années de thèse. Je tiens à le remercier pour avoir partagé pendant plusieurs années une certaine forme de curiosité et d'exigence.

Je voudrais également remercier les amis que j'ai eu la chance de continuer à fréquenter pendant ces trois années. Les moments passés en région parisienne avec les Kiwis sont toujours aussi précieux. A Lyon ou presque, je tiens à remercier particulièrement Mathilde, Clément, Gaëlle, Nicolas et Antoine, avec qui j'espère continuer de disserter de n'importe quel sujet avec une fréquente pointe de chimie.

Enfin, je tiens à remercier Amélie, qui a donné à ces années une spontanéité, une richesse et en un mot un bonheur que j'ai eu la chance de partager. Bonheur dans lequel la résonance magnétique s'est intégrée grâce à elle avec un naturel surprenant. Et comme les plus attentifs d'entre vous pourrons le constater, Amélie en aura profité pour devenir experte en diffusion de spin.

Abstract

Since its introduction by Bloembergen in 1949, nuclear spin diffusion has been a topic of significant interest in magnetic resonance. Spin diffusion, which can be defined as the transfer of spin polarisation induced by the dipolar interaction, is a ubiquitous transport mechanism in solids. Experimental observations of spin diffusion contain structural information. However, the many-body nature of the problem makes it difficult to describe from first principles. The central goal of this thesis is to obtain a quantitative description of the spin diffusion phenomenon from first-principles, through the development of suitable models of the underlying many-body dynamics. To that end we first consider an extension of an existing approach that relies on a master equation to describe the polarisations, for the case of proton-driven carbon-13 spin diffusion (PDSD). Second, a novel approach is introduced for the simulation of the time evolution of selected observables for large strongly coupled nuclear spin systems, using low-order correlations in Liouville space (LCL). Following the introduction of this new simulation method, Liouville-space reduction in solids is analysed in more detail, in order to identify the conditions under which the LCL approximation is valid. Finally, using the LCL model, simulations of proton spin diffusion (PSD) and PDSD are performed, directly from crystal geometry and with no adjustable parameters, and are found to be in excellent agreement with experimental measurements for polycrystalline organic solids.

Keywords: spin diffusion, magnetic resonance, solid-state NMR spectroscopy, computer simulation

Depuis 1949, date à laquelle Bloembergen en introduisit le concept, la diffusion de spin nucléaire suscite un vif intérêt en résonance magnétique. La diffusion de spin, qui peut être définie comme le transfert de polarisation de spin induit par l'interaction dipolaire, est un mécanisme omniprésent dans les solides. Les mesures expérimentales de ce phénomène contiennent des informations sur la structure du système étudié. La diffusion de spin est cependant un problème quantique à N corps, ce qui rend sa description *ab initio* relativement difficile. L'objectif principal de cette thèse est d'obtenir une description quantitative et *ab initio* de la diffusion de spin, en modélisant de manière adéquate la dynamique à N corps sous-jacente. Tout d'abord, nous exploitons une approche existante, reposant sur l'utilisation d'une équation maître pour les polarisations, dans le cas de la diffusion de spin entre carbones permise par les protons (PDSD). Ensuite, nous introduisons une méthode permettant de simuler l'évolution temporelle d'un ensemble d'observables pour un système de spins nucléaires fortement couplés, en utilisant les corrélations de petit ordre dans l'espace de Liouville (LCL). Le modèle LCL fournit une description précise du transfert de polarisation pour les systèmes polycristallins soumis à la rotation à l'angle magique. Après avoir décrit le modèle, nous analysons plus en détail la réduction de l'espace de Liouville pour les solides, afin d'identifier les conditions dans lesquelles l'approximation LCL est valide. Enfin, nous effectuons des simulations de la diffusion de spin entre protons (PSD) et entre carbones (PDSD), à partir de la structure des cristaux étudiés et sans aucun paramètre libre, et nous constatons pour des solides organiques polycristallins que leur accord avec les mesures expérimentales est excellent.

Mots-clés: diffusion de spin, résonance magnétique, spectroscopie RMN de l'état solide, simulation par ordinateur

Résumé de la thèse

La diffusion de spin nucléaire

La diffusion de spin nucléaire est un phénomène omniprésent dans les solides. Elle est susceptible d'intervenir dès lors qu'existe une distribution non uniforme de polarisation. Une telle distribution peut être due à la présence de sources ou de puits de polarisation. Elle peut également être induite par l'expérimentateur, avec comme objectif d'exploiter le phénomène pour obtenir des informations d'intérêt. Dans la première partie (chap. 2) différentes approches pour modéliser et observer la diffusion de spin sont présentées, ainsi que divers exemples de son utilisation pour des études structurales.

Le type de modèle pertinent pour décrire la diffusion de spin nucléaire dans une situation donnée dépend notamment des résolutions, spatiale et temporelle, avec lesquelles le phénomène est observé. Il est dans certain cas possible de considérer la polarisation comme une fonction continue de l'espace, dont l'évolution temporelle est régie par une équation de diffusion. Une équation maître pour les polarisations peut également être utilisée, lorsque plusieurs sites sont observés individuellement. Ces modèles ne prennent cependant pas en compte la nature cohérente de la dynamique de spin au cours du transfert de polarisation.

De nombreuses méthodes ont été développées afin d'observer expérimentalement la diffusion de spin nucléaire. Il est dans une certaine mesure possible de la caractériser en étudiant des phénomènes dans lesquels elle intervient indirectement, comme la relaxation longitudinale. En spectroscopie de résonance magnétique nucléaire (RMN) haute résolution, la méthode de choix pour observer la diffusion de spin de manière quantitative est la spectroscopie bidimensionnelle d'échange. Il est possible d'observer soit directement les noyaux d'intérêt, soit des noyaux "espions" qui bénéficient d'une résolution plus élevée.

La diffusion de spin nucléaire joue un rôle central dans la caractérisation structurale des solides par spectroscopie de RMN. Elle est en particulier aujourd'hui largement utilisée pour la biologie structurale, l'étude des matériaux, et la cristallographie de petites molécules par RMN du solide. Les applications présentées exploitent en général une équation de diffusion ou une équation maître pour les polarisations afin d'extraire des informations structurales des mesures expérimentales, bien que ces modèles ne soient pas toujours valides.

Equation maître et simulation de raies à zero-quantum pour décrire la diffusion de spin permise par les protons

Pour la diffusion de spin entre carbones dans des molécules organiques, l'interaction dipolaire avec les protons permet de compenser la différence d'énergie entre les états Zeeman des carbones. L'analyse de ce mécanisme conduit sous certaines hypothèses à une équation maître qui régit l'évolution temporelle des polarisations pour les carbones. Dans la deuxième partie (chap. 3), nous envisageons l'utilisation de ce modèle pour un solide polycristallin soumis à la rotation à l'angle magique.

Des courbes de diffusion de spin carbone (PDSD, pour *proton driven spin diffusion*) ont été enregistrées pour un acide aminé, la L-histidine.H_2O.HCl. Ces courbes sont raisonnablement décrites par une équation maître, et il est donc possible de définir et de mesurer des constantes de vitesse de diffusion, qui décrivent l'échange de polarisation entre groupes de carbones cristallographiquement équivalents. La qualité de la mesure des constantes de vitesse de diffusion est améliorée en analysant une série de spectres, ce qui permet notamment de prendre en compte les transferts relayés.

L'expression théorique de la constante de vitesse de diffusion montre qu'elle dépend pour une paire de carbones donnée du carré du couplage internucléaire et d'une fonction de la raie à zero quantum. Afin d'exploiter les expériences PDSD, cette fonction doit en général être déterminée de manière empirique. Ici nous utilisons des simulations numériques de l'évolution temporelle rapide des corrélations carbone-carbone sous l'effet du bain de protons. Il est possible avec des simulations exactes prenant en compte un carbone ainsi que les douze protons les plus proches d'obtenir des raies à un quantum. Les raies à zero quantum peuvent ensuite être obtenues par convolution de raies à un quantum.

L'utilisation d'une équation maître pour analyser les courbes PDSD, puis de simulations de raies à zero quantum, permet de calculer des distances internucléaires "effectives" dont l'accord avec les distances mesurées par diffraction de rayons X illustre la pertinence du modèle pour des études structurales. Les hypothèses sur lesquelles le modèle repose ne sont cependant pas toujours vérifiées, en particulier pour les constantes de couplage homonucléaire importantes l'accord entre constantes de vitesse de diffusion calculées et expérimentales n'est pas quantitatif.

Simulation numérique utilisant les corrélations de petit ordre dans l'espace de Liouville

Les simulations numériques prenant en compte un très grand nombre de spins ne peuvent pas être effectuées en décrivant de manière exhaustive l'espace des spins, car la taille de celui-ci croit de manière exponentielle lorsque le nombre de spins augmente. Nous présentons donc dans la troisième partie (chap. 5) une méthode permettant de simuler l'évolution temporelle d'observables d'intérêt pour des systèmes de spins fortement couplés et de grande taille.

Le développement de modèles alternatifs est rendu nécessaire notamment par le fait

que l'utilisation d'une équation maître n'est en principe valide que lorsqu'existe une séparation des échelles de temps sur lesquelles évoluent les polarisations d'une part et les corrélations entre spins d'autre part. Le modèle que nous proposons, nommé LCL (pour *low-order correlations in Liouville space*), repose sur l'utilisation des corrélations de petit ordre dans l'espace de Liouville. Il exploite le fait que sous certaines conditions l'effet des corrélations d'ordre élevé sur l'évolution temporelle des observables d'intérêt peut être négligé. Son principal avantage est que la taille de l'espace de Liouville réduit croit de manière polynomiale et non exponentielle lorsque le nombre de spins augmente, ce qui permet de prendre en compte un nombre bien plus élevé de spins que pour une simulation utilisant la totalité de l'espace de Liouville.

La possibilité de simuler un grand nombre de spins repose également sur le choix de l'algorithme utilisé pour intégrer l'équation du mouvement. Pour l'implémentation de LCL, nous utilisons la méthode Suzuki-Trotter, qui nécessite de stocker en mémoire un seul exemplaire de la matrice densité, et aucun opérateur agissant dans l'espace de Liouville. Cet algorithme est utilisé dans le programme Tourbillon, que nous avons développé et qui permet de simuler le transfert de polarisation dans des systèmes de plus de 100 spins.

Afin d'explorer la validité du modèle LCL, nous comparons des simulations de transfert de polarisation effectuées avec LCL et des simulations exactes. Dans le cas d'un système statique, il ne semble pas possible de réduire la taille de l'espace de Liouville sans modifier de manière excessive l'évolution des polarisations. Pour un système soumis à la rotation à l'angle magique, en revanche, les simulations LCL et les simulations exactes présentent un bien meilleur accord. Cet accord devient excellent lorsqu'une moyenne est effectuée sur toutes les orientations possibles du système.

Le modèle LCL permet donc de simuler le transfert de polarisation dans des systèmes de spins de grande taille pour des solides polycristallin soumis à la rotation à l'angle magique, ce qui correspond à des conditions expérimentales usuelles en RMN du solide.

Dynamique et thermodynamique de spin dans des espaces de Liouville réduits

L'utilisation d'espaces de Liouville réduits n'est pas toujours possible pour simuler la dynamique de spin dans les solides, et nous étudions plus en détail dans la quatrième partie (chap. 6) les propriétés de la réduction de l'espace de Liouville pour le transfert de polarisation dans les solides.

La dépendance temporelle induite par la rotation à l'angle magique, ainsi que la simplification résultant de la moyenne sur toutes les orientations possibles du système, semblent jouer un rôle essentiel dans la validité de la réduction de l'espace de Liouville. Nous illustrons cet effet avec des simulations, sans cependant réussir à fournir d'explication analytique et quantitative.

Il est intéressant d'étudier les populations des corrélations exclues de l'espace de Liouville réduit lors de l'évolution temporelle décrite dans un espace de Liouville complet.

Loin d'être négligeable, la contribution des corrélations d'ordre élevé constitue la majeure partie de la matrice densité après seulement quelques centaines de microsecondes d'évolution. Cette propriété révèle que le succès de la réduction de l'espace de Liouville dans les solides repose sur un mécanisme très différent de celui exploité pour les simulations de RMN en solution.

L'étude numérique de transferts prolongés montre par ailleurs que les simulations effectuées dans des espaces complets d'une part, réduits d'autre part, diffèrent par la valeur atteinte par les polarisations dans l'état de quasi-équilibre. Afin de caractériser cette propriété, nous adaptons un formalisme existant pour la prédiction des quasi-équilibres par un calcul dans le domaine de fréquence. Cette approche révèle que la réduction de l'espace de Liouville induit un comportement en apparence ergodique pour les observables d'intérêt.

L'ensemble des propriétés identifiées pour le modèle LCL permet d'envisager la description quantitative de certaines expériences.

Simulation *ab initio* de la diffusion de spin

Dans la cinquième partie (chap. 7), munis de l'ensemble des propriétés identifiées précédemment, nous exploitons le modèle LCL pour prédire des courbes expérimentales de diffusion de spin, en utilisant seulement la structure du système étudié, sans aucun paramètre empirique.

Pour la diffusion de spin entre protons (PSD, pour *proton spin diffusion*), le fait de pouvoir simuler un système comportant un grand nombre de spins permet de prendre en compte la totalité du contenu d'une maille primitive. Il est alors possible d'appliquer des conditions aux limites périodiques, et donc de rendre compte de la nature étendue d'un solide tout en incluant une information structurale précise. Nous utilisons le modèle LCL pour prédire les courbes de diffusion dans deux solides organiques, le thymol et la β-L-aspartyl-L-alanine; un très bon accord entre simulation et expérience est observé pour ces deux systèmes.

Pour la diffusion de spin entre carbones permise par les protons (PDSD), ce sont les propriétés thermodynamiques du modèle LCL, associées à la possibilité de prendre en compte un nombre accru de protons, qui permettent de surmonter les limites observées à la fois pour des simulations exactes et pour l'approche reposant sur une équation maître. Nous illustrons l'excellent accord entre les mesures expérimentales et les simulations avec les courbes PDSD enregistrées pour la L-histidine.H_2O.HCl.

L'utilisation d'espaces de Liouville judicieusement réduits permet donc d'obtenir, pour des solides organiques polycristallins soumis à la rotation à l'angle magique, un accord entre simulations *ab initio* et mesures expérimentales qui n'était pas envisageable précédemment.

Contents

Contents xiii

1 Introduction 1

2 Nuclear spin diffusion 5
2.1 Introduction . . . 5
2.2 Modelling spin diffusion . . . 6
2.2.1 Equation of motion . . . 6
2.2.2 Diffusion equation . . . 8
2.2.3 Master equation for the polarisations . . . 9
2.2.4 Numerical simulation of the density matrix . . . 10
2.2.5 Mixed approaches . . . 11
2.3 Observing spin diffusion . . . 12
2.3.1 Influence on other processes . . . 12
2.3.2 Spin diffusion between resolvable resonances . . . 12
2.3.3 Spin diffusion between regions with different mobility . . . 15
2.3.4 Purely spatial spin diffusion . . . 15
2.4 Structural investigation . . . 16
2.4.1 Materials . . . 16
2.4.2 Small molecules . . . 16
2.4.3 Biomolecules . . . 17
2.5 Perspectives . . . 21

3 Master-equation approach to the description of proton-driven spin diffusion 23
3.1 Introduction . . . 23
3.2 Outline of the master-equation approach . . . 24
3.2.1 Time evolution of experimental observables . . . 24
3.2.2 PDSD rate constants and effective dipolar couplings . . . 25
3.3 Characterisation of the zero-quantum lineshape . . . 26
3.3.1 Measurements of spin diffusion rate constants . . . 26
3.3.2 Comparison with squared effective dipolar couplings . . . 30
3.3.3 Numerical simulation of the zero-quantum lineshape . . . 31
3.4 Consequences for structural studies . . . 36
3.5 Conclusions . . . 38

4 Interlude: Liouville space **39**
4.1 Introduction . . . 39
4.2 System and evolution . . . 40
4.3 Projection operators and memory functions . . . 41
4.3.1 Reformulation of the equation of motion . . . 41
4.3.2 Master-equation in the short correlation time limit . . . 42
4.4 Application to proton-driven spin diffusion . . . 43
4.4.1 Interactions . . . 43
4.4.2 Existence and expression of rate constants . . . 44
4.4.3 Simulation of lineshapes . . . 46
4.5 Conclusions . . . 47

5 Numerical simulation from low-order correlations in Liouville space **49**
5.1 Introduction . . . 49
5.2 Theory . . . 51
5.2.1 Motivation . . . 51
5.2.2 Picturing Liouville space for dipolar-coupled nuclear spins . . . 51
5.2.3 Formal Liouville-space reduction . . . 54
5.2.4 Heteronuclear spin systems . . . 55
5.3 Tourbillon: 100 nuclear spins and beyond . . . 56
5.3.1 Numerical integration scheme . . . 56
5.3.2 Rotation matrices . . . 59
5.3.3 Actual Liouville-space reduction . . . 60
5.3.4 Magic-angle spinning and powder averaging . . . 61
5.4 Accurate simulation of polarisation transfer in spinning powders . . . 62
5.4.1 Comparison with exact simulations . . . 62
5.4.2 Large-scale simulation . . . 65
5.5 Conclusions . . . 65

6 Spin dynamics and thermodynamics in reduced Liouville spaces **69**
6.1 Introduction . . . 69
6.2 Validity of Liouville-space reduction . . . 70
6.2.1 Magic-angle spinning . . . 70
6.2.2 Powder averaging . . . 72
6.3 Specificity of Liouville-space reduction in solids . . . 74
6.3.1 Population of excluded coherences . . . 74
6.3.2 Change of basis set . . . 76
6.3.3 Dimension of the spin-order subspaces . . . 77
6.4 Quasi-equilibria in full and reduced Liouville spaces . . . 78
6.4.1 Calculation in the time domain . . . 78
6.4.2 Prediction of quasi-equilibrium expectation values . . . 79
6.4.3 Calculation in the frequency domain . . . 87
6.5 Conclusions . . . 89

7 *Ab initio* simulation of spin diffusion **91**
7.1 Introduction 91
7.2 Comparing simulation and experiment 92
7.2.1 Initial density matrix and observables 92
7.2.2 Extended periodic systems 93
7.2.3 Symmetry and equivalence 95
7.3 Proton spin diffusion 96
7.3.1 Accurate simulation from crystal geometry 96
7.3.2 Role of intermolecular couplings 99
7.3.3 Coherent features of the observed spin dynamics 101
7.4 Proton-driven carbon-13 spin diffusion 102
7.4.1 Thermodynamic wall of exact simulations 102
7.4.2 Accurate simulation from crystal geometry 104
7.5 Conclusions 106

8 Conclusions **107**

References **111**

Publications **127**

Chapter 1

Introduction

Over the past several decades, nuclear magnetic resonance (NMR) has been demonstrated to be uniquely suited to exploring the structure and dynamics of a large range of systems at the atomic level. In the solid state, although there still exist a number of fundamental obstacles to the full realisation of high-resolution NMR spectroscopy, there has been a steady development of methods to overcome these barriers and thus provide access to systems and information that are beyond the reach of other techniques.

The complexity of the nuclear interactions probed by solid-state NMR spectroscopy is both a blessing and a curse. The potentially rich information content of solid-state NMR spectroscopic measurements is often difficult to disentangle due to the overwhelmingly complex underlying spin dynamics. In particular, abundant nuclear spins of large magnetogyric ratio are strongly coupled by the dipolar interaction in the solid state. Due to its geometrical dependence, the dipolar interaction leads to measurements that contain extensive structural information. At the same time, the ability to remove its effect on the spin dynamics is a mandatory step towards high-resolution, because its large magnitude and homogeneous nature lead, in general, to broad and featureless spectra. Such a duality is notably found in organic solids, where protons form extended networks of strongly coupled spins.

A key feature of the dipolar interaction is that it gives rise to correlations among large numbers of spins. The resulting many-body dynamics can be treated in a collective fashion in many cases, especially when the ensemble of strongly coupled spins can be considered as a perturbation to the system of interest, or when its dynamics is monitored with a relatively coarse resolution. Such simplifications are no longer possible, however, when the correlated ensemble is observed at a high resolution in space and time. Although numerical simulation based on the Liouville von Neumann equation would in principle be fully suitable to describe coherent dipolar-driven spin dynamics, they are in practice limited to a small number of spins by the "exponential wall" met by numerical implementations of the exact description of many-body problems.

Nuclear spin diffusion is a prototypical many-body problem in magnetic resonance. Spin diffusion, which can be defined as the transfer of polarisation between spins induced by the dipolar interaction, was introduced by Bloembergen in the early days of magnetic resonance, and has since remained a topic of significant interest. Nowadays,

steady increases in the resolution with which polarisation transfer can be monitored in NMR spectroscopy provide experimental measurements that challenge existing models of this phenomenon. In particular, the description of spin diffusion from first principles at a site-specific level remains a largely open problem.

In high-resolution solid-state NMR spectroscopy, spin diffusion is at the heart of many structural studies. From mixtures of polymers to nanocrystalline proteins, an extensive set of systems has been characterised with spin-diffusion based methods that in general rely on simplified models of the spin dynamics and on numerical simulation of relatively small spin systems. Existing models have led to numerous successful applications, but they nevertheless face acknowledged limitations, and a strong impetus thus exists to make progress in this field. In addition, spin diffusion also plays a role in other processes, such as relaxation and hyperpolarisation, and is a test bed of spin dynamical concepts in quantum information processing.

The central goal of this thesis is to obtain a quantitative description of the spin diffusion phenomenon from first-principles, through the development of suitable models of the underlying many-body dynamics. A strong emphasis is put on the study of polarisation transfer among carbons and protons in polycrystalline solids under magic-angle spinning. In particular, simulation methods are introduced that can be used to predict experimental measurements of proton spin diffusion and proton-driven carbon-13 spin diffusion directly from geometry and with no adjustable parameters. The concepts discussed here are equally relevant in other areas that will, however, only be referred to infrequently.

The present manuscript reports investigations carried out at the centre de RMN à très hauts champs, from the autumn of 2008 to the spring of 2011. In order to set the stage, an overview of existing methods to observe and model spin diffusion is first given in chapter 2. A range of structural studies are also described, to simultaneously highlight the current successes and potential future developments of spin-diffusion based methods, with a focus on structural biology and NMR crystallography.

In chapter 3, we consider a master-equation approach to the description of proton-driven carbon-13 spin diffusion, which is already used extensively to interpret experimental measurements. We propose refinements to improve its accuracy, and open the possibility to employ it in a parameter-free manner. First, we illustrate how experimental measurements of spin diffusion rate constants can be made more accurate by the analysis of a series of spin exchange spectra. Second, we show that numerical simulations can provide a missing link between experimentally measurable rate constants and the structural information of interest.

The results discussed in chapter 3 provide some insight into the possibility to describe the dynamics of spin diffusion from first principles, and in particular into the distinctive features of polarisation transfer among protons and among carbons. For that reason, the theoretical basis of the master-equation approach is outlined in chapter 4, after a brief summary of the Liouville formalism employed in the rest of the manuscript. Chapter 4 gives both an interpretation of the master-equation approach, and provides a framework and a motivation for the developments of alternative models.

In chapter 5, we introduce an approach for the description of large, strongly coupled nuclear-spin systems, based on the simulation of the time evolution of selected observables from low-order correlations in Liouville space. The model, which we call LCL, is found to provide accurate simulation of polarisation transfer for polycrystalline samples under magic-angle spinning. LCL simulations, implemented in a memory-efficient way in the Tourbillon program, avoid the exponential wall of quantum simulation and make it possible to simulate the dynamics of over a hundred nuclear spins. Despite these favourable features, however, Liouville-space reduction in solids is only partly understood, and some underlying mechanisms are discussed in chapter 6. In particular, we show how the combination of Liouville-space reduction and of the time-dependence induced by magic-angle spinning dramatically affects the dynamics and thermodynamics of polarisation transfer.

Finally, building on the analysis of existing models and on the approaches developed here, we show in chapter 7 that accurate simulations can be performed for polycrystalline organic solids under magic-angle spinning, which reproduce experimental measurements of both proton spin diffusion and proton-driven carbon-13 spin diffusion. Specifically, small organic molecules with known crystal structures are used to illustrate how an appropriate choice of spin system and simulation approach, motivated by the analyses performed throughout the thesis, can lead to an unprecedented agreement between first-principles simulation and experiments.

Chapter 2

Nuclear spin diffusion

2.1 Introduction

Nuclear spin diffusion was first introduced by Bloembergen in 1949 to account for unexpected values of relaxation times in solids [1]. Paramagnetic impurities were expected to act as powerful relaxation sinks, albeit with a limited spatial range, and a mechanism was thus necessary for nuclear polarisation to travel from the bulk of the sample to the relaxing impurities. Spin diffusion has subsequently turned out to be a ubiquitous phenomenon in solids, and has over the years been regarded alternatively as a key ingredient in various types of experiments, as a spin dynamical challenge, and as a tool for a large range of applications. Several reviews have been written on spin diffusion in various contexts [2–5].

Nuclear spin diffusion can be defined as the transfer of polarisation between homonuclear spins driven by the dipolar interaction. No precise and unambiguous definition exists, however, and the phrase "spin diffusion" encompasses a variable range of processes. In this chapter, we will focus on "spontaneous" polarisation transfer, which occurs in the absence of a radio-frequency irradiation. In any case, spin diffusion in solids should be distinguished from its counterpart in solution-state NMR, where the term refers to the relayed nature of incoherent transfers of polarisation due to the Overhauser effect.

Spontaneous transfers of polarisation can occur whenever a non-uniform distribution of polarisation exists. Such a situation is found when polarisation is produced or depleted faster in certain regions of a sample, and spin diffusion is then one of the mechanisms that tends to drive the system to equilibrium. Non-uniform distributions of polarisation can also be generated by differentiating groups of spins according to a spectroscopic parameter that allows for their individual selection, typically their chemical shift. The latter situation is exploited in experimental approaches that explicitly aim at characterising the spin diffusion process, while the former explains why spin diffusion is ubiquitous as part of the longitudinal relaxation process in solids.

As the dipolar interaction depends on the length and orientation of internuclear vectors, experimental studies of spin diffusion potentially have a rich content of structural information. For that reason, spin diffusion has been a central tool in studies by solid-

state NMR for many years and for a large variety of samples. In general, however, spin diffusion is a many-body process, and the extraction of structural information from experiments is still, to a large extent, an open problem. Both the determination of pair-wise distances from experimental data and the prediction of polarisation transfer curves for a given structure are only possible in specific cases or in a qualitative manner.

Attempts to understand and to exploit spin diffusion require some degree of modelling. The pertinent approach to describe the phenomenon, however, depends significantly on the space and time resolutions with which it is observed, and on the mechanism involved. For example, in studies performed with low resolution, polarisation can often be considered as a continuous function of space, the time-evolution of which is governed by a diffusion equation. In contrast, some observations can only be accounted for by a quantum-mechanical description of all of the spins involved. These notions are illustrated qualitatively in Fig. 2.1. Although derivations from first principles exist for each approach, it should be noted that they have often been used successfully for applications far outside their range of validity.

In this chapter, we will first outline the basic principles of the spin diffusion phenomenon, and approaches that have been developed to model it in various contexts. We will then describe experimental methods that have been used to observe spin diffusion, and consider three areas in which spin diffusion plays a central role, with a strong emphasis on high-resolution solid-state NMR spectroscopy of crystalline systems.

2.2 Modelling spin diffusion

2.2.1 Equation of motion

In the solid state, nuclear spins are coupled through space by the dipolar interaction. For a homonuclear pair of spins ij, the dipolar interaction in its high-field secular form can be written:

$$H_{ij} = -\frac{\mu_0 \gamma^2 \hbar}{4\pi r_{ij}^3} \frac{1}{2} \left(3\cos^2\theta_{ij} - 1\right) \left(2 I_{iz} I_{jz} - \frac{1}{2}\left(I_{i+} I_{j-} + I_{i-} I_{j+}\right)\right), \tag{2.1}$$

where r_{ij} is the internuclear distance, and θ_{ij} is the angle between the internuclear vector and the static magnetic field. The so-called "flip-flop" term, $I_{i+}I_{j-} + I_{i-}I_{j+}$, which is non-secular for a heteronuclear spin pair, is responsible for polarisation transfer.

As illustrated experimentally by the formation of polarisation echoes [6–9], spin diffusion is a fully coherent phenomenon. That is, for a system described by a density matrix σ, the evolution of σ is governed by the Liouville-von Neumann equation

$$\frac{d}{dt}\sigma = -\mathrm{i}[H, \sigma], \tag{2.2}$$

where the Hamiltonian H consists of the dipolar interaction and of other relevant contributions. The phrase "spin diffusion", which is in apparent contradiction with the idea of a coherent process, was originally coined because the time evolution of the polarisation for

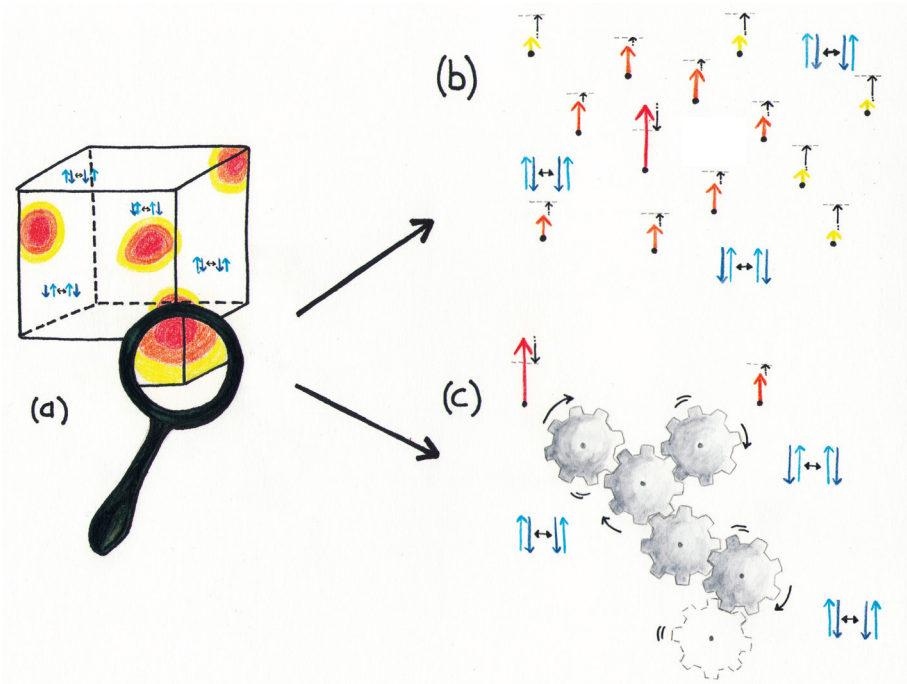

Figure 2.1: Modelling spin diffusion. (a) Diffusion equation: the spin polarisation can be considered as a function of the position in the sample; polarisation "diffuses" in the sample. (b) Master equation for the polarisation: the variables are the single-spin polarisations; nuclear spins exchange polarisation with a given rate constant. (c) Density matrix: all the multi-spin correlations are taken into accounts; the spin dynamics are fully coherent and can be regarded as a series of rotations. The spin polarisation is represented in yellow, orange and red depending on its intensity. Black arrows represent the time evolution. Spin diffusion arises in all cases from homonuclear flip-flop transitions, depicted by pairs of spins shown in blue throughout the figure.

an ensemble of spins is largely described by a diffusion law when observed with a sufficiently coarse resolution in space or in time. Even at higher resolution, the many-body dynamics of a large system can degenerate into a simplified behaviour, where the coherent nature of the phenomenon is not strikingly apparent. Out of the huge number of degrees of freedom of the system, only a few are actually observed experimentally, and a master equation for the observed polarisations can often model experimental measurements successfully.

There are also many cases in which the coherent nature of the dynamics has to be accounted for when modelling spin diffusion. In a limited number of situations, analytical solutions of the equation of motion can be found. For example, in experiments performed under magic-angle spinning where the spinning frequency matches the chemical-shift difference between two nuclei, a two-body Hamiltonian largely governs the effective spin dynamics [10–12]. In general, however, no such simplification exists. Although numerical simulation based on the Liouville von-Neumann equation could in principle be used to predict spin diffusion for a given system, such an approach is prevented by the exponential wall of quantum simulations, which puts the large nuclear spin systems that would be required out of reach. Modelling spin diffusion is thus still to some extent an open problem, for which new approaches have to be developed.

2.2.2 Diffusion equation

The use of a diffusion equation to describe polarisation transfer was first introduced on a mostly phenomenological basis by Bloembergen [1], and was later explored by several authors [13, 14] (see Ref. [15] for a review). In such a description, the polarisation is a function of the position in the sample, and its time evolution is given by:

$$\frac{d}{dt}\vec{P} = D\Delta\vec{P}, \tag{2.3}$$

where D is a diffusion coefficient and Δ is the Laplacian operator. As explained by Abragam [16], a qualitative reasoning for a regular lattice of spins yields Eq. 2.3 with a diffusion coefficient D of the form

$$D = Wa^2, \tag{2.4}$$

where a is the the lattice spacing, and W is the probability per unit time of a flip-flop transition for a pair of nearest-neighbours spins, which itself depends in a complex way on the geometry of the system. Several approaches have been suggested to derive a diffusion equation from first principles [17–24]. Although they rely on different formalisms, these derivations yield similar expressions for the diffusion coefficient.

Equation 2.3 describes the behaviour of the bulk polarisation only. In the presence of paramagnetic centres, nuclei are frequently modelled by separating bulk nuclei that are far from the centres, and core nuclei that interact directly with them. Additional terms are necessary in Eq. 2.3 to account for the interaction of the core nuclei with paramagnetic centres, and of the core nuclei with the bulk nuclei. We will not give a detailed description of these considerations here.

The use of a diffusion equation was originally introduced and derived to describe the behaviour of a system of identical spins observed with a coarse spatial resolution. As will be seen in the following sections, it has subsequently been used with success in a range of different contexts.

2.2.3 Master equation for the polarisations

With the advent of two-dimensional NMR [25, 26] and high-resolution solid-state NMR [27, 28], it became possible to observe polarisation transfer between chemical sites for nuclei of low magnetogyric ratio, such as carbon-13. This led to the notion of "spectral" spin diffusion, which can be seen as taking place in frequency space, between resonances for which there exists a difference in frequency much larger than the homonuclear dipolar coupling between them. In contrast to the case of purely "spatial" spin diffusion, which occurs between spins with identical or negligibly different resonance frequencies, in spectral spin diffusion the flip-flop process is not energy conserving, and an external source of energy is required for polarisation transfer to occur.

Suter and Ernst used a thermodynamic treatment to describe spectral spin diffusion in a system of S spins in the presence of abundant I spins of high magnetogyric ratio [29, 30]. In such a system, the energy required for polarisation transfer between S spins is provided by the dipolar reservoir of the I spins, and the process is refered to as "I-driven". In this thermodynamic treatment, the only relevant variables are the spin polarisations M_i, the time evolution of which is governed by a master equation:

$$\frac{d}{dt}\mathbf{M} = \mathbf{K}\mathbf{M}. \tag{2.5}$$

Derivations were also proposed by Henrichs *et al.* [31], and Kubo and McDowell [32] to justify the use of a master equation, and to provide expressions for the spin diffusion rate constants $k_{ij} = [\mathbf{K}]_{ij}$. The latter authors also considered the case of a sample under magic-angle spinning [33]. All derivations are based on the assumption that there exists a separation of time scales between the slow transfer of polarisation between S spins and the fast decoherence of a two-S zero-quantum coherence.

In the case of a homonuclear dipolar interaction between S spins much smaller than the SI and II dipolar interactions, the rate constant for a spin pair ij is of the general form [30–33]:

$$k_{ij} \propto \omega_{ij}^2 F[G_{ij}(\nu)], \tag{2.6}$$

where

$$\omega_{ij} = \frac{\mu_0 \gamma_S^2 \hbar}{4\pi r_{ij}^3}, \tag{2.7}$$

is the dipolar coupling and $F[G(\nu)]$ is a function of the zero-quantum lineshape $G(\nu)$. Formally, $G(\nu)$ is the Fourier transform of the free-induction decay of a two-S zero-quantum coherence under the action of the surrounding I spins; it provides a measure of the overlap between the homogeneously broadened S resonances. Suter and Ernst studied doubly ^{13}C-labelled malonic acid to illustrate the use of a kinetic model to analyse

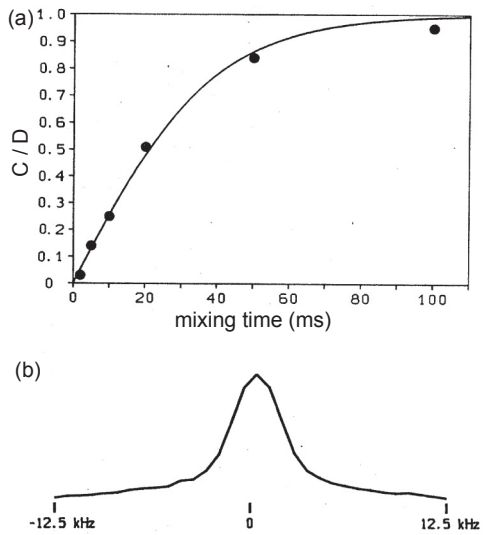

Figure 2.2: Spin diffusion in doubly ^{13}C-labelled malonic acid. (a) Time evolution of the ratio between the cross-peak volume (C) and the diagonal-peak volume (D), measured from a series of 2D spin exchange spectra recorded for various mixing times. (b) Experimental measurement of the zero-quantum lineshape. Reproduced from Ref. [30], © 1985 American Physical Society.

spectral spin diffusion [30]. Figure 2.2 shows the time evolution of the ratio between the cross and diagonal peaks that they measured with a series of 2D spin exchange spectra; a fit to an exponential was used to measure the spin diffusion rate constant. The spin diffusion rate constant was then analysed, with a zero-quantum lineshape characterised experimentally, to illustrate the validity of Eq. 2.6. The experimental technique will be described in section 2.3.2.

Equation 2.6 has been used extensively for structural studies, as it links an experimentally measurable quantity, the spin diffusion rate constant for a spin pair k_{ij}, to a geometrical information of interest, the internuclear distance r_{ij}. The zero-quantum lineshape $G(\nu)$, however, is in general unknown and difficult to determine. Kinetic models with rate constants of the form given in Eq. 2.6 have also been used to describe other types of spin diffusion experiments, with a variable degree of empiricism.

2.2.4 Numerical simulation of the density matrix

The coherent evolution of a spin system can in principle be described exactly with a numerical integration of the Liouville von-Neumann equation. In situations where a small spin system was indeed studied experimentally, numerical simulations have been used with some success to model spin diffusion [34, 35], and in particular to describe coherent oscillations that cannot be modelled by a diffusion equation or a master equation for the polarisations [36]. State-of-the-art spin simulations in solid-state NMR are, however, limited to about a dozen strongly coupled spins, and thus cannot be used to model quantitatively spin diffusion within large nuclear-spin systems, as observed in Ref. [37], for example.

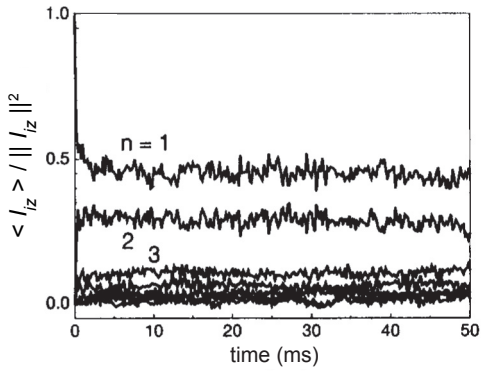

Figure 2.3: Polarisation transfer in a linear chain of 8 protons, aligned parallel to the magnetic field B_0. The initial polarisation is concentrated on the first spin, and the normalised polarisation of each spin is observed. Atomic coordinates are given in Ref. [38]. Reproduced from Ref. [38], © 1997 Elsevier Science.

Numerical simulations of spin diffusion performed with small spin systems can be difficult to interpret and to relate to experimental observations. For example, the observation of so-called non-ergodic quasi-equilibria in small spin system has raised questions about the long term behaviour of large nuclear-spin systems [38], which are still largely open to this day [39], and led to a discussion of the interpretation of spin thermodynamics for small spin systems [40, 41]. Figure 2.3 shows an example of quasi-equilibrium obtained by Brüschweiler and Ernst with numerical simulations of polarisation transfer in a linear chain of 8 protons [38]. In such a simulation, the total polarisation does not equilibrate, even after a very long simulation time.

Even when a diffusion equation or a master equation is empirically observed to model experimental data with reasonable accuracy and with a limited number of free parameters, there is sometimes no detailed understanding of how the underlying many-body dynamics result in a simplified behaviour. The inability to perform direct numerical simulations for large spin systems is also a limitation in these cases.

2.2.5 Mixed approaches

In order to model the time-evolution of experimental observables for large systems of dipolar coupled spins, a full quantum description of a small fraction of the total number of variables has to be associated with a simplified description of the remaining immense number of variables involved. For example, R. R. Ernst and co-workers have introduced the use of a spin diffusion superoperator to describe the effect of a large number of strongly coupled protons on a small number of carbons and protons [42]. This superoperator approach was used by M. Ernst and co-workers to describe spin diffusion between S spins in the presence of a bath of strongly coupled I spins [43]. In another study, Meier and co-workers treated the effect of passive spins as a perturbation of the spin dynamics of a pair of active spins [44, 45].

Waugh and co-workers have explored the possibility of using classical gyromagnets

to describe spin diffusion [46, 47], and one could think of a separation between a core of quantum spins surrounded by a bath of classical spins. In this thesis, we will explore an alternative separation between a core and a bath, performed in Liouville space between low-order and high-order correlations [48, 49], and show how it can be used to model spin diffusion [50]. We will also consider the use of numerical simulation of the density matrix to describe the dynamics on a short time-scale, coupled to a master equation to model the polarisation transfer process [51].

2.3 Observing spin diffusion

2.3.1 Influence on other processes

In many experiments, spin diffusion plays a role as a mechanism for polarisation transfer towards a sink or from a source of polarisation. Spin diffusion is then in general modelled as a diffusive process, and a value of the diffusion coefficient D can be determined from experimental measurements of relaxation times. We will not describe this approach in more detail, and in the following we will focus instead on experimental methods that aim at recording the time evolution of the polarisations for several sites during the spin exchange process.

2.3.2 Spin diffusion between resolvable resonances

In NMR spectroscopy, multidimensional experiments are a powerful way to observe spin diffusion between spins that have different chemical shifts, as first demonstrated by Szeverenyi *et al.* for carbon-13 nuclei [52] and by Caravatti *et al.* for proton nuclei [53]. Figure 2.4 shows spin diffusion spectra recorded by these authors. In a typical 2D spin exchange experiments, the spins precess under the sole effect of their chemical shift during the evolution and detection periods, and polarisation transfer occurs during the mixing period [54]. The 2D spectrum at a given mixing time then provides a quantitative depiction of the exchange process, and full spin diffusion build-up curves can be obtained by recording a set of experiments for a series of mixing times. The 2D spin exchange pulse sequence and spectrum are depicted in Fig. 2.5. Selective excitations can also be used to monitor spin diffusion from a given site in a one-dimensional experiment.

In solid-state NMR, achieving sufficient resolution to obtain site-specific information in systems of increasing sizes is a continuing challenge. The dipolar interaction, which is at the origin of the spin diffusion process, leads to homogeneously broadened NMR peaks, and its effect on the spin dynamics thus has to be, in general, suppressed during the evolution and detection periods of a spin exchange experiment. For nuclei of relatively low magnetogyric ratio, such as carbon-13, the combination of magic-angle spinning [55–57] and heteronuclear decoupling pulse sequences [58] can provide high-resolution, and 2D spin exchange pulse sequences based on the paradigmatic CPMAS concepts [27, 28, 59] are routinely used. For nuclei of high magnetogyric ratio, and in particular for protons, removing the effect of the dipolar interaction on spectral resolution while simultaneously

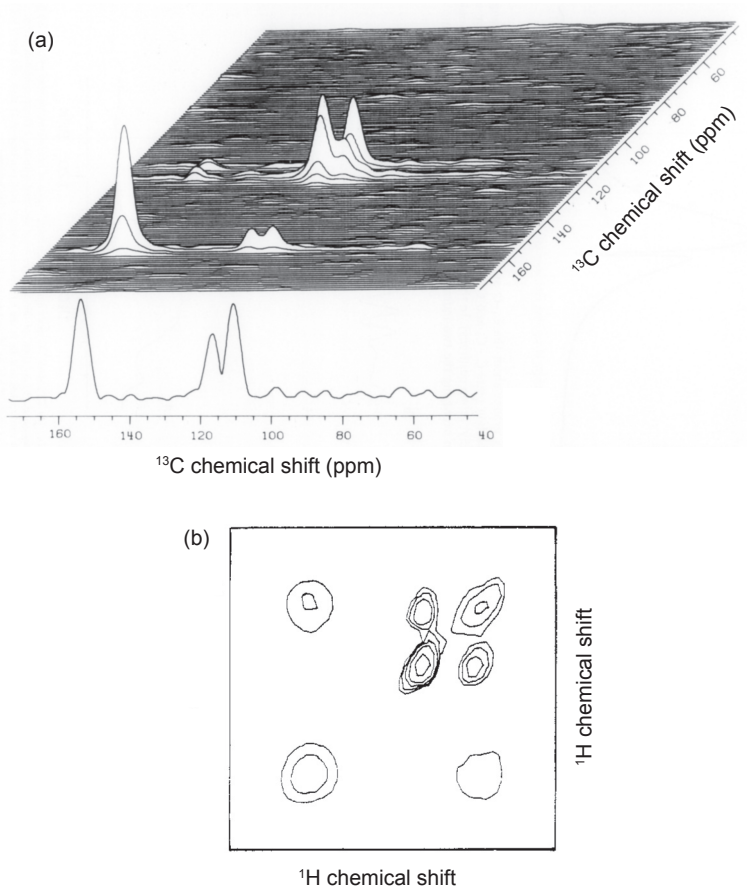

Figure 2.4: 2D spin diffusion spectra. (a) 2D ^{13}C-^{13}C spin diffusion spectrum of powdered 1,4 dimethoxybenzene at natural abundance, recorded with 2.5 kHz MAS and a mixing time of 90 s. (b) 2D ^{1}H-^{1}H spin diffusion spectrum of a blend of polystyrene and poly(vinyl methyl ether) cast from chloroform, recorded with 2.8 kHz MAS and a mixing time of 100 ms. Reproduced from Ref. [52], © 1982 Academic Press and Ref. [53], © 1985 American Chemical Society.

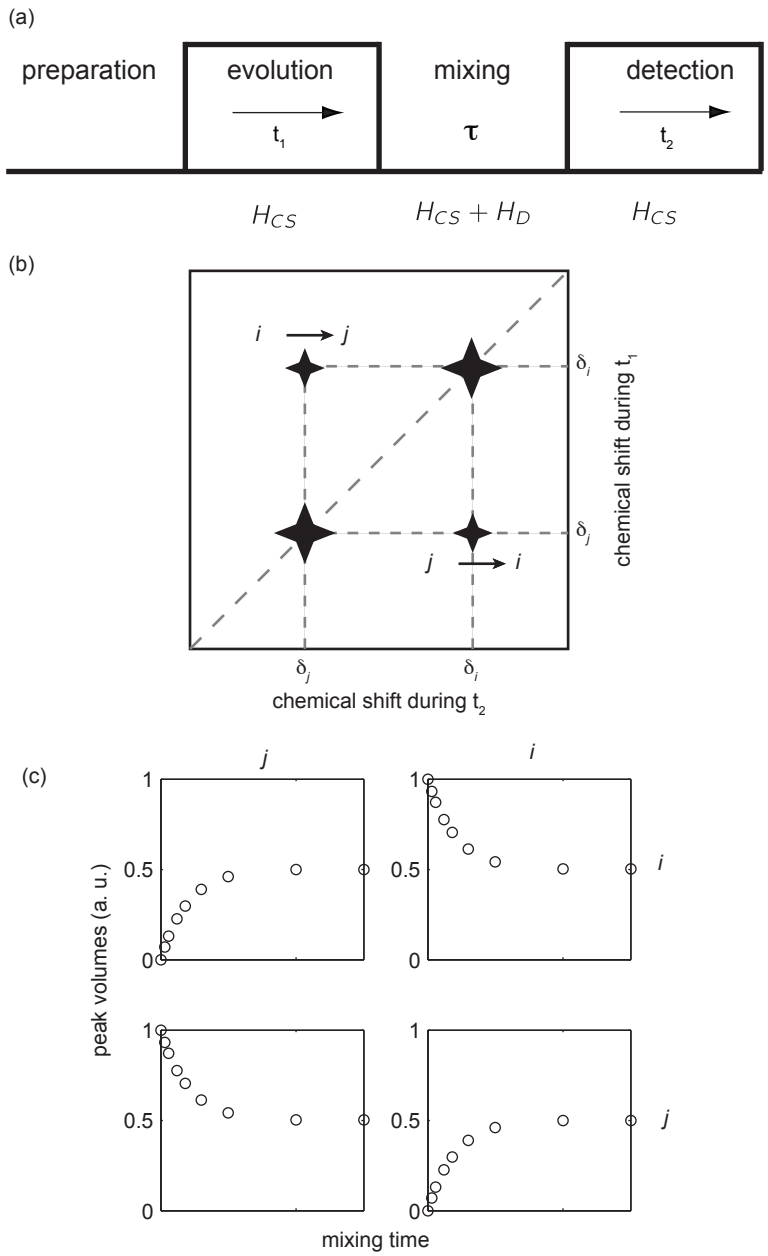

Figure 2.5: (a) 2D spin exchange pulse sequence. (b) Schematic spectrum. (c) Schematic build-up curves. For spin diffusion experiments, the chemical-shift interaction H_{CS} is encoded during the evolution and detection period, and the dipolar interaction H_D induces spin diffusion during the mixing period. In a 2D spectrum, off-diagonal peaks correspond to a transfer of polarisation during the mixing period; an example is shown here for two types of spins i and j.

leaving as much of the chemical shift interaction as possible unaltered has proved to be a difficult challenge. Homonuclear dipolar decoupling pulse sequences can nevertheless now provide site-specific information for a large range of systems [60], and have been used to record 2D proton spin diffusion experiments.

Spin diffusion between I spins can also be monitored with a "spy detection" scheme introduced by Zhang *et al.* [61], which relies on a heteronuclear polarisation transfer step to and from neighbouring S spins. This approach was extended to 2D experiments to observe spin diffusion between protons, with S spins chosen to provide high-resolution during evolution and detection [62, 63]; it is today widely exploited in biomolecular NMR for uniformly ^{13}C and ^{15}N labelled systems. An alternative monitoring scheme has also been proposed by Scholz *et al.*, who exploited the mixed rotary and rotational resonance conditions to follow the decay of the difference in polarisation between two carbons with radio-frequency irradiation on protons only [64].

It should be noted that the ability to individually monitor resonances does not imply that they are spectrally separated in the sense of the spectral spin diffusion process described in section 2.2.3. The homonuclear dipolar interaction, which is not suppressed during the mixing period, can still be significantly larger than the frequency differences between the observed resonances.

2.3.3 Spin diffusion between regions with different mobility

A non-uniform distribution of polarisation can also be generated by exploiting a difference of mobility between several groups of spins in a given sample. This approach is notably used to study spin diffusion between regions in a sample that have different relaxation times. For example, in the Goldman-Shen experiment [65], which is one of the early experiments introduced to monitor spin exchange, a free-precession delay is used to selectively depolarise regions of a sample that have shorter transverse relaxation times. Polarisation transfer from the slow-relaxing regions to the fast-relaxing regions is then monitored with a series of 1D experiments. Variations on this approach have been developed, where the free-precession delay is replaced, for example, by a multiple quantum filter that selects the less mobile regions. Various examples are discussed in Refs. [66] and [67].

2.3.4 Purely spatial spin diffusion

All the approaches described above rely to some extent on a source of non-equivalence to study the spin diffusion process, be it a difference in chemical shift or in relaxation time. Purely spatial diffusion between equivalent spins, although it has been subject of extensive theoretical investigation, has to date only been measured experimentally twice. Zhang and Cory [68] used a method inspired by incoherent NMR scattering experiments to measure the spin diffusion coefficient in reciprocal space and Meier and co-workers performed a real-space measurement using spatially and time resolved magnetic resonance force microscopy [69]. Both groups studied a sample of calcium fluoride, one of

the prototypical solids for the study of spin diffusion [1], where the ensemble of fluorine forms a regular network of equivalent spins that are strongly coupled by the dipolar interaction.

2.4 Structural investigation

2.4.1 Materials

Spin diffusion experiments have been used extensively to study the morphology of polymers, and in particular to determine the size of domains in mixtures of polymers [4]. Because of their high magnetogyric ratio and high natural abundance, protons are a probe of choice for this class of samples, and many methods have been developed to create gradients of polarisation and to study polarisation transfer over long distances. In a typical application, polarisation is depleted selectively in the least mobile region of a polymer blend, and the build-up back to equilibrium is monitored and used to obtain structural information. For this type of measurement, diffusion coefficients have to be either estimated with standard formulae or determined independently from a different sample.

Spin diffusion between carbons has also been explored as a tool to study polymers, for both ^{13}C-enriched [70] and natural-abundance [71] samples. Carbon spin diffusion in natural-abundance samples occurs, however, on much longer time-scales [52, 70–73]. Spin diffusion in polymers has been reviewed by several authors [22, 66, 74], and is covered in the book by Schmidt-Rhor and Spiess [4].

Spin diffusion between protons and driven by protons has also been used to characterise hydrated inorganic materials and hybrid materials. For example, Alonso, Massiot and co-workers have studied organically modified silicates and mesoporous silica membranes, on scales of up to several hundreds of nanometers [75, 76].

We will not review the methods developed to study these materials in further detail, instead we will focus in the rest of this section on methods that exploit the link between crystal geometry and high-resolution spin diffusion data.

2.4.2 Small molecules

As in the case of polymers, protons are in principle the nuclei of choice for NMR-based structural studies in organic solids [77]. The practical use of spin diffusion between protons for structure determination of small molecules with atomic resolution remains, however, a challenging task, which requires both a way to monitor polarisation transfer with sufficient resolution, and a reliable model to link experimental data and structural information. Several groups have started to address this challenge, which is made particularly critical by the fact that the resulting protocols are suitable for powdered samples, for which diffraction-based methods are not generally applicable.

Baldus and co-workers have used a spy detection scheme to observe spin diffusion between protons in isotopically enriched molecules, in the so-called XHHY experiments, with X,Y $\in$ {C, N} [78]. The resulting spin diffusion build-up curves, analysed in the

initial regime with a spin pair approximation, were used to define distance restraints and thus drive the structure determination of a tripeptide [79]. In a similar approach, classifications of ^{1}H-^{1}H contacts were used to study L-tyrosine-ethylester [80], and to determine the structure of an anti-cancer agent, epothilone B [81], shown in Fig. 2.6 with a CHHC spectrum. In all three cases, a diluted sample was used, so that only intermolecular contacts had to be taken into account in the analysis.

Polarisation transfer between protons can also in some cases be observed directly with ^{1}H-^{1}H spin exchange pulse sequences that employ homonuclear dipolar decoupling during evolution and detection. With this approach, Brus and co-workers measured proton spin diffusion in glycine, and tried to model polarisation transfer between spin pairs as a diffusive process [82], optionally taking motional effects into account [83]. In a more comprehensive study, Elena *et al.* recorded full build-up curves for a dipeptide, β-L-aspartyl-L-alanine, and used a master-equation approach to predict spin diffusion build-up curves for a given crystal structure [84]. The comparion between predicted and experimental build-up curves was then successfully used to drive a structure search [85]. The resulting structure and a proton spin diffusion spectrum are shown in Fig. 2.7. This protocol, which is applicable to compounds at natural abundance, was subsequently used to study thymol [86].

As an alternative to spy detection and homonuclear dipolar decoupling, Fujiwara and co-workers have suggested using stereo array isotope labelling to obtain high-resolution for proton detection. They performed experiments with the amino acid valine [87], and analysed them with a recently developed model [88].

Carbon-13 spin exchange experiments have also been performed on small molecules. In a series of studies, Luz, Tekely and co-workers monitored proton-driven spin diffusion in organic solids and used a master-equation approach to its description [89–92]. For samples of tropolone and durene, they assessed the relative contributions of spin diffusion and self-diffusion to the spin exchange process [89, 90]; it was necessary to take into account the statistical distribution of carbon-13 to model the exchange process. For a set of selectively labelled compounds, they used one-dimensional experiments to monitor spin diffusion between chemically equivalent nuclei and to determine internuclear distances [91, 92].

Information about the relative orientation of interaction tensors can also be obtained from spin diffusion experiments, as first illustrated by Henrichs *et al.* [93], and later exploited quantitatively by Ernst and co-workers [94, 95] and Tycko and co-workers [96, 97]. In this type of studies, the dynamics of the spin-exchange process are less relevant and the shapes of the correlation peaks are analysed after a long equilibration time.

2.4.3 Biomolecules

Spin diffusion played a central role in the first use of solid-state NMR to determine the structure of a protein, α-spectrin SH3, reported by Castellani *et al.* [98]. More precisely, 2D ^{13}C experiments with a proton-driven carbon-13 spin diffusion mixing time, collo-

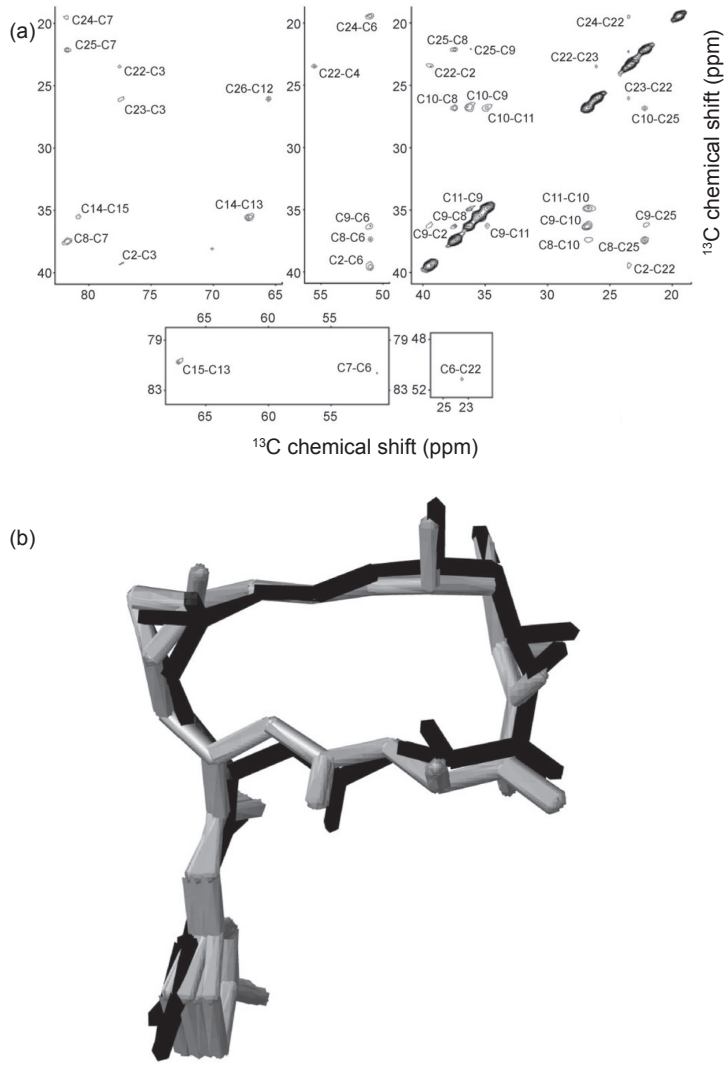

Figure 2.6: Structure determination of epothilone B. (a) 2D CHHC spectrum of ^{13}C-labelled powdered epothilone B, recorded with 11 kHz MAS and a mixing time of 100 μs. (b) Comparison of the 10 lowest-energy solid-state NMR structures derived from CHHC data (grey) and the x-ray structure (black). Reproduced from Ref. [81], © 2007 Wiley.

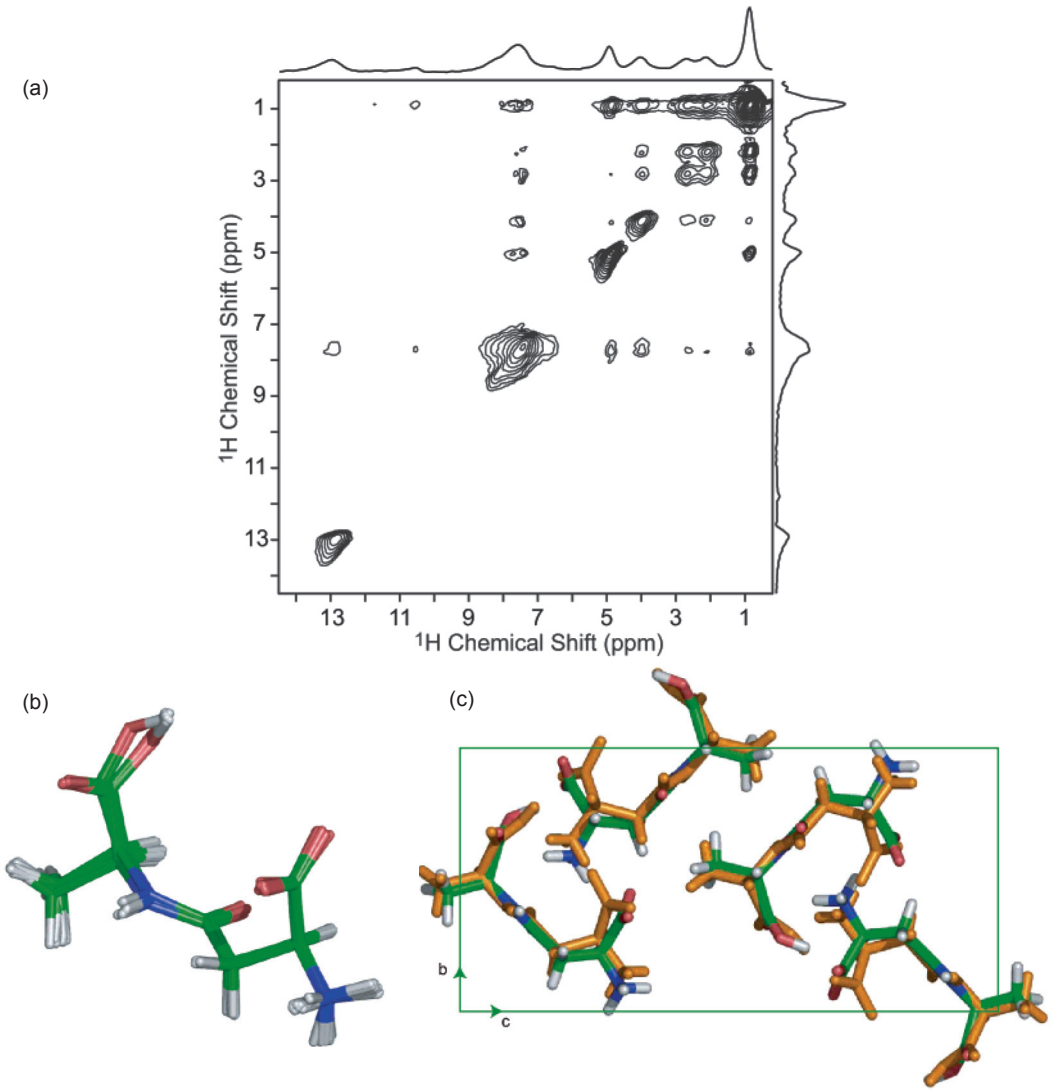

Figure 2.7: NMR crystallography of β-L-aspartyl-L-alanine. (a) 2D ^{1}H-^{1}H spin diffusion spectrum of powdered β-L-aspartyl-L-alanine, recorded with 22 kHz MAS and a mixing time of 220 μs. (b) 16 lowest-energy solid-state NMR structures derived from PSD data. (c) Comparison between the structure obtained from the averaged of the 16 lowest-energy structures and the x-ray structure (orange). Reproduced from Ref. [84], © 2005 American Chemical Society and Ref. [85], © 2006 American Chemical Society.

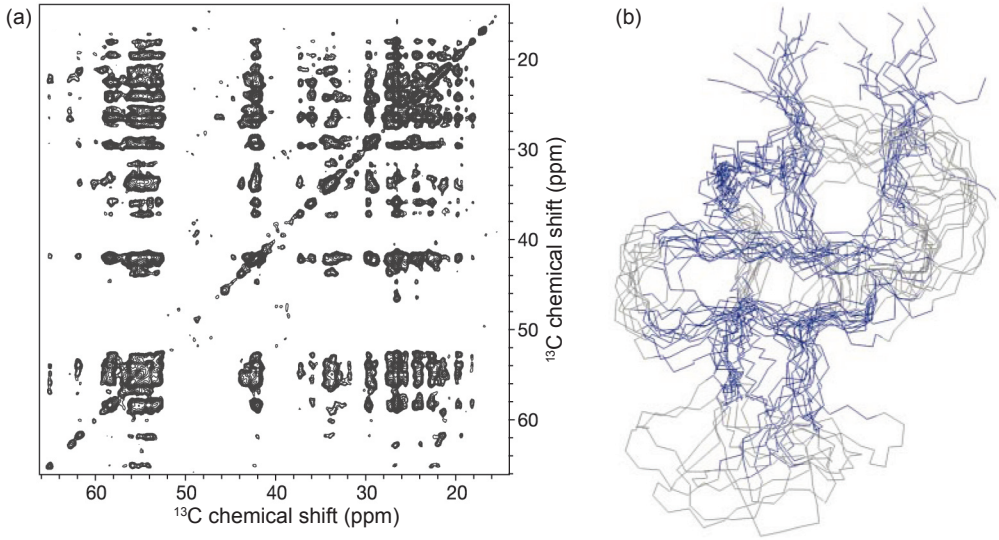

Figure 2.8: Structure determination of α-spectrin SH3. (a) 2D ^{13}C-^{13}C PDSD spectrum of selectively ^{13}C-labelled α-spectrin SH3, recorded with 8 kHz MAS and a mixing time of 500 ms. The sample was grown on [2-^{13}C]glycerol. (b) 12 of the 15 lowest-energy solid-state NMR structures derived from PDSD data, representing the fold of α-spectrin SH3. Reproduced from Ref. [98], © 2002 Nature Publishing Group.

quially referred to as PDSD experiments, were used to define carbon-carbon distance restraints. The structure and a 2D ^{13}C-^{13}C PDSD spectrum are shown in Fig. 2.8. Spin diffusion between protons has also been used to define distance restraints, with XHHY experiments, which have been subsequently used in combination with other restraints to determine the structure of a protein. In fact, several protein structures determined so far were obtained with some information derived from PDSD or XHHY experiments [99–107].

Even when a large number of correlations are observed in multidimensional spin exchange experiments, their usefulness for structural investigation is not guaranteed. In particular, long-range distance constraints, which are most useful to determine the structure of a macromolecule, are in general not straightforward to obtain. Spin diffusion among protons is well adapted for the collection of non-trivial constraints, as illustrated by Lange *et al.* [78] and de Boer *et al.* [108]. For carbon-13 spin diffusion, Grommek *et al.* have argued that long-range information could be obtained from PDSD experiments even in fully-labelled samples [43], and such experiments have indeed been used to determine the structure of the small protein ubiquitin [101]. It has also been shown, however, that a straightforward interpretation of PDSD spectra was hindered by the complex underlying dynamics of the spin diffusion process [101]. Many other techniques based on homonuclear dipolar recoupling have been developed to collect distance information; they are reviewed in, e.g., Ref. [109] and their relative merits will not be discussed here.

A more advanced analysis of PDSD experiments has been used by Fujiwara and coworkers to determine the structure of the light-harvesting bacteriochlorophyll c assembly

[110]. They used a kinetic model to account for relayed transfer in the analysis of a series of PDSD spectra. In order to exploit the relationship expressed in Eq. 2.6 and to obtain distance restraints, they approximated zero-quantum lineshapes by convolutions of experimentally measured single-quantum lineshapes.

A kinetic model has also been used by Hong and co-workers to extract structural information from a series of CODEX experiments performed on a membrane protein. The equilibrium magnetisation obtained in CODEX experiments was used to determine the oligomeric number of the protein [111], and the analysis of the time-dependent polarisation transfer between carbon-13 and between fluorine-19 made it possible to determine intermolecular distances [112]. CODEX experiments have also been used to study the tertiary structure of a cell wall [113].

Interestingly, no boundaries exist between the various forms that spin diffusion can take and the domain in which it is used, and approaches inspired by studies of polymers, both in terms of experiment and modelling, are being developed to study the interaction between water and membrane proteins [114–116].

2.5 Perspectives

Spin diffusion has been a topic of interest since the early days of magnetic resonance and is still fuelling intensive methodological developments. Although many successful applications continue to be reported, in particular for structural studies, the question of describing spin diffusion from first principles, at the level of resolution with which it can today be observed, is still to a large extent unaddressed. A better understanding of spin diffusion from first principles is not only a subject of academic interest, it is also expected to lead to an improvement in existing methods and to the emergence of new approaches to structure determination.

Chapter 3

Master-equation approach to the description of proton-driven spin diffusion

3.1 Introduction

The spontaneous transfer of polarisation among carbons in organic molecules, which is made possible by their interaction with surrounding protons and therefore named proton-driven spin diffusion (PDSD), is currently being used extensively for structural studies [101, 104–107]. PDSD experiments and their applications have been described in chapter 2. The through-space transfer of polarisation that the dipolar interaction induces between homonuclear spins encodes structural information [4], and in contrast to transfer mechanisms relying on dipolar recoupling, spontaneous spin diffusion can be observed with one of the simplest possible two-dimensional correlation experiments. PDSD spectra, which are expected to contain not only short-range information [43, 117], provide qualitative information about spatial proximity that can be turned into coarse distance restraints. Such qualitative models are known to be flawed [101], but since the PDSD process involves not only a large assembly of carbon nuclei but also an even larger number of protons, a direct numerical simulation of the underlying spin dynamics is in general not possible, and simplified models are therefore necessary to make a quantitative link between structure and spectra [2–4].

Master-equation approaches to the description of polarisation transfer have been used extensively to analyse incoherent dipolar-driven processes in solution-state NMR [54]. In the solid-state, several studies have shown that the coherent action of surrounding protons can in some cases be described with a simple kinetic model [16, 30–33], and master-equation approaches have been used to study ^{13}C PDSD in a variety of systems [70–72, 89–92, 110, 112, 118–120], as well as other related polarisation transfer processes [79, 80, 84–86, 121–126]. In particular, the structure of a large ^{13}C-labelled biomolecular assembly has recently been derived from PDSD data with a kinetic model [110]. In this simplified description, the rate constants involve both internuclear distances and a quantity

that captures the contribution of the proton bath to the polarisation transfer process. This latter quantity, discussed in detail below, in general has to be determined empirically.

In this chapter, we illustrate the use of a master-equation approach to the description of PDSD in polycrystalline L-histidine.H_2O.HCl under magic-angle spinning. We first show that full PDSD build-up curves can be accurately described with a kinetic model. We then consider the link between the rate constants and the effective dipolar couplings, which can be calculated from the known crystal structure. We then show that numerical simulations of the zero-quantum lineshapes, directly from crystal geometry and with no adjustable parameters, are accurate enough to capture the contribution of the proton bath to the proton-driven spin diffusion rate constants. Finally, using carbon-carbon internuclear distances we illustrate the potential of the master-equation approach for structural studies.

3.2 Outline of the master-equation approach

3.2.1 Time evolution of experimental observables

As explained in section 2.2.3, in a master-equation approach to the description of polarisation transfer for a system of N homonuclear spins, the time evolution of the polarisations is described by:

$$\frac{d}{dt}\mathbf{M} = \mathbf{K}\mathbf{M}. \tag{3.1}$$

$\mathbf{M}$ is a vector of coefficients of the carbon polarisations $\{M_i\}$, and $[\mathbf{K}]_{ij}$, hereafter noted k_{ij}, is the rate constant for the transfer from spin j to spin i. For a system containing groups of equivalent spins, it is useful to introduce the summed polarisations M'_p for groups of equivalent spins

$$M'_p = \sum_{i=1}^{N_p} M_{a_i}, \tag{3.2}$$

where p denotes a group of N_p equivalent spins, and the sum is over all spins $\{a_i\}$ in the group. Spins can be considered as equivalent if they are related by a symmetry operation that leaves the exhange matrix unchanged. Using this set of variables, the rate matrix becomes block-diagonal, and only the block involving the summed polarisations has to be taken into account. The other variables, the detailed expression of which is irrelevant, can be dropped from the description. The kinetic model then simplifies to

$$\frac{d}{dt}\mathbf{M}' = \mathbf{K}'\mathbf{M}', \tag{3.3}$$

where

$$k'_{pq} = \frac{1}{N_p}\sum_{i=1}^{N_p}\sum_{j=1}^{N_q} k_{a_i b_j}. \tag{3.4}$$

This simplification would not be possible for groups that include non-equivalent spins, as discussed by Robyr *et al.* in Ref. [119]. Equation 3.4 can be simplified by considering the

fact that, because the spins in a given group are equivalent, the sum $\sum_{j=1}^{N_q} k_{a_i b_j}$ is identical for all values of i :

$$k'_{pq} = \sum_{j=1}^{N_q} k_{a_1 b_j}. \tag{3.5}$$

For proton-driven spin diffusion in polycrystalline solids under magic-angle spinning, assuming that a single rate constant can be defined for a given pair of spins, nuclear spins are equivalent if they are crystallographically equivalent according to the definition introduced by Haeberlen [127], i.e., if the nuclei are related by a symmetry operation of the crystal. There are then as many groups of equivalent spins as there are spins in the asymmetric unit, and the sums over all spins in a group are sums over asymetric units. In consequence, for a system where all the carbons in the asymmetric unit are resolved in the experimental spectra, Eq. 3.3 describes the time evolution of the peak volumes in a PDSD experiment.

3.2.2 PDSD rate constants and effective dipolar couplings

In proton-driven spin diffusion, the transfer of polarisation between carbons, which would in the absence of protons be quenched by the large energy difference between the Zeeman energy levels of the carbons, is made possible by the dipolar interaction of the carbons with surrounding protons, which act as an energy bath. Building on this qualitative description, several studies have shown that, under certain conditions, the rate constant for the transfer of polarisation between two carbons k_{ij} is expected to be proportional to the square of the dipolar coupling ω_{ij} between these two carbons and can be expressed as

$$k_{ij} = \kappa \omega_{ij}^2 F[G_{ij}(\nu)], \tag{3.6}$$

where

$$\omega_{ij} = \frac{\mu_0 \gamma_C^2 \hbar}{4\pi r_{ij}^3}; \tag{3.7}$$

γ_C is the carbon magnetogyric ratio, r_{ij} is the internuclear distance between spin i and j, and κ is a geometrical factor [30–33]. $F[G_{ij}(\nu)]$ is a function of the zero-quantum lineshape $G_{ij}(\nu)$, which is the Fourier transform of the free-induction decay of a transverse two-carbon zero-quantum correlation under the action of the surrounding protons. This term captures the contribution of the proton bath to the polarisation transfer process.

Combining Eq. 3.5 and 3.6, the rate constant for the transfer between groups of crystallographically equivalent spins can be written:

$$k'_{pq} = \kappa \sum_{j=1}^{N_q} \omega_{a_1 b_j}^2 F[G_{a_1 b_j}(\nu)]. \tag{3.8}$$

For a given pair of carbons, if the ensemble of protons acting on a each carbon are independent, the zero-quantum lineshape for the carbon pair can be approximated by the

convolution of the single-quantum lineshape for each carbon [2]. This assumption of uncorrelated proton baths is not strictly valid for a ^{13}C-labelled polycrystalline system [128]. If such an approximation is made for all the carbon pairs in the system, then, as all the spins in the group q are equivalent, the term $F[G_{a_1b_j}(\nu)]$ becomes identical for all spin pairs (a_1,b_j), regardless of the value of j. Equation 3.8 can then be factored as,

$$k'_{pq} = \kappa\omega^2_{pq,\mathrm{eff}}F[G_{a_1b_1}(\nu)], \tag{3.9}$$

where

$$\omega^2_{pq,\mathrm{eff}} = \sum_{j=1}^{N_q}\omega^2_{a_1b_j}. \tag{3.10}$$

The quantity $\omega_{pq,\mathrm{eff}}$, sometimes called "effective dipolar coupling", is straightforward to calculate for a given crystal structure. Effective dipolar couplings have been suggested as a measure of the overall coupling between groups of nuclei [129], and have notably been used in earlier studies of spin diffusion [32].

3.3 Characterisation of the zero-quantum lineshape

3.3.1 Measurements of spin diffusion rate constants

Proton-driven spin diffusion, like many other polarisation transfer processes, can be monitored experimentally using a pseudo-3D setup, which consists of recording 2D NMR spectra for a series of mixing times, as explained in section 2.3.2. The pulse sequence used in PDSD experiments and a representative spectrum are shown in Fig. 3.1. In PDSD, the system evolves freely during the mixing period, and polarisation transfer occurs spontaneously. The evolution of the peak volumes as a function of the mixing time can be organised into an array of build-up curves, which reflects the structure of 2D spectra and provides a convenient way to visualise and analyse the data.

Figure 3.2 shows experimental PDSD build-up curves for a polycrystalline sample of ^{13}C-labelled L-histidine.H_2O.HCl (**1**, see Fig. 3.3), measured at 10 kHz MAS; build-up curves were also recorded at 15 and 20 kHz MAS. PDSD spectra are commonly recorded at spinning frequencies of 12 kHz or less, which provide a compromise between the facts that increasing the spinning frequency simultaneously leads to an improved resolution and to a slow down of the polarisation transfer process. In particular, it has been observed that PDSD is virtually quenched at spinning frequencies of 60 kHz and above [132]. The fact that the mixing period is free of radio-frequency irradiation makes the PDSD sequence particularly robust with respect to experimental imperfections. However, the link between PDSD data and structure is difficult to make.

The full quantum-mechanical description of spin diffusion in large nuclear spin systems is not possible in the general case, and drastic simplifications are necessary. As explained in section 3.2, in a master-equation approach to the description of polarisation transfer in polycrystalline samples under magic-angle spinning, the only variables are the summed polarisations M'_p for groups of crystallographically equivalent carbons,

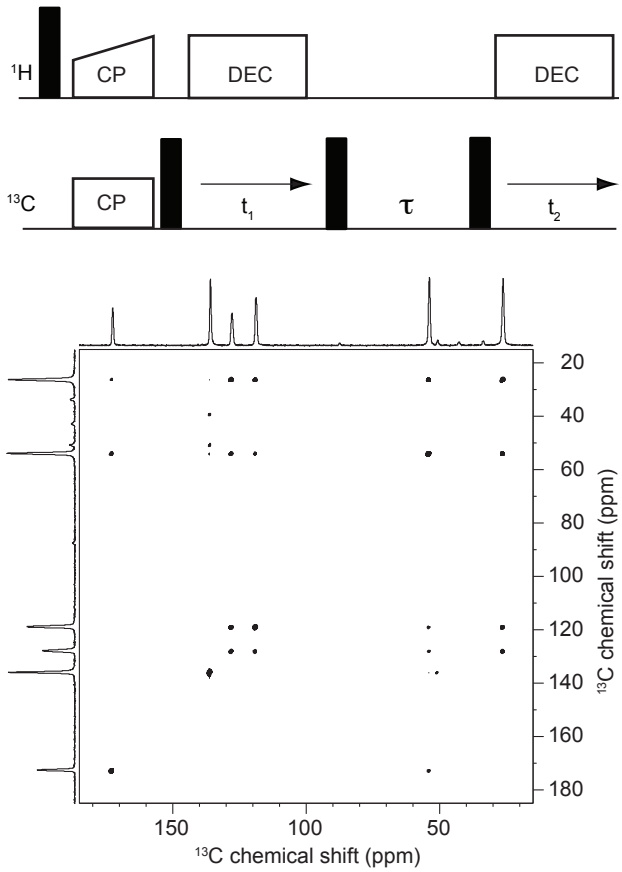

Figure 3.1: Pulse sequence for the 2D ^{13}C-^{13}C PDSD experiment and 2D ^{13}C-^{13}C PDSD spectrum recorded with 15 kHz MAS and a mixing time τ of 25 ms for L-histidine.H_2O.HCl. Experiments were performed on a standard-bore Bruker Avance II NMR spectrometer operating at a ^{1}H Larmor frequency of 700 MHz using a 2.5 mm double-resonance MAS probe spinning the sample at frequencies of 10, 15, and 20 kHz. Two-dimensional PDSD experiments with values of the mixing time of up to 500 ms were recorded in random order. The CP contact time was 1 ms, and the acquisition time was 30 ms. SPINAL-64 [130] at a nutation frequency of 80 kHz was used for heteronuclear decoupling during the evolution and detection period. 512 increments of 8 transients each were recorded using the States method [131], with a recycle delay between scans of 3 s, resulting in a total experimental time of about 3.5 h for each spectrum.

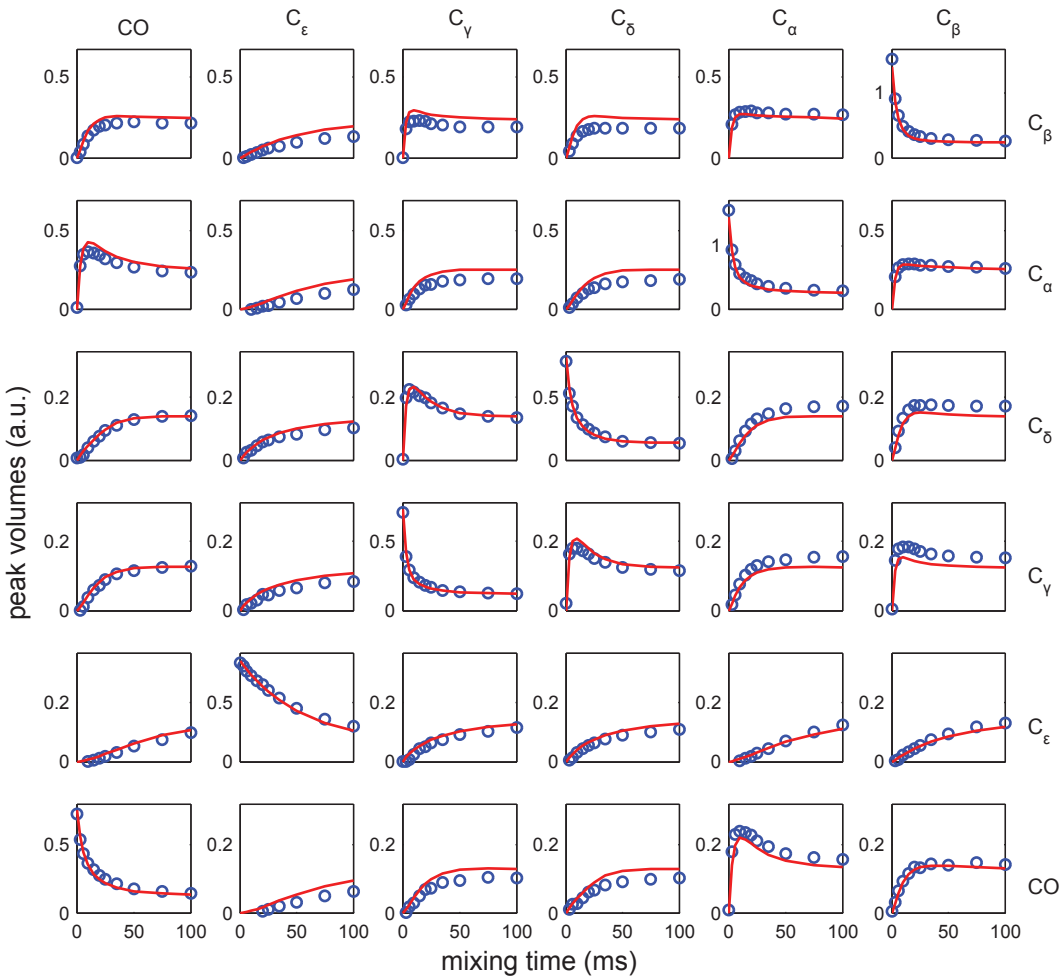

Figure 3.2: PDSD build-up curves recorded for a polycrystalline sample of L-histidine.H_2O.HCl with 10 kHz MAS. Experimental measurements (blue) and curves calculated with a kinetic model (red) are shown. Experimental curves were obtained by integrating peak volumes in a series of 2D PDSD experiments. The rate constants used in the kinetic model were determined from the experimental curves using a least-error matrix analysis.

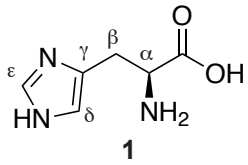

Figure 3.3: Chemical structure of L-histidine.H_2O.HCl.

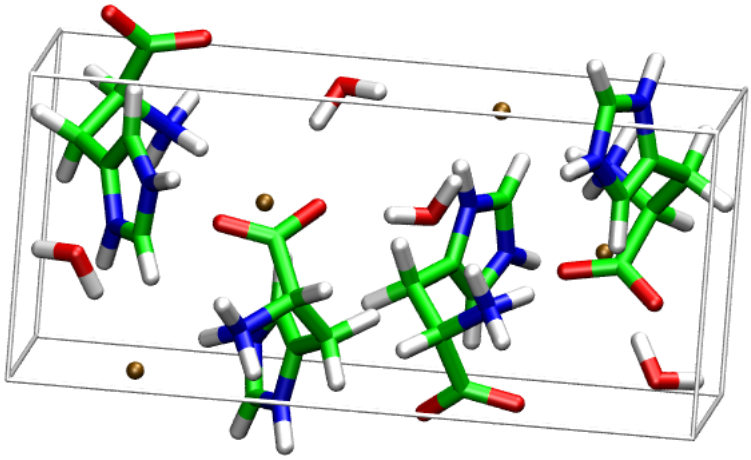

Figure 3.4: Crystal structure of L-histidine.H_2O.HCl. Carbon atoms are depicted in green, hydrogen in white, oxygen in red, nitrogen in blue and chlorine in brown.

the time evolution of which is governed by a kinetic model. Here we chose to study L-histidine.H_2O.HCl, which has a well-resolved peak for each carbon in the asymmetric unit, i.e., for each group of crystallographically equivalent carbons, and a single known polymorphic form, the structure of which, shown in Fig 3.4, has been determined accurately by neutron diffraction on a single crystal sample (refcode histcm12 in the Cambridge Structural Database [133]).

Although rate constants can be measured in the initial regime [134] or in principle calculated from a single spectrum [135, 136], considering the full build-up curves makes it possible to assess the accuracy with which experimental data can be described with a master-equation approach. The curves calculated with Eq. 3.3 for rate constants determined with the least-error matrix analysis introduced by Macura and co-workers [137] are also shown in Fig. 3.2, illustrating the fact that the master equation approach is appropriate for this polycrystalline amino acid. It should be noted that the least-error matrix analysis also makes it possible to assess the information content of each spectrum [137], and reveals here that mixing times longer than 75 ms contribute very little to the measured values of the rate constants.

Some key features of the PDSD process are well illustrated by this study. In particular, the role of relayed transfer can be noticed by comparing the intensity of some cross-peaks, which, after only a few tens of milliseconds, are relatively intense although they correspond to a small rate constant for direct transfer. Values of PDSD rate constants k'_{pq} obtained with a least-error matrix analysis of the full experimental build-up curves are given in table 3.1, and it can be seen, for example, that after 50 ms the C_β/C_γ and C_β/C_δ cross peaks have comparable volumes, although the corresponding rate constants for the direct transfer differ by an order of magnitude. Also, as will be discussed in more detail in

Table 3.1: Measured PDSD rate constants, in Hertz, for L-histidine.H_2O.HCl with 10 kHz MAS, determined using a least-error matrix analysis of a series of 2D PDSD spectra. Rate constants were obtained from PDSD build-up curves using the least-error matrix analysis developed by Macura and co-workers [137], which consists of taking a weighted average of the rate constants determined by an independent full-matrix analysis of each 2D spectrum, with weights determined by an iterative least squares approach. Estimates of the uncertainty for the rate constants were obtained using the formula given in Ref. [137] with a uniform estimated measurement uncertainty for the experimental peak volumes of 0.5% of the initial volume of a diagonal peak. A spectrum with $\tau = 0$ ms is also needed for the full-matrix analysis, as the non-uniform CP efficiencies result in non-uniform total volumes for each row of the 2D spectra [138].

	CO	C_ε	C_δ	C_γ	C_α	C_β
C_β						*
C_α					*	67.9-72.8
C_γ				*	2.8-5.9	7.1-10.3
C_δ			*	111-115	2.2-6.6	86.1-90.7
C_ε		*	6.2-7.9	4.7-5.8	< 1	1.4-3.1
CO	*	< 1	1.3-4.2	6.7-8.7	90.5-93.5	5.8-9.0

the next section, although they vary over a large range of values, the PDSD rate constants are not related in a simple way to structural information.

3.3.2 Comparison with squared effective dipolar couplings

As explained in section 3.2, under the assumption of uncorrelated proton baths, the elements of the rate matrix $\mathbf{K}'$ can then be written as

$$k'_{pq} \propto \omega^2_{pq,\mathrm{eff}} F[G_{a_1 b_1}(\nu)], \tag{3.11}$$

where $\omega^2_{pq,\mathrm{eff}}$ is the effective dipolar coupling between two groups of crystallographically equivalent spins. The crystal structure of L-histidine.H_2O.HCl has been determined by neutron diffraction, and it is thus possible to calculate, from the crystal geometry, effective dipolar coupling constants between groups of equivalent spins, which include both intramolecular and intermolecular couplings. It can be noted that in a larger biomolecular system, the effective dipolar couplings would in most cases not be significantly different from the dipolar coupling corresponding to the shortest inter-spin distance, but that in crystals of a small organic molecule the difference can be significant; the approach here is fully general. For L-histidine.H_2O.HCl, effective dipolar couplings can differ from the dipolar coupling for a single pair by more than 50 % in extreme cases, with in most cases differences ranging from less than 1 % to 25 %.

If we assume that Eq. 3.11 is applicable, although the assumption of uncorrelated proton baths is not strictly valid for a ^{13}C-labelled polycrystalline system [128], we should compare the experimentally measurable quantity k'_{pq} with the structural information of interest $\omega^2_{pq,\mathrm{eff}}$ for all pairs of groups of equivalent nuclei. Table 3.2 shows the ratios between the PDSD rate constants measured experimentally and the squared effective dipolar

Table 3.2: Ratios, in microseconds, between PDSD rate constants and squared effective dipolar couplings for L-histidine.H_2O.HCl with 10 kHz MAS. Squared effective dipolar couplings were determined from a single-crystal neutron diffraction structure.

	CO	C_ε	C_δ	C_γ	C_α	C_β
C_β						*
C_α					*	0.8
C_γ				*	2.0-4.2	1.7-2.4
C_δ			*	0.6-0.7	0.5-1.4	0.8-0.9
C_ε		*	0.6-0.8	0.4-0.5	< 2.5	1.7 - 3.8
CO	*	< 1.3	0.7-2.4	4.4-5.7	1.1	1.4-2.2

couplings. It can be seen that they vary by more than one order of magnitude, which would result in a factor of more than 50 % in distance estimates if the contribution of the proton baths to the PDSD rate constants is not accounted for in a pair-specific manner. From a practical point of view, this issue can be circumvented by empirically determining the ratios $k'_{pq}/\omega^2_{pq,\mathrm{eff}}$ for reference compounds [112], or by using experimentally measured single-quantum lineshapes [110]. Here we assess the possibility to use numerical simulations of zero-quantum lineshapes to predict the ratios $k'_{pq}/\omega^2_{pq,\mathrm{eff}}$, starting from the crystal geometry.

3.3.3 Numerical simulation of the zero-quantum lineshape

Exact numerical simulations of NMR experiments can routinely be used to describe systems of about a dozen strongly coupled nuclear spins [139–141], and such a system size is in general insufficient to perform a direct simulation of the PDSD process. It has recently been shown, however, that numerical simulations can be used to describe homogeneously broadened ^{1}H lineshapes under magic-angle spinning [129, 142]. Here we explore the possibility to describe carbon lineshapes homogeneously broadened by carbon-proton and proton-proton dipolar interactions.

A study of the convergence behaviour of carbon single-quantum lineshapes as the number of surrounding protons is increased shows that 10 protons or more are required to obtain a reasonably converged lineshape, as illustrated in Fig. 3.5 with example free-induction decays and lineshapes. In order to perform a direct simulation of zero-quantum lineshapes, a system consisting of two carbons and of the unions of two groups of about 10 protons each would be thus be required. Such a system size, even if there exists some overlap between the groups of protons, is in general not manageable with numerical simulations performed by programs that rely on a full description of the spin space. In consequence, all the zero-quantum lineshapes considered here were obtained as convolutions of single-quantum lineshapes.

Here we used SPINEVOLUTION [141] to simulate single-quantum lineshapes for all the carbons in the asymmetric unit of L-histidine.H_2O.HCl. For each simulation, the spin system consisted of a single carbon and the 12 protons that are nearest to this carbon;

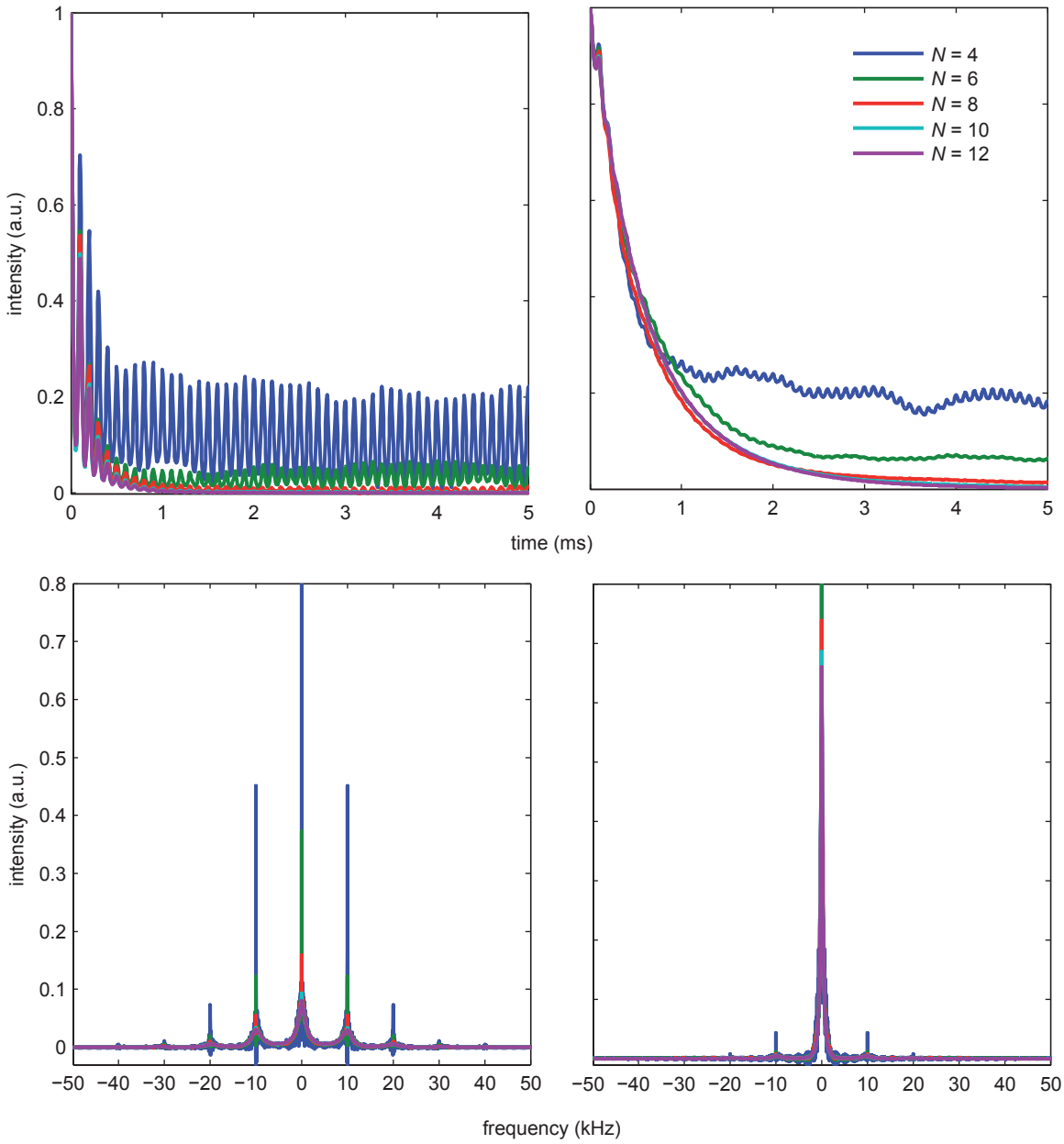

Figure 3.5: Examples of simulated powder-averaged carbon single-quantum free-induction decays and lineshapes with 10 kHz MAS. Curves are shown for the C_α (left) and the C_γ (right) of L-histidine.H_2O.HCl. In each simulation, the system consisted of a single carbon and of the N protons that are the closest to this carbon. Atomic coordinates were taken from a crystal structure (CSD entry: histcm12), and a ZCW set of 144 orientations was used for the simulation.

such a 13-spin system corresponds to the current maximum number of spins that can be simulated with SPINEVOLUTION. Once a single-quantum lineshape had been simulated for each carbon in the asymmetric unit, zero-quantum lineshapes were obtained as convolutions of single-quantum lineshapes, with each single-quantum lineshape centred at the chemical shift precession frequency of the corresponding carbon. Both heteronuclear carbon-proton and homonuclear proton-proton dipolar couplings were taken into account in the simulations, and they lead to a homogeneously broadened single-quantum lineshape. Chemical shift anisotropies (CSAs) are not, however, expected to have a significant effect on the zero-quantum lineshapes, and they were thus not included in the simulations reported here; we have verified the validity of this approximation by comparing simulations with and without CSA. Other polarisation-transfer mechanisms involving CSA cannot be excluded.

A selection of zero-quantum lineshapes calculated in this manner is shown in Fig. 3.6, where it can be seen that they vary significantly from one pair of carbons to another. Using the expression for the rate constant for the transfer of polarisation in polycrystalline systems under magic-angle spinning derived by Kubo and McDowell [33], the element of the rate matrix can be written

$$k'_{pq} = \frac{1}{15}\omega^2_{pq,\mathrm{eff}}\left(G_{a_1b_1}(\nu_r) + \frac{1}{2}G_{a_1b_1}(2\nu_r)\right). \tag{3.12}$$

The ratios between the PDSD rate constants and the effective dipolar couplings can thus be estimated by summing the intensity of the simulated lineshapes at the spinning frequency and at twice the spinning frequency, indicated by crosses in Fig. 3.6. It should be noted that Eq. 3.12 provides PDSD rate constants for powder-averaged PDSD build-up curves, and involves powder-averaged zero-quantum lineshapes. Although there exists in principle a distribution of rate constants for a polycrystalline sample, we have in this study followed Kubo and McDowell and considered only powder-averaged quantities.

Figure 3.7 shows the comparison between the calculated value of the function of the zero-quantum lineshape and the experimentally determined ratio $15k'_{pq}/\omega^2_{pq,\mathrm{eff}}$, for spinning frequencies of 10, 15 and 20 kHz. Remarkably, the non-trivial influence of the spinning frequency on the rate constants is overall correctly reproduced, and the quantitative agreement between the predicted and measured values is, with a few exceptions, very good. Notably, the spinning frequency dependence is not monotonic in many cases, but varies in a complex manner, which depends strongly on the pairwise chemical-shift differences. When chemical-shift differences are not taken into account, then the predicted values typically lie above (50 μs or larger) the measured values, and they either decay monotonically or do not change significantly with spinning frequency. The complex dependence of the rate constants on spinning frequency is found to be dominated by the proximity to rotational-resonance [10, 11] due to varying chemical shift differences. Not accounting for the pair-specific nature of the ratios would lead to an incorrect relationship between internuclear distances and PDSD rate constants.

It can be seen in Fig. 3.7 that the ratios that are unambiguously overestimated by the calculation correspond to pairs of carbons for which there exists a very short internuclear distance, such as C_α and C_β. For such pairs, the approximation of uncorrelated

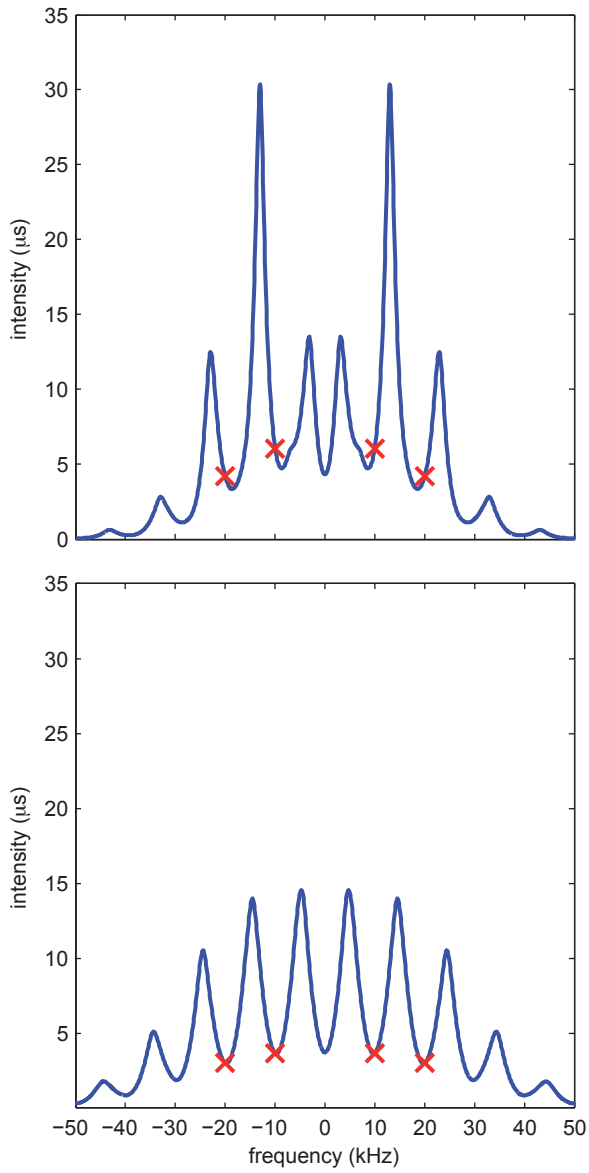

Figure 3.6: Examples of simulated powder-averaged zero-quantum lineshapes for L-histidine.H_2O.HCl with 10 kHz MAS. The lineshapes are shown for the C_α-C_δ pair (top) and the C_α-C_ε pair (bottom). Red crosses indicate the intensity of the zero-quantum lineshape at the spinning frequency and at twice the spinning frequency. Zero-quantum lineshapes were obtained as convolution of single-quantum lineshapes; each single quantum lineshape was simulated with a system consisting a single carbon and of the 12 protons that are closest to this carbon. Atomic coordinates were taken from a crystal structure (CSD entry: histcm12), and a ZCW set of 538 orientations was used for the simulation.

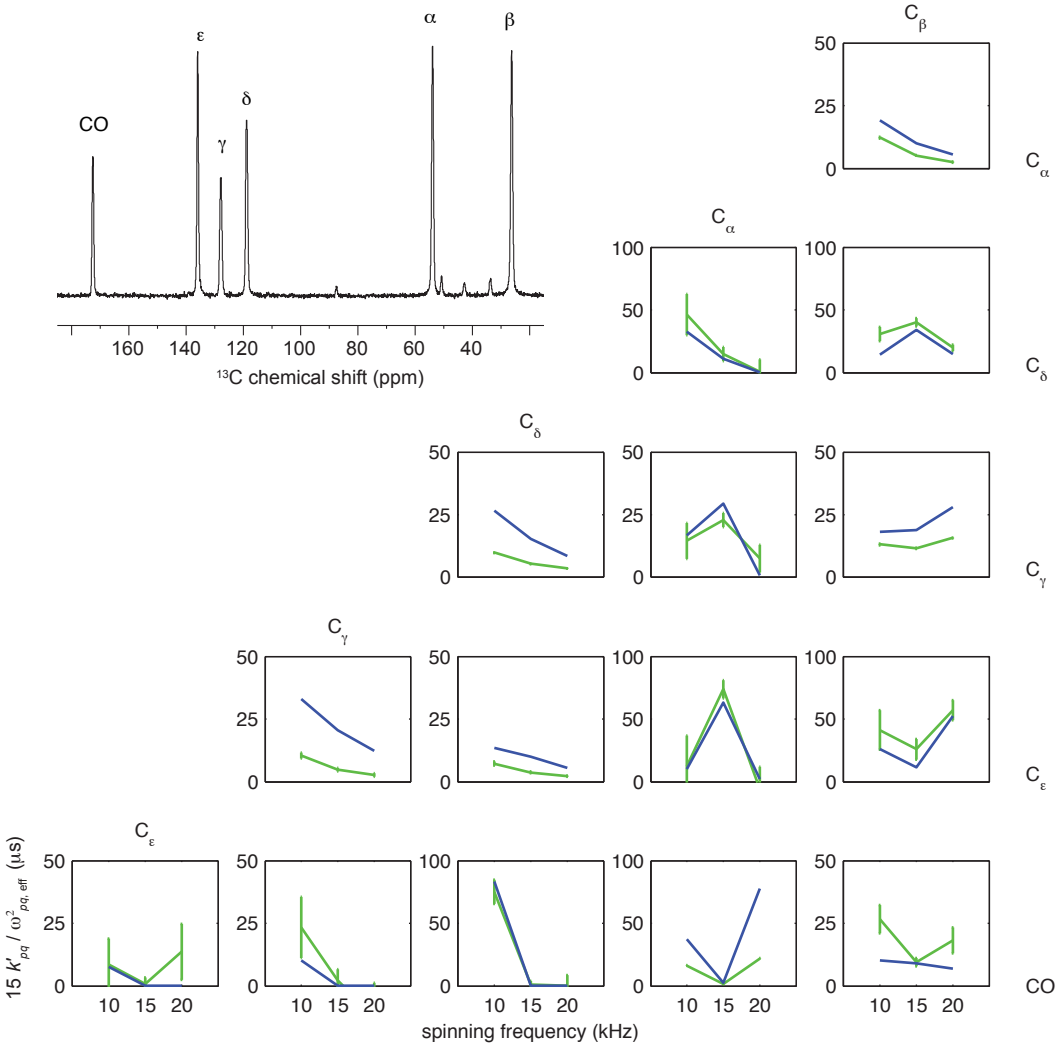

Figure 3.7: Ratios between PDSD rate constants and squared effective dipolar couplings for L-histidine.H_2O.HCl. Experimental (green) and calculated (blue) values are shown for three spinning frequencies. Experimental values were obtained by dividing experimental PDSD rate constants by squared effective dipolar couplings determined from a single-crystal neutron diffraction structure. Calculated values were obtained from numerical simulations of zero-quantum lineshapes. A 1D ^{13}C CPMAS spectrum is shown as an inset.

proton baths is questionable and may be the cause of the observed discrepancy; also, the homonuclear carbon-carbon coupling is not always much smaller than the heteronuclear carbon-proton couplings. For the other ratios, such as the ratios for $C_{\alpha/\beta}$ and $C_{\delta/\varepsilon}$, there is good agreement between calculation and experiments.

Most importantly, it should be noted that the comparison shown here is parameter-free, and in particular involves no overall scaling of the experimental and calculated quantities, with the latter being obtained from first principles. Numerical simulations of the zero-quantum lineshapes can thus provide a more quantitative link between structural information and experimentally measurable quantities.

3.4 Consequences for structural studies

As both a summary and a perspective, the link between structural information and NMR data made possible by a master-equation approach to the description of PDSD using simulated zero-quantum lineshapes can be evaluated using carbon-carbon internuclear distances. Using PDSD rate constants determined by a least-error matrix analysis of a series of 2D PDSD spectra, and ratios between PDSD rate constants and squared effective dipolar couplings determined with numerical simulations of zero-quantum lineshapes, the following "effective distances" can be calculated:

$$r_{pq,\mathrm{eff}}^{\mathrm{nmr}} = A_{pq}\left(k'_{pq}\right)^{-1/6}, \tag{3.13}$$

where the prefactor is

$$A_{pq} = \left(\frac{\mu_0 \gamma_{\mathrm{C}}^2 \hbar}{4\pi}\right)^{1/3} \left(\frac{1}{15}\left(G_{a_1 b_1}(\nu_r) + \frac{1}{2} G_{a_1 b_1}(2\nu_r)\right)\right)^{1/6}. \tag{3.14}$$

These effective distances, which are the structural information of interest for the PDSD experiments, can be compared with the corresponding values determined by neutron diffraction:

$$r_{pq,\mathrm{eff}}^{\mathrm{neutron}} = \left(\sum_{j=1}^{N_q}\left(r_{a_1 b_j}^{\mathrm{neutron}}\right)^{-6}\right)^{-1/6}. \tag{3.15}$$

The comparison between $r_{pq,\mathrm{eff}}^{\mathrm{nmr}}$ and $r_{pq,\mathrm{eff}}^{\mathrm{neutron}}$ for L-histidine.H_2O.HCl with 10 kHz MAS is shown in Fig. 3.8, and the strong observed correlation illustrates from a structural point of view the fact that the spin dynamics relevant to the PDSD phenomenon are well described, without any adjustable parameters, by the approach outlined in this study.

This becomes particularly pertinent if we consider a more traditional approach to the analysis of PDSD data. Figure 3.8 also shows distance estimates obtained by analysing a single 2D PDSD spectrum recorded with a mixing time of 25 ms. The analysis assumes a linear relationship between normalised cross-peak volumes and the inverse sixth power of internuclear distances, and uses directly-bonded carbons for calibration (as described in the figure caption). Large systematic errors are observed for the distance estimates obtained with this approach, which neither accounts for relayed transfer nor accounts for

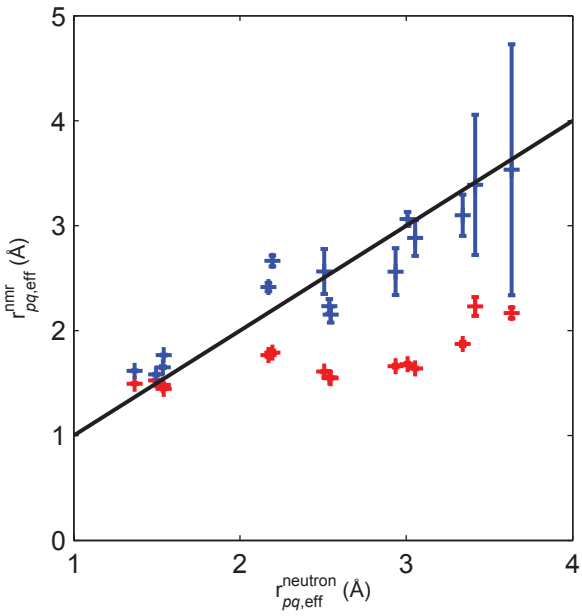

Figure 3.8: Effective internuclear distances in L-histidine.H_2O.HCl, as obtained in a master-equation approach to the description of PDSD (blue) and estimated with the analysis of a single 2D PDSD spectrum (red), plotted against reference values calculated from a crystal structure determined by neutron diffraction. Values shown in blue were obtained using PDSD rate constants determined with a least-error matrix analysis of a series of 2D PDSD spectra, and ratios between PDSD rate constants and squared effective dipolar couplings determined with numerical simulations of zero-quantum lineshapes. Values shown in red were obtained from a single PDSD spectrum recorded with a mixing time of 25 ms. First, each row was normalised to a total intensity of one, and then the spectrum was symmetrised with respect to the diagonal. Finally, cross-peak volumes were converted into distance estimates by assuming a linear relationship between the cross-peak volumes and the inverse sixth power of effective distances, with a proportionality factor chosen to give the best agreement with neutron diffraction data for effective distances that involve pairs of directly-bonded carbons. PDSD spectra were recorded with 10 kHz MAS.

the variable ratios between PDSD rate constants and squared effective dipolar couplings [101]. Figure 3.8 thus illustrates the shortcoming of a straightforward analysis of the PDSD phenomenon, and the possibility to link structural information and NMR data accurately in a parameter-free manner with the method developed here, which could help overcome these shortcomings.

3.5 Conclusions

A master-equation approach to the description of proton-driven spin diffusion has been shown to be appropriate for a ^{13}C-labelled polycrystalline amino acid under magic-angle spinning. The ratios between the rate constants for the transfer of polarisation and effective dipolar couplings are found to vary by more than one order of magnitude, a fact that in conjunction with relayed transfer makes the quantitative use of PDSD data difficult. Numerical simulations are shown, however, to be accurate enough to capture the contribution of the proton bath to the PDSD rate constants, and thus to provide an estimate of the ratio between the structural information of interest and an experimentally measurable quantity. This provides the missing quantitative link between measured polarisation exchange rate constants and internuclear distances. Generalisation to PDSD in biomolecular solids is readily envisaged, providing potential for a central role in structure determination by solid-state NMR.

Chapter 4

Interlude: Liouville space

4.1 Introduction

When modelling spin diffusion, complexity arises from the fact that the small set of variables of interest, the single-spin polarisations, are coupled to an immense number of additional variables, the multi-spin correlations. Modelling spin diffusion is thus a specific instance of a general undertaking, for which many approaches have been developed. In particular, simplified descriptions become possible when there exists a separation of time-scales between the slow evolution of the system of interest and the fast evolution of the bath of additional variables. In nuclear magnetic resonance, for example, Redfield relaxation theory relies on such a separation of time-scales to treat the coupling between nuclear-spin degrees of freedom and atomic motion [16].

For spin diffusion, a separation of time-scales can exist between the slow transfer of polarisation and the much faster dynamics of multi-spin correlations. These correlations can then be considered as a bath, and such a picture leads to a master-equation for the polarisations [30–32]. In general, however, both the polarisations and multi-spin correlations evolve on comparable time-scales.

In this chapter, we give a brief overview of the projection-operator method, which is a possible approach to describe the time evolution of a system of interest coupled to a bath [143, 144]. We then show how this method can be used to derive expressions of spin diffusion rate constants, for polarisation transfer among weakly coupled S spins in the presence of strongly coupled I spins. No new results are introduced, but a single consistent framework is provided to discuss existing analyses, such as the one exploited in chapter 3, and to introduce alternative models. All derivations are given here using a Liouville-space formalism [54, 143, 144], which we briefly summarise. Although the consequences are mostly notational in this chapter, the Liouville-space formalism is an integral part of the methods introduced in subsequent chapters.

4.2 System and evolution

For a given system, a Liouville space can be defined by considering operators in Hilbert space as vectors in Liouville space. Operators that act on Liouville-space vectors are usually called "superoperators", and the term "operator" then refers to a vector in Liouville space.

The density matrix σ that describes the system is a vector in Liouville space, and the time evolution of the density matrix is governed by the Liouville-von Neumann equation of motion:

$$\frac{d}{dt}|\sigma\rangle = \hat{L}|\sigma\rangle, \tag{4.1}$$

where $\hat{L}$ is the Liouvillian, defined here as the superoperator that describes a commutator with the Hamiltonian H in Hilbert space:

$$\hat{L}|\sigma\rangle = |-i[H,\sigma]\rangle. \tag{4.2}$$

The Liouvillian can in general also include a relaxation superoperator, but only coherent contributions to the time evolution will be considered here.

A formal solution of the equation of motion can be written by introducing the propagator $\hat{U}(t,0)$ defined by the relationship

$$\frac{d}{dt}\hat{U}(t,0) = \hat{L}(t)\hat{U}(t,0). \tag{4.3}$$

The propagator can formally be written

$$\hat{U}(t,0) = \hat{\hat{T}}\exp\left(\int_0^t \hat{L}(t')dt'\right), \tag{4.4}$$

where $\hat{\hat{T}}$ is the time-ordering operator. It should be noted that in the following, the time-dependence of the density matrix and of superoperators will not always be made explicit.

The scalar product between two operators A and B is defined in Liouville space as

$$\langle A|B\rangle = \mathrm{Tr}(A^\dagger B). \tag{4.5}$$

The expectation value of a physical observable Q is then given by

$$\langle Q\rangle = \langle Q|\sigma\rangle. \tag{4.6}$$

In the following, we will frequently consider the expectation value of an observable Q after an evolution during t under the effect of a Liouvillian L for an initial density matrix $\sigma_0 = \sigma(0)$, which is given by:

$$\langle Q\rangle(t) = \langle Q|\hat{U}(t,0)|\sigma_0\rangle. \tag{4.7}$$

4.3 Projection operators and memory functions

4.3.1 Reformulation of the equation of motion

There are many situations in which only a small number of observables are of interest to the experimentalist. It is then pertinent to derive an equation of motion that involves only a restricted set of variables. The projection-operator method is a possible approach to the derivation of such an equation, which involves a reformulation of the Liouville-von Neumann equation in a form that is amenable to the development of approximate models [143, 144].

The time-derivative of the expectation value of an observable can be written

$$\frac{d}{dt}\langle Q\rangle = \langle Q|\hat{L}|\sigma\rangle. \tag{4.8}$$

In order to derive a set of equations that involve the expectation values of a selection of operators of interest Q_i, the description of the system is separated into two contributions, that of the operators of interest and that of the rest of Liouville space. A projection superoperator on the operators of interest is defined as

$$\hat{P} = \sum_i \frac{|Q_i\rangle\langle Q_i|}{\langle Q_i|Q_i\rangle}. \tag{4.9}$$

The density matrix can then be written:

$$|\sigma\rangle = \hat{P}|\sigma\rangle + (\hat{1}-\hat{P})|\sigma\rangle. \tag{4.10}$$

With such a decomposition, Eq. 4.8 becomes

$$\frac{d}{dt}\langle Q_i\rangle = \langle Q_i|\hat{L}\hat{P}|\sigma\rangle + \langle Q_i|\hat{L}(\hat{1}-\hat{P})|\sigma\rangle. \tag{4.11}$$

As explained in Ref. [143, 144], after introducing a formal expression of $(\hat{1}-\hat{P})|\sigma\rangle$ the following equation is obtained

$$\frac{d}{dt}\langle Q_i\rangle(t) = K + L + M, \tag{4.12}$$

where

$$K = \sum_{j=1}^{m} \frac{\langle Q_i|\hat{L}(t)|Q_j\rangle}{\langle Q_j|Q_j\rangle}\langle Q_j\rangle(t); \tag{4.13}$$

$$L = \langle Q_i|\hat{L}(t)\hat{S}(t,0)(\hat{1}-\hat{P})|\sigma_0\rangle; \tag{4.14}$$

$$M = \sum_{j=1}^{m}\int_0^t dt' \frac{\langle Q_i|\hat{L}(t)\hat{S}(t,t')(\hat{1}-\hat{P})\hat{L}(t')|Q_j\rangle}{\langle Q_j|Q_j\rangle}\langle Q_j\rangle(t), \tag{4.15}$$

and

$$\hat{S}(t,t') = \hat{\hat{T}}\exp\left(\int_{t'}^{t}(\hat{1}-\hat{P})\hat{L}(t'')dt''\right). \tag{4.16}$$

In Eq. 4.12, the term K describes the dynamics within the set of operators of interest, and the term M describes the effect of the discarded operators on the operators of interest. In most experimental situations, the initial state is prepared as a combination of operators of interest, and the term L is zero. Equation Eq. 4.12 is still fully general and is of little practical use as such. It does provide, however, a convenient framework to develop approximate descriptions.

4.3.2 Master-equation in the short correlation time limit

The projection-operator method is notably appropriate when a separation of timescales exists between the slow evolution of the variables of interest and the fast evolution of the discarded variables. As explained in Refs [143, 144], it is in most cases possible to assume that the operators of interest satisfy

$$[Q_i, Q_j] = 0, \tag{4.17}$$

and that the initial density matrix is prepared as a combination of operators of interest only

$$(\hat{1} - \hat{P})|\sigma_0\rangle = 0. \tag{4.18}$$

Under these assumptions, only the term M in Eq. 4.12 is non-zero and the equation becomes

$$\frac{d}{dt}\langle Q_i\rangle(t) = \sum_{j=1}^{m} \int_0^t dt' K_{ij}(t,t')\langle Q_j\rangle(t), \tag{4.19}$$

where the memory functions $K_{ij}(t,t')$ have been introduced:

$$K_{ij}(t,t') = \frac{\langle Q_i|\hat{L}(t)\hat{S}(t,t')(\hat{1}-\hat{P})\hat{L}(t')|Q_j\rangle}{\langle Q_j|Q_j\rangle}. \tag{4.20}$$

Memory functions involve the dynamics of discarded variables; they often only depend, exactly or within a reasonable approximation, on the time difference $\tau = t - t'$. If the memory functions decay as τ increases and the relevant correlation time τ_c that is very small compared to the timescale on which the variables of interest evolve, a simple master equation is obtained for the variables of interest:

$$\frac{d}{dt}\langle Q_i\rangle(t) = \sum_{j=1}^{m} k_{ij}\langle Q_j\rangle(t), \tag{4.21}$$

where

$$k_{ij} = \int_0^\infty d\tau K_{ij}(\tau). \tag{4.22}$$

The memory functions and the resulting rate constants k_{ij} are in general impossible to calculate exactly, because they involve the very large set of discarded operators. Once a master-equation has been derived, empirical expression of the rate constants or approximate expressions of the memory functions are thus in general employed.

4.4 Application to proton-driven spin diffusion

4.4.1 Interactions

The projection-operator method can be used to derive a master equation for the description of polarisation transfer among weakly coupled S spins in the presence of strongly coupled I spins. The relevant interactions are recalled here before deriving expressions for the spin diffusion rate constants. For a system of S and I spins the Liouvillian can be written

$$\hat{L} = \hat{L}^{SS} + \hat{L}^{SI} + \hat{L}^{II} + \hat{L}^{S}, \tag{4.23}$$

where $\hat{L}^{AB}$ is the dipolar interaction between spins A and B and $\hat{L}^{A}$ is the chemical-shift interaction for spins A. Spins one-half are considered here, and it is assumed that the chemical-shift interaction for I spins is negligible compared to the homonuclear dipolar interaction $\hat{L}^{II}$. These assumptions correspond notably to the case of spin diffusion among carbons made possible by surrounding protons.

For a system of S spins, the high-field secular homonuclear dipolar interaction can be written

$$H^{SS} = \sum_{i>j} \omega_{ij} \left(2S_{iz}S_{jz} - \frac{1}{2}\left(S_{i+}S_{j-} + S_{i-}S_{j+}\right)\right), \tag{4.24}$$

where

$$\omega_{ij} = -\frac{\mu_0 \gamma_S^2 \hbar}{4\pi r_{ij}^3} \frac{1}{2}\left(3\cos^2\theta_{ij} - 1\right) \tag{4.25}$$

is the dipolar coupling between i and j in the laboratory frame; r_{ij} is the internuclear distance, and θ_{ij} is the angle between the internuclear vector and the static magnetic field. For a heteronuclear pair, the "flip-flop" term is non secular and the high-field secular heteronuclear dipolar Hamiltonian is thus

$$H^{SI} = \sum_i \sum_u \omega_{iu} 2S_{iz}I_{uz}. \tag{4.26}$$

For a system under magic angle spinning, the Liouvillian is time dependent and the dipolar coupling in the laboratory frame can be written

$$\omega_{ij}(t) = \omega_{ij}^P \sum_m A_m e^{im\omega_r t}, \tag{4.27}$$

where

$$\omega_{ij}^P = -\frac{\mu_0 \gamma_S^2 \hbar}{4\pi r_{ij}^3} \tag{4.28}$$

is the dipolar coupling in the principal axis frame. The coefficient A_m can be expressed with Wigner rotation matrices, as explained for example in Ref. [12]

$$A_m = D_{0-m}^{(2)}(\Omega_{PR}) d_{-m0}^{(2)}(\theta_m); \tag{4.29}$$

Ω_{PR} is the set of Euler angles that relates the principal axis frame P to the rotor frame R, and $\theta_m = \cos^{-1}(1/\sqrt{3})$ is the magic angle.

4.4.2 Existence and expression of rate constants

4.4.2.1 General expression

If the homonuclear dipolar interaction between S spins is much smaller than the other interactions, the evolution of the carbon polarisations occurs on a long time scale, while multi-spin correlations evolve on a shorter time-scale. The projection-operator method can then be applied in the short correlation time limit to derive a master equation for the polarisations S_{iz}

$$\frac{d}{dt}\langle S_{iz}\rangle(t) = \sum_{j=1}^{m} k_{ij}\langle S_{jz}\rangle(t), \tag{4.30}$$

where

$$k_{ij} = \int_0^\infty d\tau \frac{\langle S_{iz}|\hat{L}(t)\hat{S}(t,t-\tau)(\hat{1}-\hat{P})\hat{L}(t-\tau)|S_{jz}\rangle}{\langle S_{jz}|S_{jz}\rangle}. \tag{4.31}$$

The total Liouvillian can be separated into two contributions

$$\hat{L} = \hat{L}_1 + \hat{L}_0, \tag{4.32}$$

where

$$\hat{L}_1 = \hat{L}^{SS} \tag{4.33}$$

governs the slow dynamics of the polarisations and

$$\hat{L}_0 = \hat{L}^{SI} + \hat{L}^{II} + \hat{L}^{I} \tag{4.34}$$

governs the fast dynamics of the multi-spin correlations. As the evolution caused by $\hat{L}_1$ is slow, the expression for the rate constant becomes

$$k_{ij} = \frac{1}{\|S_{jz}\|^2}\int_0^\infty \langle S_{iz}|\hat{L}_1(t)\hat{U}_0(t,t-\tau)\hat{L}_1(t-\tau)|S_{jz}\rangle d\tau, \tag{4.35}$$

where

$$\hat{U}_0(t,t-\tau) = \hat{\hat{T}}\exp\left(\int_{t-\tau}^{t}\hat{L}_0(t)dt\right), \tag{4.36}$$

and where the relationships $\hat{L}|S_{iz}\rangle = \hat{L}_1|S_{iz}\rangle$ and $\langle S_{iz}|\hat{L}_1|S_{jz}\rangle = 0$, valid for any pair of S spins (i,j), have been taken into account.

4.4.2.2 Time-independent interaction

For a time-independent Liouvillian, the expression for the rate constant becomes:

$$k_{ij} = \frac{1}{\|S_{jz}\|^2}\int_0^\infty \langle S_{iz}|\hat{L}_1\hat{U}_0(\tau,0)\hat{L}_1|S_{jz}\rangle d\tau. \tag{4.37}$$

Considering the relationship:

$$\hat{L}_1 S_{iz} = -i\sum_{j\neq i}\omega_{ji}\frac{1}{2}\left(S_{i+}S_{j-} - S_{i-}S_{j+}\right), \tag{4.38}$$

the rate constant can be written

$$k_{ij} = \frac{1}{2}\omega_{ij}^2 \frac{1}{\|S_{Y,ij}\|^2} \int_0^\infty \langle S_{Y,ij}|\hat{U}_0(\tau,0)|S_{Y,ij}\rangle d\tau. \tag{4.39}$$

where the two-S zero-quantum transverse coherence $S_{Y,ij} = S_{i+}S_{j-} - S_{i-}S_{j+}$ has been introduced.

Introducing the zero-quantum lineshape

$$G_{ij}(\nu) = \frac{1}{\|S_{Y,ij}\|^2} \int_0^\infty \langle S_{Y,ij}|\hat{U}_0(\tau,0)|S_{Y,ij}\rangle e^{2i\pi\nu\tau} d\tau, \tag{4.40}$$

which is the Fourier transform of the free-induction decay of a two-S zero-quantum transverse coherence under the action of the SS and SI dipolar interaction and of the S chemical-shift interaction, the rate constant becomes:

$$k_{ij} = \frac{1}{2}\omega_{ij}^2 G_{ij}(0). \tag{4.41}$$

This expression for the rate constant, which is applicable to proton-driven spin diffusion in static solids, has been derived by several groups [30–32]. Several approaches were employed for the derivation, and Suter and Ernst for example used second-order perturbation theory [30], while Henrichs *et al.* employed the projection-operator method [31].

4.4.2.3 Periodic interaction

For a system under magic-angle spinning, the interactions are time-dependent and the expression for the rate constant becomes:

$$\begin{aligned} k_{ij} &= \frac{1}{2}\left(\omega_{ij}^P\right)^2 \\ &\times \sum_{m,m'} A_m A_{m'} \frac{1}{\|S_{jz}\|^2} \int_0^\infty \langle S_{Y,ij}|\hat{U}_0(t,t-\tau)|S_{Y,ij}\rangle e^{i(m+m')\omega_r t} e^{-2i\pi m\nu_r\tau} d\tau. \end{aligned} \tag{4.42}$$

At this stage, an approximation is made by assuming that the rate constant is time-independent. This approximation consists of assuming that the time-periodic contributions to the rate constant are negligible, and that the propagator $\hat{U}_0(t,t-\tau)$ depends negligibly on t. Under these assumptions the expression of the rate constant is

$$k_{ij} = \frac{1}{2}\left(\omega_{ij}^P\right)^2 \sum_m A_m A_{-m} \frac{1}{\|S_{jz}\|^2} \int_0^\infty \langle S_{Y,ij}|\hat{U}_0(\tau,0)|S_{Y,ij}\rangle e^{-2i\pi m\nu_r\tau} d\tau. \tag{4.43}$$

Introducing the zero-quantum lineshape defined in Eq. 4.40:

$$k_{ij} = \frac{1}{2}\left(\omega_{ij}^P\right)^2 \left(A_1 A_{-1}\left(G_{ij}(\nu_r) + G_{ij}(-\nu_r)\right) + A_2 A_{-2}\left(G_{ij}(2\nu_r) + G_{ij}(-2\nu_r)\right)\right). \tag{4.44}$$

In order to describe polarisation transfer in a polycrystalline sample, an approximation is made by assuming that a single rate constant can be defined and obtained as an average

over all orientations. In addition, the coefficients $A_m A_{-m}$ and the zero-quantum lineshape are averaged separately. If these approximations were valid, the rate constant would be:

$$k_{ij} = \frac{1}{30}\left(\omega_{ij}^{P}\right)^2 \left(\left(\overline{G}_{ij}(\nu_r) + \overline{G}_{ij}(-\nu_r)\right) + \frac{1}{2}\left(\overline{G}_{ij}(2\nu_r) + \overline{G}_{ij}(-2\nu_r)\right) \right), \tag{4.45}$$

where $\overline{G}_{ij}$ is the powder-averaged zero-quantum lineshape for the spin pair ij. Equation 4.45 has been derived by Kubo and McDowell with a related approach [33]. A final simplification is possible by taking into account the symmetry of the zero-quantum lineshape:

$$k_{ij} = \frac{1}{15}\left(\omega_{ij}^{P}\right)^2 \Re\left[\overline{G}_{ij}(\nu_r) + \frac{1}{2}\overline{G}_{ij}(2\nu_r)\right]. \tag{4.46}$$

4.4.3 Simulation of lineshapes

4.4.3.1 Motivation

The projection-operator method in the short correlation time limit provides a justification for the use of a master equation to describe proton-driven spin diffusion, and a formal expression for the spin diffusion rate constants. However, the zero-quantum lineshapes, which capture the contribution of the bath of protons to the transfer of polarisations among carbons, in general do not have a known analytical form. A possibility to address this problem is to assume a simple analytical form that involves a small number of empirical parameters. In chapter 3 of this thesis, we have developed a parameter-free description that relies on numerical simulations of the zero-quantum lineshapes. These simulations, which can also be seen as explicit calculations of memory functions for a bath of multi-spin correlations, involve further simplifications that are described here.

4.4.3.2 Implementation

Several properties of the zero-quantum lineshapes can be exploited in the calculation of polarisation-transfer rate constants from first principles. As the coherence order is conserved for each S spin individually for an evolution governed by $\hat{L}_0$, Eq. 4.40 can also be written

$$G_{ij}(\nu) = \frac{1}{\|I_{i+}I_{j-}\|^2}\int_0^\infty \Re\left[\langle I_{i+}I_{j-}|\hat{U}_0(t,0)|I_{i+}I_{j-}\rangle\right] e^{2i\pi\nu t}dt, \tag{4.47}$$

If the system can be divided into groups consisting of a single S spin and a number of surrounding I spins, such that the interactions between groups are negligible, the Liouvillian $\hat{L}_0$ can be approximated as

$$\hat{L}_0 \simeq \sum_{i=1}^{N_S} \hat{L}_{0,i}, \tag{4.48}$$

where each $\hat{L}_{0,i}$ describes the interactions within a given group. The free-induction decay of a zero-quantum coherence can then be written as the product of the free-induction decay of single-quantum coherences

$$\langle I_{i+}I_{j-}|\hat{U}_0(t,0)|I_{i+}I_{j-}\rangle = \langle I_{i+}|\hat{U}_{0,i}(t,0)|I_{i+}\rangle\langle I_{j-}|\hat{U}_{0,j}(t,0)|I_{j-}\rangle, \tag{4.49}$$

where

$$\hat{U}_{0,i}(t,0) = \hat{\hat{T}}\exp\left(\int_0^t \hat{L}_{0,i}(t')dt'\right). \tag{4.50}$$

The zero-quantum lineshape is then equal to the convolution of two single-quantum lineshapes. Although the assumption of non-interacting groups of I spins was not always justified, such an approximation was made in chapter 3 to simulate zero-quantum lineshapes.

It can also be noted that, as the chemical-shift interaction for the S spins commutes with the SI and II dipolar interaction, its action can be calculated as

$$\langle I_{i+}I_{j-}|\hat{U}_0(t,0)|I_{i+}I_{j-}\rangle = \exp\left(-i(\omega_i+\omega_j)t\right)\langle I_{i+}I_{j-}|\hat{U}_{II,SI}(t,0)|I_{i+}I_{j-}\rangle. \tag{4.51}$$

where

$$\hat{U}_{II,SI}(t,0) = \hat{\hat{T}}\exp\left(\int_0^t \left(\hat{L}_{II}(t')+\hat{L}_{SI}(t')\right)dt'\right), \tag{4.52}$$

and where only isotropic chemical shifts have been taken into account. Numerical simulations of single-quantum free-induction decays thus do not have to include chemical-shift evolution. In practice, the quantities were thus calculated:

$$\langle I_{i+}|\hat{U}_{II,SI}(t,0)|I_{i+}\rangle. \tag{4.53}$$

4.5 Conclusions

The Liouville-space formalism and the projection-operator method have been outlined and used to derive a master equation for proton-driven spin diffusion. In this framework, numerical simulations of zero-quantum lineshapes, such as the ones employed in chapter 3, can be seen as explicit calculations of memory functions for a bath of multi-spin correlations. However, the separation of time-scales on which the master-equation approach relies does not always exist. In particular, a separation of time-scales is not expected for spin diffusion among strongly coupled spins. This limitation provides a motivation for the development of alternative models, which can be cast in a similar framework, as will be shown in the following chapters.

Chapter 5

Numerical simulation from low-order correlations in Liouville space

5.1 Introduction

Numerical simulations play a significant role in the understanding and development of magnetic resonance experiments [139–141, 145, 146], as they can provide access to the structural and dynamical properties of a large variety of systems, as well as insight into the underlying spin dynamics [4, 54]. In solid-state NMR spectroscopy, the dynamics of the observables are dominated by coherent interactions, and the ability to understand and manipulate these interactions is of central importance. Simulations based on numerical integration of the Liouville-von-Neumann equation are therefore appropriate in this context, and they today routinely complement or even replace analytical treatments. In many cases, relatively small spin systems are sufficient to characterise the parameter space of a pulse sequence, and, for example, to identify the regime in which it is expected to perform best. Such simulations are limited, even with highly optimised algorithms [141, 147] and methods exploiting translational symmetry [148], to systems of about fifteen spins, due to the exponential scaling of the size of the spin space. Solid-state simulation programs usually give an explicit description of all coherent evolution occurring in the spin space, and such a description is currently out of reach for large spin systems.

In the course of solid-state NMR experiments, correlations can build up within extended networks of strongly coupled spins [149–152], and the simulation of large nuclear spin systems is thus a key objective. In organic solids, the dipolar interaction with and among protons in general dominates the spin dynamics; describing large systems is thus relevant not only for proton experiments, but also for experiments involving rare nuclei of lower magnetogyric ratio, such as carbon-13. In order to capture the dynamics of dipolar-coupled systems, simplified models of the spin systems and of the interactions have been developed [30, 47, 142, 153–157] and used, for example, to understand ^{1}H [142] or ^{13}C [155] lineshapes under magic-angle spinning. Such models either sacrifice structural information or else rely on an incoherent description of the spin dynamics, and they usually require the use of empirical parameters. These limitations are particularly

relevant in the case of structural studies of organic solids, where a coherent description of relatively small spin systems cannot reproduce experimental measurements quantitatively on the full experimental timescale [37, 88, 158].

An alternative approach to approximating the coherent dynamics of large spin systems is to exclude a portion of the full Liouville space from the simulation. NMR simulation using a reduced Liouville space was first introduced in solids by Brüschweiler and Ernst, who used a "cogwheel" model of spin motion in a solid to simulate the short-term dynamics of a chain of 10 spins [159]. In solution-state magnetic resonance, Kuprov and coworkers have developed efficient strategies to identify and remove negligibly populated spin states [160–164], and have used these strategies for applications in biomolecular NMR [165] and spin chemistry [160]. In their scheme, small clusters of nearest-neighbor spins are defined, and spin i interacts directly with spin j in the simulation only if the two spins belong to the same cluster. However, in the case where each spin is strongly coupled to many other spins, e.g., a strongly coupled lattice of protons in a solid, the applicability of this approach has not been established.

The number of spins that can be simulated, either in full or reduced Liouville spaces, depends critically on the scheme used to numerically integrate the equations of motion. Commonly-used NMR simulation programs depend on a variety of numerical schemes; while diagonalisation and exponentiation of the Hamiltonian provides an intuitive and reliable approach [139], other methods have been shown to perform significantly better in many cases [141, 147, 148]. Current methods of implementing any of these numerical schemes require that the Hamiltonian or the Liouvillian of the system be stored in the computer memory, along with one or more propagators, or at least their non-zero elements. Memory requirements are commonly dominated by the need to store such evolution matrices. Alternative numerical approaches exists, in which the memory requirement scales as the vector describing the spin state, rather than the evolution matrices that act on that vector. They have notably been explored in the closely related field of quantum computing [166], in particular to simulate the decoherence process [167].

In this chapter, we introduce a method of simulating large, densely coupled nuclear spin systems in a reduced Liouville space. First, we make a case for Liouville-space reduction in solids, and discuss the design of reduced Liouville spaces for an evolution governed by the dipolar interaction. The resulting model, which we call LCL, describes the time evolution of experimental observables from low-order correlations in Liouville space. Then, we describe a numerical scheme based on the Suzuki-Trotter algorithm [168], which allows for high-order numerical accuracy without requiring storage of a large evolution matrix. Finally, we show that our approach can be used to simulate the coherent dynamics of a powdered sample under magic-angle spinning for over 100 nuclear spins.

5.2 Theory

5.2.1 Motivation

Simulation of the full Liouville space for large, densely coupled spin systems is hindered by the requirement to take into account explicitly all possible multi-spin correlations that can develop during the course of a process of interest. In general, however, only a small fraction of Liouville space is observed experimentally; in most solid-state NMR experiments, only single-spin and few-spin coherences are observed. Accurate description of a fraction of Liouville space only is in itself a goal of significant interest, for which no general approach exists.

Several methods have been developed to describe the time-evolution of a limited set of variables of interest, when their evolution occurs on a time-scale much shorter than that on which additional variables evolve. For densely coupled nuclear spin systems, no such separation of time-scales exists between the evolution of experimental observables and that of the rest of Liouville space. There is a possibility, however, that a reduced Liouville space can nevertheless be found, so that an exact description of the reduced Liouville space associated with a simplified description of the rest of Liouville space makes it possible to capture the coherent dynamics of experimental observables, while keeping the total number of variables manageable.

There are reasons to expect the effect of high-order correlations on the evolution of experimental observables to be relatively simple in a number of situations. For example, in multiple-quantum NMR [151] phase interference among high-order coherences hinders the observation of their excitation, and special efforts have to be made to obtain multiple-quantum spectra [150]. For experiments performed with magic-angle spinning, there is an additional expectation that the region of Liouville space which effectively contributes to the time evolution of detected observables might shrink. For example, it has been shown that sample rotation at frequencies of the order of the highest couplings often allows analysis of sideband intensities using only two-spin coherences [169].

In the following, we explore the possibility to simulate polarisation transfer in a reduced Liouville space that includes only low-order correlations, an approach that we call LCL. The LCL model can be seen as a projection-operator method, where the operators of interest are extended to include a selection of low-order correlations. From this point of view, LCL exploits the fact that the "memory" of high-order correlations has in some cases a negligible effect on the evolution of experimental observables.

5.2.2 Picturing Liouville space for dipolar-coupled nuclear spins

The density matrix σ that describes a system of N nuclear spins $I = 1/2$ can be considered as a vector of dimension 2^{2N} in Liouville space [54], and can be expressed as a linear

combination of basis vectors B_r:

$$\sigma(t) = \sum_{r=1}^{2^{2N}} b_r(t) B_r. \tag{5.1}$$

Here we use a basis set consisting of products of single-spin operators [170]

$$B_r = 2^{q_r - 1} \prod_{i=1}^{N} I_{i,r}, \tag{5.2}$$

where

$$I_{i,r} \in \{E_i, I_{iz}, \frac{I_{i+}}{\sqrt{2}}, \frac{I_{i-}}{\sqrt{2}}\}. \tag{5.3}$$

The product is over all spins i, and q_r is the number of spins i for which the single-spin operator $I_{i,r}$ is not the identity operator E_i. For a given product operator B_r of the form given in Eq. 5.2, a spin order and a coherence order can be defined. The spin order is given by q_r, and can be seen as the number of spins that are correlated in the state B_r. The coherence order is $q_+ - q_-$, where q_+ (resp. q_-) is the number of raising operators $I_{i+}/\sqrt{2}$ (resp. lowering operators $I_{i-}/\sqrt{2}$) appearing in the product. Both quantities are useful in designing reduced Liouville spaces.

In the solid state, the spin dynamics for abundant nuclear spins $I = 1/2$ of high magnetogyric ratio, such as protons, are dominated by the dipolar interaction. For a system of N homonuclear spins the high-field secular dipolar Hamiltonian is

$$H^{II} = \sum_{i>j} -\frac{\mu_0 \gamma^2 \hbar}{4\pi r_{ij}^3} \frac{1}{2} (3\cos^2\theta_{ij} - 1)(2I_{iz}I_{jz} - \frac{1}{2}\left(I_{i+}I_{j-} + I_{i-}I_{j+}\right), \tag{5.4}$$

where the sum is over all pairs of nuclei (i, j), r_{ij} is the internuclear distance, and θ_{ij} is the angle between the internuclear vector and the static magnetic field. In the following, we will sometimes refer to the dipolar coupling between i and j in the laboratory frame, defined as

$$\omega_{ij} = -\frac{\mu_0 \gamma^2 \hbar}{4\pi r_{ij}^3} \frac{1}{2} (3\cos^2\theta_{ij} - 1). \tag{5.5}$$

The time evolution of the density matrix σ under the action of a Hamiltonian H is governed by the Liouville-von Neumann equation:

$$\frac{d\sigma}{dt} = \hat{L}|\sigma\rangle = |-i[H, \sigma]\rangle, \tag{5.6}$$

where $\hat{L}$ is the Liouvillian of the system. For strongly coupled systems, the dipolar interaction results in the growth of correlations among large numbers of spins. However, this growth occurs through well defined pathways, which can be determined by mapping the connectivity between coherences in Liouville space: the action of the dipolar Liouvillian on any product operator of the type described in Eq. 5.2 can be calculated using the relations given in Table 5.1. For example, the two-spin coherence $I_{1+}I_{2-}$ is connected to the

Table 5.1: Commutators of the homonuclear dipolar Hamiltonian $H_{ij}^{II} = \omega_{ij}\left(H_{ij}^{1} - \frac{1}{2}H_{ij}^{2}\right)$ and operators A, where $H_{ij}^{1} = 2I_{iz}I_{jz}$ and $H_{ij}^{2} = I_{i+}I_{j-} + I_{i-}I_{j+}$. Operators that commute with Hamiltonian H_{ij}^{II} are not shown.

A	$[H_{ij}^{1},A]$	$[H_{ij}^{2},A]$
I_{iz}	0	$-2\frac{I_{i+}}{\sqrt{2}}\frac{I_{j-}}{\sqrt{2}} + 2\frac{I_{i-}}{\sqrt{2}}\frac{I_{j+}}{\sqrt{2}}$
$\frac{I_{i+}}{\sqrt{2}}$	$2\frac{I_{i+}}{\sqrt{2}}I_{jz}$	$-2I_{iz}\frac{I_{j+}}{\sqrt{2}}$
$\frac{I_{i-}}{\sqrt{2}}$	$-2\frac{I_{i-}}{\sqrt{2}}I_{jz}$	$2I_{iz}\frac{I_{j-}}{\sqrt{2}}$
$2I_{iz}\frac{I_{j+}}{\sqrt{2}}$	$\frac{I_{j+}}{\sqrt{2}}$	$-\frac{I_{i+}}{\sqrt{2}}$
$2I_{iz}\frac{I_{j-}}{\sqrt{2}}$	$-\frac{I_{j-}}{\sqrt{2}}$	$\frac{I_{i-}}{\sqrt{2}}$
$2\frac{I_{i+}}{\sqrt{2}}\frac{I_{j-}}{\sqrt{2}}$	0	$I_{jz} - I_{iz}$

one-spin coherences I_{1z} and I_{2z} and to the three-spin coherences $2I_{iz}I_{1+}I_{2-}$, where i is any spin different from 1 and 2:

$$\begin{aligned} I_{1+}I_{2-} &\xrightarrow{H_{12}^{II}} I_{1z} - I_{2z} \\ I_{1+}I_{2-} &\xrightarrow{H_{i1}^{II},H_{i2}^{II}} 2I_{iz}I_{1+}I_{2-}. \end{aligned} \tag{5.7}$$

It can be noted that, as the coherence order is conserved during evolution under the secular Hamiltonian, and as the initial density matrix for polarisation-transfer processes has a coherence order of zero, the basis set can be rigourously restricted to product operators of coherence order zero, for the special case of polarisation transfer [54].

For simulations in reduced Liouville spaces, the central hypothesis is that not all correlations among spins in the system have to be taken into account to reproduce accurately the time evolution of observables of interest. The spin order provides a simple and reasonable criterion for selecting the set of product operators to be included in the reduced Liouville space, and we have used this criterion in choosing reduced spaces for simulations of spontaneous polarisation transfer. As illustrated in Fig. 5.1, the zero-quantum subspace for spins $I = 1/2$ can be pictured as successive layers that correspond to correlations among an increasing number of spins, i.e, to increasing spin orders; LCL simulations are carried out within a reduced space that consists of the minimum number of layers that enable an accurate simulation of the polarisations. Figure 5.1 is inspired by a picture previously introduced for multiple-quantum NMR [171], based on the notion of a walk in Liouville space. Such a picture has also been used to study the growth of multi-spin correlations in the NMR free-induction decay [172]. As will be shown in section 5.3, it is convenient to visualise the evolution in Liouville space as the motion of a collection of interconnected cog-wheels, as initially suggested by Brüschweiler and Ernst [159]. These cog-wheels are represented by circles in Fig. 5.1.

Although spin-space reduction in solids is explored here for dipolar-coupled nuclear

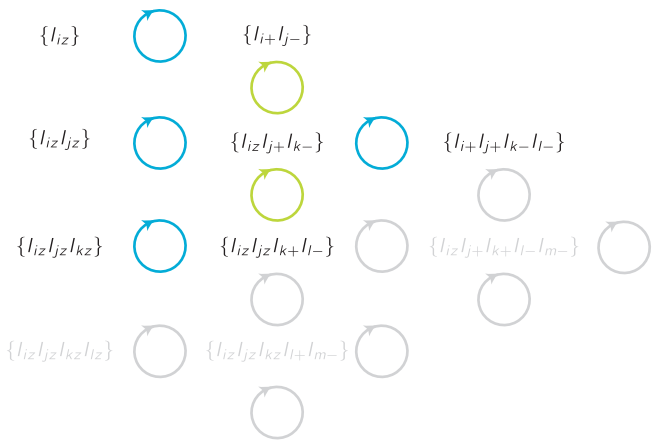

Figure 5.1: Schematic representation of the zero-quantum subspace for a homonuclear system of $I = 1/2$ spins. Groups of product operators are connected by the homonuclear dipolar interaction, and the cyclical evolution under the couplings is represented by circles. Green (resp. blue) circles correspond to the action of Hamiltonian H^1 (resp. H^2) defined in table 5.1. In a reduced Liouville space with $q_{\max} = 4$, product operators in grey are excluded.

spins $I = 1/2$, the same formalism can in principle be applied to spins $I > 1/2$ and other interactions.

5.2.3 Formal Liouville-space reduction

A reduced Liouville space X can be defined by excluding from the full Liouville space correlations among more than $q_{\max}$ spins. Such a reduction can formally be obtained by using a reduced Liouvillian $\hat{L}_X$ defined as

$$\hat{L}_X = \hat{P}_X \hat{L} \hat{P}_X, \tag{5.8}$$

where $\hat{P}_X$ is a projection operator for the the reduced Liouville space. Expressed in the product-operator basis set introduced above, $\hat{P}_X$ is a $2^{2N} \times 2^{2N}$ diagonal matrix that has 1 on the diagonal for basis operators that are kept in the reduced Liouville space, and 0 everywhere else. It can be noted that, within the reduced Liouville space, the time evolution of the system is still unitary, as the anti-Hermicity of the Liouvillian is preserved by the reduction process.

The size of a reduced Liouville space that excludes all coherences involving more than $q_{\max}$ spins, where $q_{\max}$ is small with respect to the number of spins, scales polynomially instead of exponentially with the number of spins. This key feature of LCL simulations is illustrated in Fig. 5.2 for the case of polarisation transfer in a homonuclear system of $I = 1/2$ spins. In combination with numerical methods described in section 5.3, this scaling property makes it possible to simulate a number of spins that is an order of magnitude larger than the number that can be handled by exact simulations.

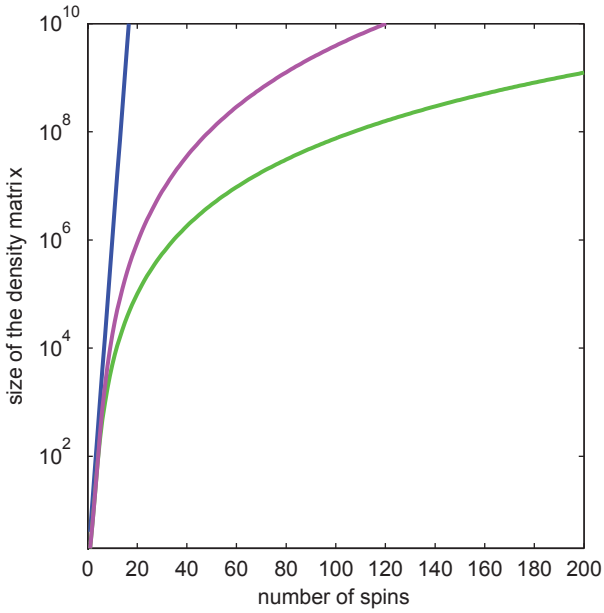

Figure 5.2: Scaling property of the density matrix for a simulation of polarisation transfer in a homonuclear system of $I = 1/2$ spins. The number of elements in the density matrix is shown for the full Liouville space (blue) and for reduced Liouville spaces that excludes all coherences involving more than $q_{\max} = 4$ (green) or $q_{\max} = 5$ spins (magenta).

5.2.4 Heteronuclear spin systems

Reduced spin spaces can also be appropriate to describe a heteronuclear spin system, when there is one or more group of densely coupled spins. Here we consider the case of a system of N_C carbons and N_H protons, for which it is convenient to expand the density matrix using the following product operators:

$$B_r = 2^{q_r - 1} \prod_{u=1}^{N_C} S_{u,r} \prod_{i=1}^{N_H} I_{i,r}, \tag{5.9}$$

where

$$\begin{aligned} S_{u,r} &\in \{E_u, S_{uz}, \frac{S_{u+}}{\sqrt{2}}, \frac{S_{u-}}{\sqrt{2}}\} \\ I_{i,r} &\in \{E_i, I_{iz}, \frac{I_{i+}}{\sqrt{2}}, \frac{I_{i-}}{\sqrt{2}}\}. \end{aligned} \tag{5.10}$$

Here the products are over all carbons u and all protons i, and q_r is the spin-order for the product operator B_r. Carbons and protons are chosen for illustrative purposes and can be replaced by any other group of abundant or rare spins.

The action of the homonuclear carbon-carbon and proton-proton dipolar Liouvillian on any product operator of the form given in Eq. 5.9 can be calculated using the relations

Table 5.2: Commutators of the heteronuclear dipolar Hamiltonian $H_{ui}^{SI} = 2\omega_{ui}S_{uz}I_{iz}$ and operators A. Operators that commute with Hamiltonian H_{ui}^{SI} are not shown.

A	$[H_{ui}^{l}, A]$
$\frac{S_{u+}}{\sqrt{2}}$	$2\frac{S_{u+}}{\sqrt{2}}I_{iz}$
$\frac{S_{u-}}{\sqrt{2}}$	$-2\frac{S_{u-}}{\sqrt{2}}I_{iz}$
$\frac{I_{i+}}{\sqrt{2}}$	$2S_{uz}\frac{I_{i+}}{\sqrt{2}}$
$\frac{I_{i-}}{\sqrt{2}}$	$-2S_{uz}\frac{I_{i-}}{\sqrt{2}}$
$2\frac{S_{u+}}{\sqrt{2}}I_{iz}$	$\frac{S_{u+}}{\sqrt{2}}$
$2\frac{S_{u-}}{\sqrt{2}}I_{iz}$	$-\frac{S_{u-}}{\sqrt{2}}$
$2S_{uz}\frac{I_{i+}}{\sqrt{2}}$	$\frac{I_{i+}}{\sqrt{2}}$
$2S_{uz}\frac{I_{i-}}{\sqrt{2}}$	$-\frac{I_{i-}}{\sqrt{2}}$

given in table 5.1. For the heteronuclear dipolar Liouvillian

$$H^{IS} = \sum_{u=1}^{N_C}\sum_{i=1}^{N_H} -\frac{\mu_0\gamma_C\gamma_H\hbar}{4\pi r_{ui}^3}\frac{1}{2}(3\cos^2\theta_{ui}-1)2S_{uz}I_{iz}, \tag{5.11}$$

the relations given in table 5.2 can be used.

A reduced Liouville space can be designed by excluding from the full Liouville space all correlations among more than $q_{\mathrm{C,max}}$ carbons or $q_{\mathrm{H,max}}$ protons. Again, it can be helpful to picture the connectivity among coherences due to the dipolar interaction, and an example is shown in Fig. 5.3.

5.3 Tourbillon: 100 nuclear spins and beyond

5.3.1 Numerical integration scheme

The density matrix σ after an evolution of duration τ under the action of the time-dependent Liouvillian $\hat{L}$ can formally be written as

$$\begin{aligned} |\sigma(\tau)\rangle &= \hat{U}(\tau,0)|\sigma(0)\rangle \\ &= \hat{\hat{T}}\exp\left(\int_0^\tau \hat{L}(t)dt\right)|\sigma(0)\rangle, \end{aligned} \tag{5.12}$$

where $\hat{U}(\tau,0) = \hat{\hat{T}}\exp\left(\int_0^\tau \hat{L}(t)dt\right)$ is the time-evolution operator, and where $\hat{\hat{T}}$ is the Dyson time-ordering operator. For time-dependent homonuclear dipolar interactions, the Liouvillian is dynamically homogeneous, i.e., it does not commute with itself at different times [173], and in general $\hat{U}(\tau,0)$ cannot be calculated analytically.

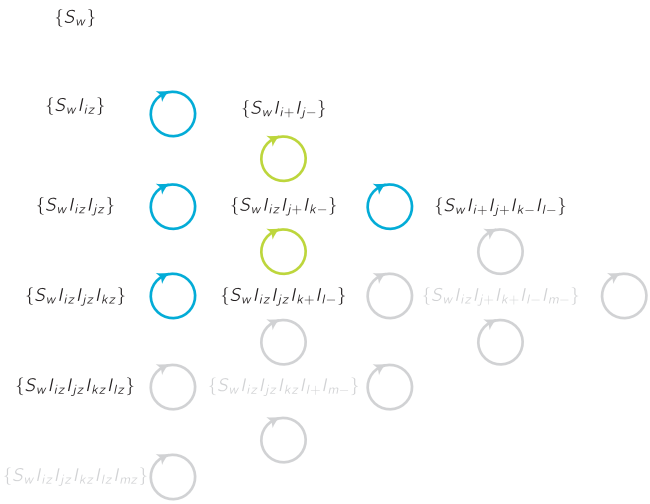

Figure 5.3: Schematic representation of part of the zero-quantum subspace for a heteronuclear system of $I = 1/2$ and $S = 1/2$ spins. Groups of product operators are connected by the homonuclear II dipolar interaction, and the cyclical evolution under the couplings is represented by circles. Green (resp. blue) circles correspond to the action of Hamiltonian H^1 (resp. H^2) defined in table 5.1. In a reduced Liouville space with $q_{I,\max} = 4$, product operators in grey are excluded. S_w represents any product operator involving only S single spin operators, and the effect of the SI and SS dipolar interactions are not shown.

A first approximation is made by considering that the Liouvillian is piecewise time-independent during steps of duration Δt. Under this approximation, the density matrix becomes:

$$|\sigma(\tau)\rangle \simeq \left(\prod_{p=0}^{P-1} \exp\left(\hat{L}(t_p)\Delta t\right) \right) |\sigma(0)\rangle, \tag{5.13}$$

where $\tau = P\Delta t$ and $t_p = p\Delta t$. The task then consists of calculating the product $|\sigma(t_p)\rangle = \exp(\hat{L}(t_{p-1})\Delta t)|\sigma(t_{p-1})\rangle$ for a time-independent $\hat{L}(t_{p-1})$ (in the rest of this section, the time-dependence of $\hat{L}$ will not be shown explicitly, and $\hat{L}$ is taken to represent the Liouvillian at a given time-step).

Various algorithms exist to calculate the propagator $\exp(\hat{L}\Delta t)$, which can be used to perform matrix-vector multiplications. An alternative is to calculate directly the density matrix $|\sigma'\rangle = \exp(\hat{L}\Delta t)|\sigma\rangle$ for a given $|\sigma\rangle$ without explicitly calculating the propagator. In choosing a numerical algorithm to implement the LCL scheme, we have considered efficient use of memory to be the top priority and have therefore selected a scheme which does not explicitly calculate the propagator. The motivation for this choice can be seen by considering the number of coherences included in an LCL simulation of 100 protons, using $q_{\max} = 4$. For a simulation of spin diffusion which has an initial state consisting of polarisation on certain spins, the number of basis elements needed for an LCL simulation is 7.6×10^7. If the coefficient of each of these is stored as an 8-byte double-length float, then the memory required to store the density matrix is about 600 MB. Since a given spin is coupled to all other spins through the dipolar interaction, the reduced Liouvillian

$\hat{L}_X$ contains many couplings between coherences, and the number of non-zero matrix elements is 2 to 3 orders of magnitude larger than the number of coherences.

For the Suzuki-Trotter (ST) algorithm [168], only a single copy of the density matrix has to be stored in computer memory, and no explicit storage is needed for a Liouvillian, a propagator, or an object of similar size such as an eigenvector matrix [166]. For this reason, we used the ST algorithm, although faster algorithms exist; it should be noted that such a choice is in general not compatible with methods that make full use of the time and γ-angle periodicity inherent to solid-state NMR simulations, and in particular with the COMPUTE family of algorithms [141, 174–176].

To apply the ST algorithm, the total Liouvillian $\hat{L}$ is written as a sum of terms $\hat{L} = \sum_{m=1}^{M} \hat{L}_m$, chosen such that the evolution under each $\hat{L}_m$ can be calculated analytically in small subspaces that are invariant under $\hat{L}_m$. The decomposition is in general not unique, and neither is the number of terms M in the decomposition. In the context of NMR, spin dynamics are often visualised and calculated as successive rotations in low-dimensional subspaces, so the ST algorithm can be applied in a natural way. In its simplest form, the ST algorithm is a first order (ST1) method where the rotations are implemented successively for each term in the decomposition of the Liouvillian:

$$\exp\left(\sum_{m=1}^{M} \hat{L}_i \Delta t\right) = \prod_{m=1}^{M} \exp\left(\hat{L}_m \Delta t\right) + O(\Delta t^2). \tag{5.14}$$

The ST1 scheme is identical to the use of the Zassenhaus formula suggested by Brüschweiler and Ernst in their cogwheel model [159]. The Suzuki-Trotter scheme, however, can be taken to higher orders by using an appropriately ordered sequence of rotations; for example, the second-order (ST2) propagator, which we use here, is given by:

$$\begin{aligned} \exp\left(\sum_{m=1}^{M} \hat{L}_m \Delta t\right) &= \prod_{m=1}^{M} \exp\left(\hat{L}_m \frac{\Delta t}{2}\right) \\ &\quad \times \prod_{m=M}^{1} \exp\left(\hat{L}_m \frac{\Delta t}{2}\right) \\ &\quad + O(\Delta t^3). \end{aligned} \tag{5.15}$$

For both ST1 and ST2, memory requirements and CPU requirements per timestep scale linearly with the number of elements in the density matrix. For polarisation transfer in a system of homonuclear spins $I = 1/2$, they are thus well described by the curves shown in Fig. 5.2. As the simulations are performed "directly" in the time domain, and as the accumulated error grows as $\tau(\Delta t)^k$ for a scheme of order k, the CPU requirements scale in principle as $\tau^{1+1/k}$ if the accumulated error is kept constant [166, 167].

It should be noted that there are other ways to propagate the density matrix without an explicit calculation of the propagator. Some of these methods require storing the Liouvillian, usually in sparse format, and some simply require a function that returns the product $\hat{L}|\sigma\rangle$ for a given $|\sigma\rangle$ [166]. Here we chose a method that only requires a single copy of the density matrix and that can nevertheless be taken to higher-order in a systematic manner.

In addition, when a product-operator basis set is used, only a few matrices of size 4×4 or smaller are needed to describe NMR interactions with the ST algorithm.

5.3.2 Rotation matrices

To implement the ST algorithm, it is first necessary to select an appropriate decomposition of the total Liouvillian. For the dipolar interaction various decompositions have been suggested [166], and here we use the pair decomposition

$$\hat{L} = \sum_{i>j} \hat{L}_{ij}, \tag{5.16}$$

where each term $\hat{L}_{ij}$ in the sum corresponds to the interaction between a pair of nuclear spins.

For each term $\hat{L}_{ij}$ in equation 5.16, the total Liouville space, described with the product-operator basis set introduced in section 5.2, can be decomposed into one-, two-, and four-dimensional subspaces, in which the progagator $\exp(\hat{L}_{ij}\Delta t)$ has a simple analytical expression. Moreover, the time evolution in these subspaces corresponds to the usual rotations among product operators, and the block-diagonal propagators can be expressed in terms of a small number of closed-form matrices. We will use the notation $\hat{R}(\theta)$ to represent these rotation matrices, where $\theta = \omega_{ij}\Delta t$ is the angle of rotation associated with the propagator $\exp(\hat{L}_{ij}\Delta t)$. Matrix elements for the various $\hat{R}(\theta)$ can be obtained using the commutators given in table 5.1 and a generalised sandwich formula [177],

$$\exp(\hat{L}\phi)|A\rangle = |A\rangle\cos(\phi) - i|B\rangle\sin(\phi), \tag{5.17}$$

which is valid for $|A\rangle$ and $|B\rangle$ such that $\hat{L}|A\rangle = -i|B\rangle$ and $\hat{L}|B\rangle = -i|A\rangle$.

5.3.2.1 Homonuclear dipolar interaction

For the secular dipolar interaction between two homonuclear spins i and j, any product operator of the basis set introduced in section 5.2 either is invariant under $\hat{L}_{ij}$ or belongs to a subspace of dimension 4 in which the time evolution is described by the following matrices:

$$\hat{R}_0(\theta) = \frac{1}{2}\begin{pmatrix} 1+\cos(\theta) & 1-\cos(\theta) & -i\sin(\theta) & i\sin(\theta) \\ 1-\cos(\theta) & 1+\cos(\theta) & i\sin(\theta) & -i\sin(\theta) \\ -i\sin(\theta) & i\sin(\theta) & 1+\cos(\theta) & 1-\cos(\theta) \\ i\sin(\theta) & -i\sin(\theta) & 1-\cos(\theta) & 1+\cos(\theta) \end{pmatrix} \tag{5.18}$$

in subspaces of the form $(I_{iz}B'_r, I_{jz}B'_r, 2\frac{I_{i+}}{\sqrt{2}}\frac{I_{j-}}{\sqrt{2}}B'_r, 2\frac{I_{i-}}{\sqrt{2}}\frac{I_{j+}}{\sqrt{2}}B'_r)$;

$$\hat{R}_+(\theta) = \tag{5.19}$$
$$\begin{pmatrix} \cos(\theta)\cos(\theta/2) & -\sin(\theta)\sin(\theta/2) & -i\sin(\theta)\cos(\theta/2) & -i\cos(\theta)\sin(\theta/2) \\ -\sin(\theta)\sin(\theta/2) & \cos(\theta)\cos(\theta/2) & -i\cos(\theta)\sin(\theta/2) & -i\sin(\theta)\cos(\theta/2) \\ -i\sin(\theta)\cos(\theta/2) & -i\cos(\theta)\sin(\theta/2) & \cos(\theta)\cos(\theta/2) & -\sin(\theta)\sin(\theta/2) \\ -i\cos(\theta)\sin(\theta/2) & -i\sin(\theta)\cos(\theta/2) & -\sin(\theta)\sin(\theta/2) & \cos(\theta)\cos(\theta/2) \end{pmatrix}$$

in subspaces of the form$(\frac{I_{i+}}{\sqrt{2}}B'_r, \frac{I_{j+}}{\sqrt{2}}B'_r, 2\frac{I_{i+}}{\sqrt{2}}I_{jz}B'_r, 2\frac{I_{j+}}{\sqrt{2}}I_{iz}B'_r)$;

$$\hat{R}_-(\theta) = \hat{R}^*_+(\theta) \tag{5.20}$$

in subspaces of the form $(\frac{I_{i-}}{\sqrt{2}}B'_r, \frac{I_{j-}}{\sqrt{2}}B'_r, 2\frac{I_{i-}}{\sqrt{2}}I_{jz}B'_r, 2\frac{I_{j-}}{\sqrt{2}}I_{iz}B'_r)$, where in each case B'_r represents a product operator involving neither spin i nor spin j.

5.3.2.2 Heteronuclear dipolar interaction

For the dipolar interaction between two heteronuclear spins i and j, only the longitudinal part of the dipolar interaction is secular, and subspaces of dimension 2 can be identified. The rotation matrices are:

$$\hat{R}'_+(\theta) = \begin{pmatrix} \cos(\theta) & -i\sin(\theta) \\ -i\sin(\theta) & \cos(\theta) \end{pmatrix} \tag{5.21}$$

in subspaces of the form $(\frac{S_{u+}}{\sqrt{2}}B'_r, 2\frac{S_{u+}}{\sqrt{2}}I_{iz}B'_r)$, and $(\frac{I_{i+}}{\sqrt{2}}B'_r, 2S_{uz}\frac{I_{i+}}{\sqrt{2}}B'_r)$;

$$\hat{R}'_-(\theta) = \hat{R}'^*_+(\theta) \tag{5.22}$$

in subspaces of the form $(\frac{S_{u-}}{\sqrt{2}}B'_r, 2\frac{S_{u-}}{\sqrt{2}}I_{iz}B'_r)$ and $(\frac{I_{i-}}{\sqrt{2}}B'_r, 2S_{uz}\frac{I_{i-}}{\sqrt{2}}B'_r)$, where in each case B'_r represents a product operator involving neither spin u nor spin j.

5.3.2.3 Chemical shift

The chemical-shift interaction can be taken into account by adding to the decomposition of the total Liouvillian a term $\sum_i \hat{L}_i$, where each term $\hat{L}_i$ corresponds to the chemical-shift Liouvillian for a given spin i. For the product-operator basis set used here, which involves single-spin shift operators, the action of the Liouvillian $\hat{L}_i$ consists of a change of phase for all shift operators that involve spin i. For example, the two spin coherence $I_{1+}I_{2-}$ evolves under the chemical-shift Liouvillian $\hat{L}_1$ according to

$$\exp(\hat{L}_1\Delta t)|I_{1+}I_{2-}\rangle = \exp(i\omega_1\Delta t)|I_{1+}I_{2-}\rangle, \tag{5.23}$$

where ω_1 is the precession frequency of spin 1 in the rotating frame.

5.3.3 Actual Liouville-space reduction

For the second-order Suzuki-Trotter scheme using the pair decomposition, the propagator can be written

$$\begin{aligned} \hat{U}(\Delta t) &= \left(\prod_{i=1}^{N}\prod_{j=1}^{i-1}\exp\left(\hat{L}_{ij}\frac{\Delta t}{2}\right)\right) \\ &\quad \times \left(\prod_{i=N}^{1}\prod_{j=i-1}^{1}\exp\left(\hat{L}_{ij}\frac{\Delta t}{2}\right)\right). \end{aligned} \tag{5.24}$$

This propagator is not calculated explicitly; instead, for each pair (i, j), the coefficients in the expansion of the density matrix are grouped in vectors of size 1, 2 or 4, and multiplied by appropriate rotation matrices.

For a simulation in a reduced Liouville space X, where the time evolution is governed by the reduced Liouvillian $\hat{L}_X$, the rotations are implemented only for coherences that belong to the reduced space.

5.3.4 Magic-angle spinning and powder averaging

As is usual in NMR simulations, spherical tensors are used to describe the spatial part of the dipolar interaction and its transformations. This topic has been discussed extensively before (see for example Ref. [178] and [140]) and will not be reviewed in detail here.

For a given pair of spins (i, j), the spatial part of the secular dipolar coupling expressed in the laboratory frame, ω_{ij}, is obtained by a series of rotations, starting with a rotation from the principal axis system of the interaction (P) to the crystal frame of reference (C), and then to the rotor frame (R), and finally to the laboratory frame (L). These rotations are described by the set of Euler angles Ω_{PC}^{ij}, Ω_{CR} and Ω_{RL}, respectively.

The crystal frame is the same for all spin pairs, and the set of Euler angles Ω_{CR} thus describes the orientation of the whole system with respect to the rotor. Powder-averaged quantities are obtained by running separate simulations for an ensemble of sets of angles $\{\Omega_{CR,p}\}$, where each angle set $\Omega_{CR,p}$ corresponds to a given crystallite, and then averaging the expectation values of the observables of interest over the ensemble of orientations. Note that this process is perfectly adapted for parallelisation.

For a system under magic-angle-spinning, the time-dependent coupling constants involved in the secular dipolar Hamiltonian (see Eq. 5.4) can be written

$$\omega_{ij}(t) = \sum_{m=-2}^{2} \sum_{m'=-2}^{2} \omega_{ij}^{P} \quad D_{0m}^{(2)}(\Omega_{PC}) D_{mm'}^{(2)}(\Omega_{CR}) \times \exp(im'\omega_r t)\, d_{m'0}^{(2)}(\theta_m) \tag{5.25}$$

where

$$\omega_{ij}^{P} = -\frac{\mu_0 \gamma_i \gamma_j \hbar}{4\pi r_{ij}^3} \tag{5.26}$$

is the dipolar coupling in the principal axis frame, $\theta_m = \cos^{-1}(1/\sqrt{3})$ is the magic angle, ω_r is the spinning frequency of the rotor, and the $D_{mm'}^{(l)}$ are Wigner rotation matrices. In our simulation, magic-angle spinning is taken into account by updating the laboratory-frame dipolar coupling $\omega_{ij}(t)$ at each step of the simulation.

We have explained in detail how LCL simulations of free evolution can be performed for powdered samples under magic-angle spinning, using an algorithm that involves minimal memory requirements. This approach has been implemented in a program which we call Tourbillon, a name chosen in reference to the cog-wheel model of Brüschweiler and Ernst [159].

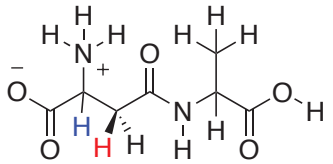

2

Figure 5.4: Chemical structure of β-L-aspartyl-L-alanine.

5.4 Accurate simulation of polarisation transfer in spinning powders

5.4.1 Comparison with exact simulations

In order to assess the applicability of the LCL model, exact simulations carried out with the software SPINEVOLUTION [141] on molecules containing up to 12 protons were compared with simulations performed in reduced Liouville spaces. Figure 5.5 illustrates typical results obtained for a single orientation of a static molecule containing 12 protons, β-L-aspartyl-L-alanine (**2**, see Fig. 5.4). The simulations using only low-order correlations in Liouville space reproduce the exact evolution for a very short initial time period, but after 100 μs, large errors develop in the simulations having $q_{\max} = 5$ (dashed curves), i.e., in the simulations for which product operators involving more than 5 correlated spins were excluded. The simulations performed in a further reduced space, $q_{\max} = 4$ (dotted curves), show pathological departure from the exact simulations (solid curves) as well as from the curves corresponding to $q_{\max} = 5$. Similar short-term accuracy was reported using a cogwheel model to propagate the density matrix in a reduced Liouville space which excluded product operators involving more than 3 correlated spins [159]. The error present in these LCL simulations shows that the excluded regions of Liouville space are relevant for simulations of a single static crystal. Although it may be possible to account for the effect of high-order correlations in a simplified manner, we explored here instead regimes in which it can be entirely neglected.

The accuracy of the LCL simulations is significantly improved by adding spinning to the simulation, as shown in Fig. 5.6. Whereas in the static case, agreement was obtained for about 50 μs, the agreement with exact simulations (solid curves) is preserved under 10 kHz MAS for longer time periods (around 250 μs), and the decay of the initial polarisation, although not reproduced exactly, is qualitatively correct for both $q_{\max} = 4$ (dotted curves) and $q_{\max} = 5$ (dashed curves). The accuracy of the LCL simulations is further improved by the combination of spinning and powder averaging, as shown in Fig. 5.7, in which the exact curves are now quantitatively reproduced using the LCL scheme for times up to 1000 μs, corresponding to the whole of the experimentally relevant timescale. The Liouville space that includes 4-spin correlations ($q_{\max} = 4$) is now sufficient to reproduce detailed features of the spin diffusion curves. Further Liouvilles-space reduction is detrimental, however, and simulations performed with $q_{\max} = 3$ only show a short-term

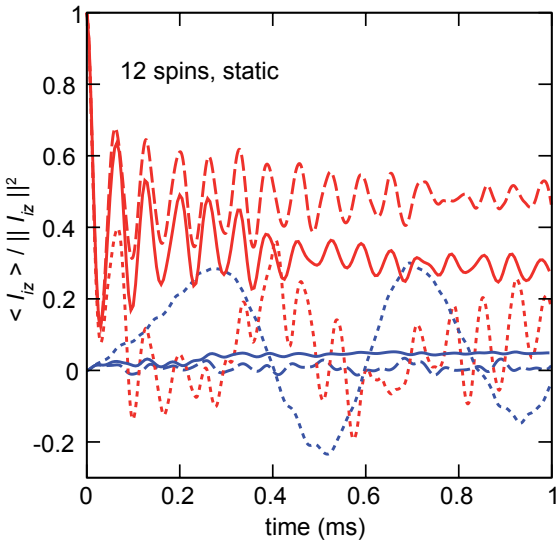

Figure 5.5: Simulations of polarisation transfer for a single molecule of β-L-aspartyl-L-alanine. Exact simulations (solid) of this system of 12 protons are compared to simulations performed in reduced Liouville spaces that exclude coherences involving more than $q_{\max} = 4$ spins (dotted) or $q_{\max} = 5$ spins (dashed). The initial density matrix is $\sigma(0) = I_{\mathrm{CH2},z}$, and the observables $\langle I_{\mathrm{CH2},z}\rangle$ (red) and $\langle I_{\mathrm{CHasp},z}\rangle$ (blue) are plotted. The colour code is shown in Fig. 5.4. Atomic coordinates for a single molecule are taken from a crystal structure (CSD entry: fumtem). The time step in the simulation is 1 μs.

agreement with exact simulations.

To validate the observations made for β-L-aspartyl-L-alanine, LCL simulations were compared with exact simulations performed for a collection of 25 10-proton organic molecules and 15 12-proton organic molecules randomly selected from the Cambridge Structural Database (CSD) [133]. The simulations were performed for systems under magic-angle spinning. For a system containing N protons, an exact powder-averaged simulation was performed for each of the N distinct initial states $\sigma(0) = I_{iz}$, and each of these simulations yielded N curves $\langle I_{iz}\rangle/||I_{1z}||^2$; i.e., a total of 4660 exact curves were compared against LCL curves. The full set of curves is available in the supplementary information of Ref. [48]. The error in the LCL simulations was characterised by calculating a root-mean square (rms) error for each curve, and the distribution of rms errors for the set of 10-proton curves and the set of 12-proton curves was found to be to be similar. Among the $q_{\max} = 4$ and $q_{\max} = 5$ curves, respectively, 78% and 95% had an rms error of 0.01 or less, as shown in Fig. 5.8.

These results support the hypothesis that for spinning organic powders, the dynamics of spin diffusion among protons can be accurately modelled using a small fraction of the full Liouville space. In the case of a 12-proton system, for instance, Table 5.3 shows that the dimension of the $q_{\max} = 4$ reduced Liouville space is less than 0.1% as large as that of the full Liouville space. An additional finding is that reduced Liouville spaces adequate for simulating these dynamics can be obtained simply by excluding all products of single-spin operators involving more than $q_{\max} = 4$ or $q_{\max} = 5$ correlated spins.

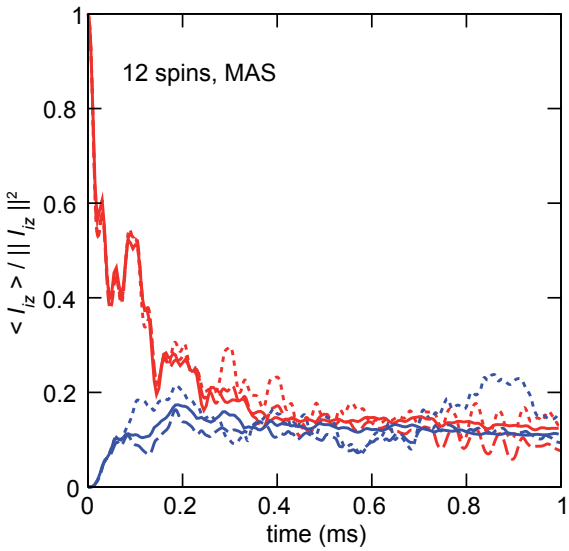

Figure 5.6: Simulations of polarisation transfer for a single molecule of β-L-aspartyl-L-alanine under 10 kHz MAS. Exact simulations (solid) of the 12-proton system are compared to simulations performed in reduced Liouville spaces that exclude coherences involving more than $q_{\max} = 4$ spins (dotted) or $q_{\max} = 5$ spins (dashed). The initial state, observables, atomic coordinates and time step are the same as in Fig. 5.5.

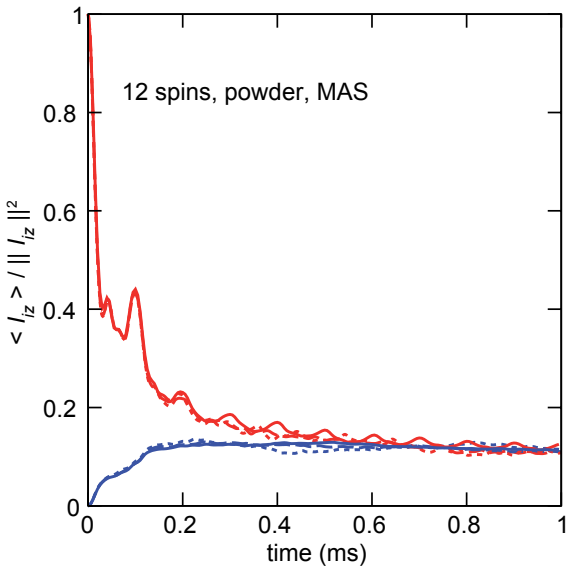

Figure 5.7: Powder-averaged simulations of polarisation transfer for a single molecule of β-L-aspartyl-L-alanine under 10 kHz MAS. Exact simulations (solid) of the 12-proton system are compared to simulations performed in reduced Liouville spaces that exclude coherences involving more than $q_{\max} = 4$ spins (dotted) or $q_{\max} = 5$ spins (dashed). The initial state, observables, atomic coordinates and time step are the same as in Fig 5.5, and a ZCW set of 50 orientations is used for the powder average.

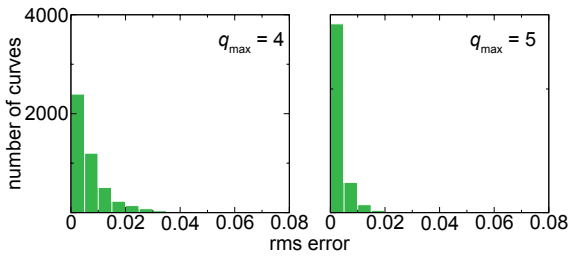

Figure 5.8: The rms error for 4660 polarisation curves obtained from 25 10-proton systems and 15 12-proton systems. For each curve, exact simulations were compared with simulations performed in reduced Liouville spaces that excluded coherences involving more than $q_{\max} = 4$ or $q_{\max} = 5$ spins.

Table 5.3: The dimensions of Liouville spaces that can be used for simulation of polarisation transfer within 10-proton and 12-proton systems. The full Liouville space includes all possible spin correlations among the N protons. Given an initial state defined by polarisations on certain protons, exact simulations of the evolution under a secular spin Hamiltonian can be performed with the zero-quantum subspace. The reduced Liouville spaces are subspaces of the zero-quantum subspace, formed by excluding product operators involving more than $q_{\max}$ correlated spins.

	Full Liouville space	Zero-quantum subspace	Reduced spaces $k = 4$	Reduced spaces $k = 5$
10 protons	1.0×10^6	1.8×10^5	5.0×10^3	1.8×10^4
12 protons	1.7×10^7	2.7×10^6	1.1×10^4	5.2×10^4

5.4.2 Large-scale simulation

A key feature of the LCL simulation scheme is that its favourable scaling properties allow simulation of large systems. As a demonstration, we have simulated powder-averaged spin diffusion curves for a spinning lattice of 144 protons, i.e., the twelve molecules contained in three primitive unit cells of β-L-aspartyl-L-alanine. We used a maximum spin order $q_{\max} = 4$, which will provide a sufficient accuracy to make comparisons with experimental data, while enabling efficient simulations for large numbers of spins. We note that Fig. 5.9 shows the expected qualitative similarity between the curves for the two systems, although quantitative differences are present. The full Liouville space for the 144-proton system has dimension 5×10^{86}, which makes the full density matrix impossible to simulate. The reduced Liouville space has dimension 3×10^8, and the LCL simulation for a single orientation used 1 GB of random-access memory and required only 8 hours of computing time on a single 2.8 GHz processor.

5.5 Conclusions

It has been found that exact powder-averaged simulations of polarisation transfer within spinning organic crystals can be quantitatively reproduced over the full experimentally

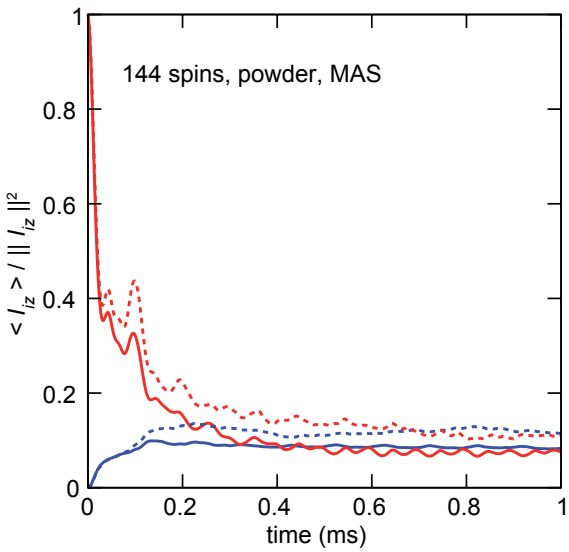

Figure 5.9: Powder-averaged simulations of polarisation transfer in a system of 144 protons (solid) and a system of 12 protons (dotted) under 10 kHz MAS. The simulations are performed in a reduced Liouville space that excludes coherences involving more than $q_{\max} = 4$ spins. The 12-proton system is a single molecule of β-L-aspartyl-L-alanine, while the 144-proton system is a rectangular block of three primitive unit cells of the same molecule. For the system of 144 spins, the minimum image convention [179] is used to define periodic boundary conditions, and the observables are summed over crystallographically equivalent spins. The initial density matrix is $\sigma(0) = I_{\mathrm{CH2},z}$, and the observables $\langle I_{\mathrm{CH2},z}\rangle$ (red) and $\langle I_{\mathrm{CHasp},z}\rangle$ (blue) are plotted. Atomic coordinates are taken from a crystal structure (CSD entry: fumtem). The time step in the simulation is 1 μs, and a ZCW set of 50 orientations is used for the powder average.

relevant timescale using reduced Liouville spaces that include only low-order correlations. The simulation model, which uses only low-order correlations in Liouville space, has been implemented by means of an algorithm that minimises memory requirements. Since the dimension of the reduced spaces scales polynomially rather than exponentially with the number of spins, simulations are feasible for over 100 nuclear spins. LCL simulations have been shown to be accurate under certain conditions, which are relevant for many solid-state NMR experiments, but empirical testing is still needed to determine the limits of this simulation method.

Chapter 6

Spin dynamics and thermodynamics in reduced Liouville spaces

6.1 Introduction

Numerical simulation based on the Liouville-von Neumann equation is used intensively in magnetic resonance to understand and control the behaviour of nuclear spins [139–141, 145, 146]. However, the size of the density matrix that describes a spin system increases exponentially with the number of spins, and such simulation is intrinsically limited to relatively small systems. As some processes cannot be described with only about a dozen spins, a strong incentive exists to develop alternative schemes that provide access to larger spin systems. Spin-space reduction has been introduced as a way to increase the capacity of spin simulation, ideally at no cost in terms of accuracy. For the sparsely coupled networks of spins found in solution, spin-space reduction schemes aim at identifying and removing regions in Liouville space that remain unpopulated throughout the simulation, and systematic approaches have been developed to reliably prune and propagate density matrices [160–163]. In solids, although the existence of densely coupled networks could seem to preclude attempts at reduction, simulations of polarisation transfer in reduced Liouville spaces have been found to be accurate for powdered systems under magic-angle spinning, a regime which is particularly relevant in solid-state NMR spectroscopy. The so-called LCL scheme is not always a valid approach, however, and in particular for a static solid it has been observed that an exact description of high-order correlations is in general needed to capture the dynamics of polarisation transfer [159]. The validity of the LCL approximation has been confirmed in a largely empirical way, by a comparison between exact and LCL simulations for a large set of systems. The lack of better understanding of Liouville-space reduction in solids prevents the use of a systematic approach to identify other situations in which reduced Liouville spaces could successfully describe the spin dynamics of large, strongly coupled systems.

The long-term behaviour of a closed quantum system can to some extent be studied computationally, and for systems of nuclear spins several authors have explored the numerical spin thermodynamics of polarisation transfer. In particular, the prediction of

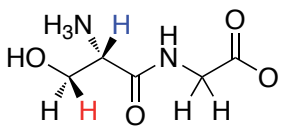

Figure 6.1: Chemical structure of a molecule of L-serylglycine

quasi-equilibrium states, and the possible manifestation of such states in actual experiments, have been considered for spin diffusion and cross-polarisation [38, 40, 41, 156, 180–182]. The concepts of spin thermodynamics in magnetic resonance have emerged well before the advent of intensive numerical simulations [183], and have notably been used to study double-resonance experiments [154]. For example, the existence of subtle quasi-equilibria has proved to be relevant for the understanding of the cross polarisation process [154]. Also, the existence of bounds for polarisation transfer in closed nuclear spin systems has been analysed by Sorensen and Levitt [177, 184–186]. There are still several open questions about the relationships between computational and experimental spin thermodynamics [40, 41], but the underlying formalisms can provide significant insight into a range of processes in magnetic resonance.

In this chapter, we describe an investigation into the dynamics and thermodynamics of spin systems described in reduced Liouville spaces. First, we consider the influence of magic-angle spinning and powder averaging on the accuracy of LCL simulations of polarisation transfer. Then, we illustrate the unusual nature of the approximation introduced by Liouville-space reduction in a spinning solid, by showing that the reduction scheme excludes coherences making a large contribution to the exact density matrix but a negligible net contribution to the evolution of experimental observables. Finally, we introduce an approach for numerical studies of quasi-equilibria in reduced Liouville spaces, which we use to characterise the long-term behaviour of LCL simulations.

6.2 Validity of Liouville-space reduction

6.2.1 Magic-angle spinning

The influence of magic-angle spinning on LCL simulations of polarisation transfer can be illustrated by a series of simulations for a system of strongly coupled protons. A comparison between powder-averaged exact and LCL simulations for a 10-spin system consisting of the protons of a molecule of L-serylglycine (see scheme in Fig. 6.1) is shown in Fig. 6.2. It can be seen that a progressive increase of the spinning frequency dramatically increases the time period during which the exact time evolution of the experimental observables is correctly reproduced by an LCL simulation, up to the point where the exact curve is well approximated throughout the experimentally relevant time period.

For a spinning frequency of 10 kHz, the spinning frequency and the dipolar couplings are of comparable magnitude. In addition, the typical time resolution of the experimental

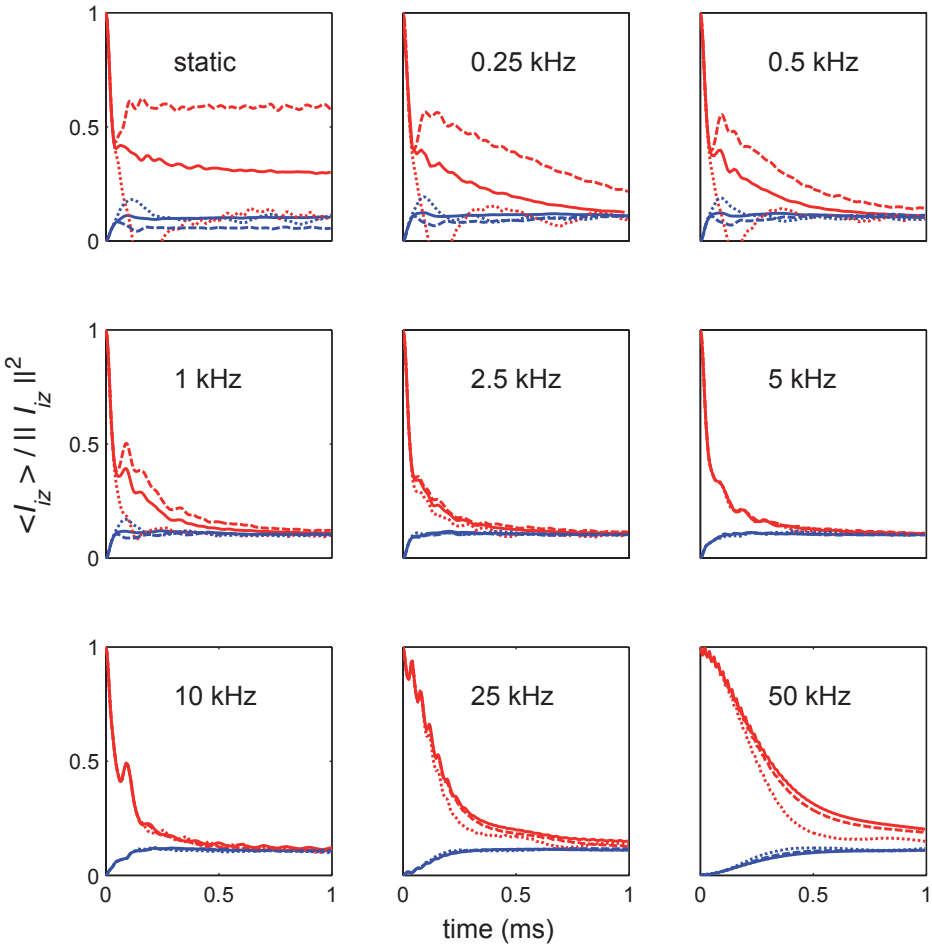

Figure 6.2: Influence of the spinning frequency on a powder-averaged simulation of polarisation transfer for a 10-spin system consisting of the protons in a single molecule of L-serylglycine. Simulations are performed in the full Liouville space (solid), and in reduced Liouville spaces where all coherences involving more than $q_{\max} = 4$ (dotted) or $q_{\max} = 5$ (dashed) spins are excluded. The initial density matrix is $\sigma(0) = I_{\mathrm{CH2_{ser},}z}$, and the observables are $\langle I_{\mathrm{CH2_{ser},}z} \rangle$ (red) and $\langle I_{\mathrm{CH_{ser},}z} \rangle$ (blue). The colour code is shown in Fig. 6.1. Atomic coordinates for a single molecule are taken from a crystal structure (CSD entry: sergly). The timestep in the simulation is 0.5 μs, and a ZCW set of 50 orientations is used for powder averaging.

observation is smaller than the rotor period, especially for the short-term dynamics, which are of particular interest in the context of structural studies. For these reasons, the accuracy of LCL simulations under MAS cannot be simply understood in terms of an effective interaction that would describe the time evolution over a rotor period. In particular, the hypothesis of an effective dipolar coupling greatly reduced by MAS does not account for the observed behaviour. This is illustrated in Fig. 6.2, where the initial transfer rates are not significantly reduced by magic-angle spinning for spinning frequencies of up to 10 kHz.

A formal analysis of the time-dependent expectation values of the single-spin polarisations could explain the influence of magic-angle spinning both on the exact spin dynamics and on the agreement between exact and LCL simulations. Such an analysis has been developed by Mark Butler, who used a Taylor expansion to compare the contribution of low-order correlations to the dynamics of the observables in static systems and in systems under magic-angle spinning [187]. Although the analytical expressions obtained are encouraging, they do not account so far for the time-scale during which LCL simulations are accurate for systems under MAS. Filip *et al.* have combined Floquet theory and perturbation theory in a Liouville-space formalism to describe the dynamics of strongly coupled spins under fast magic-angle spinning [169, 188, 189]. They found that under fast magic-angle spinning, spinning sideband intensities can be analysed by taking into account few-spin correlations [169]. Their approach or a similar approach relying on Floquet theory [190–194] could potentially be adapted to the case of polarisation transfer under magic-angle spinning.

6.2.2 Powder averaging

The error in LCL simulations, which can be quantified by a comparison between exact and LCL simulations, can be mapped as a function of crystallite orientation for a given polarisation curve. The orientation of a crystallite is here defined by the set of Euler angles (α, β, γ) that relates an arbitrary crystal frame of reference to the rotor frame. A large number of hypotheses can be formulated and explored with numerical simulations. Here we will give two specific examples, illustrated with a simulation of polarisation transfer among the protons of a molecule of L-alanine.

Figure 6.3 shows the time evolution of the error for a set of crystallite orientations that differ by their value of the angle γ. First, it can be seen that the error seems to be simply shifted in time for crystallite orientations that differ only by their value of the angle γ, i.e., for crystallites that belong to a given carousel [195]. Second, it can also be observed that after an initial monotonic increase, the error undergoes a periodic oscillation with time. Magic-angle spinning thus seems to refocus the difference between exact and LCL results over a rotor period.

Figure 6.4 shows the orientation dependence of the error over the unit sphere, which is mapped by the angles (α, β). The polarisation curve was averaged over the angle γ, as additional symmetries are known to exist in some cases for such carousel averages [174, 195]. No particular pattern has been identified in this and in similar figures, and the

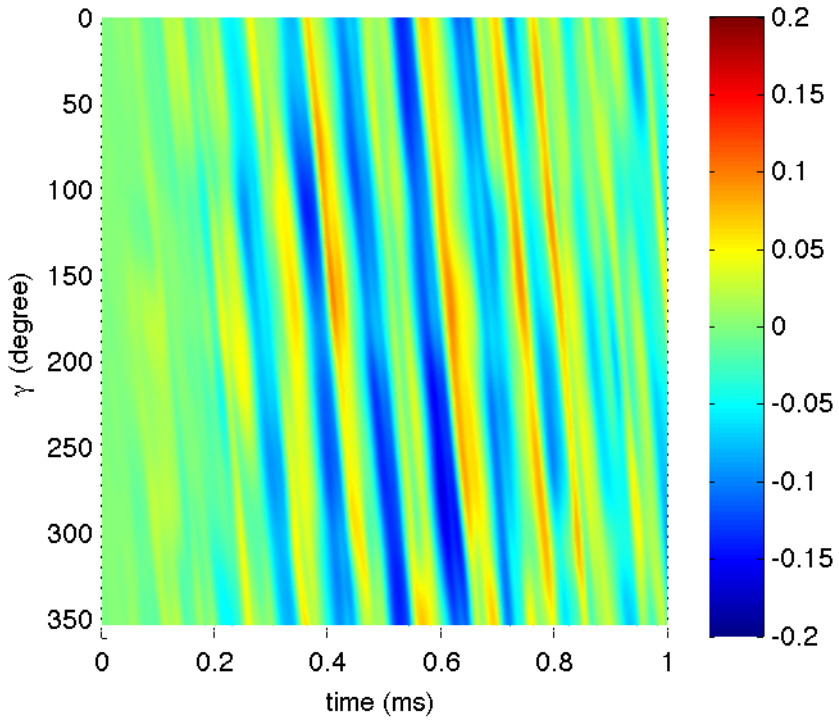

Figure 6.3: Time evolution of the error for an LCL simulation of polarisation transfer for a set of crystallite orientations that differ by their value of the angle γ. The system consists of the 7 protons in a molecule of L-alanine. The error is calculated as the difference between an exact simulation and a simulation performed in a reduced Liouville space that excludes coherences involving more than $q_{\max} = 4$ spins Atomic coordinates for a single molecule are taken from a crystal structure (CSD entry: lalnin12). The initial density matrix is $\sigma(0) = I_{CH,z}$ and the observable is $\langle I_{NH_3a,z} \rangle$. The timestep in the simulation is 0.5 μs.

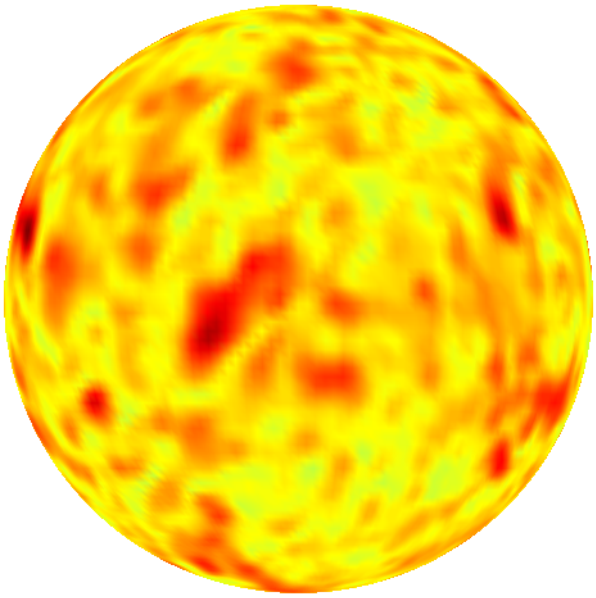

Figure 6.4: Orientation dependence of the error for an LCL simulation of polarisation transfer. The system consists of the 7 protons in a molecule of L-alanine. The unit sphere mapped by the angles (α, β) is shown. The error is calculated as the root-mean square difference between an exact simulation and a simulation performed in a reduced Liouville space that excludes coherences involving more than $q_{\max} = 4$ spins. The timestep, atomic coordinates, initial density matrix and observable are the same as in Fig. 6.3. The error is calculated for the whole polarisation curve; for both simulations the polarisation curve is averaged over the angle γ.

accuracy of LCL simulation for powder-averaged quantities thus does not seem to result from a regular behaviour of the error as a function of crystallite orientation.

Additional simulations were performed, with different parameters, but they did not provide further insight into the influence of powder averaging on the accuracy of LCL simulations.

6.3 Specificity of Liouville-space reduction in solids

6.3.1 Population of excluded coherences

Some insight into the spin dynamics can be obtained by analysing a spin-order decomposition of the density matrix, i.e., by analysing the way in which high-order correlations develop during the evolution. For a density matrix expressed using the product operators

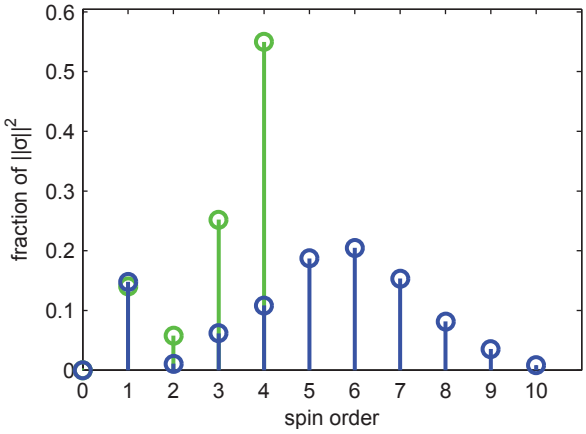

Figure 6.5: Spin-order decomposition of the density matrix for a 10-spin system consisting of the protons in a molecule of L-serylglycine, after 200 μs of evolution under 10 kHz MAS for an initial density matrix $\sigma(0) = I_{\mathrm{CH2_{ser},z}}$. The decomposition is shown for simulations performed in the full Liouville space (blue) and in a reduced Liouville space that excludes all coherences involving more than $q_{\max} = 4$ spins (green). The decomposition shown here corresponds to a single orientation, and is representative of most orientations.

given in Eq. 5.2, the spin-order decomposition $\{I_p\}_{p=0,N}$ can be calculated as

$$I_p = \sum_{q_r=p} |b_r|^2, \tag{6.1}$$

where the sum is over values of r for which $q_r = p$. For example, I_3 is evaluated at a given time t during the evolution by summing the squared coefficients $|b_r(t)|^2$ for all product operators involving 3 correlated spins. For LCL simulations, which are performed using a basis set for which each basis vector has a well-defined spin order, the coefficients I_p are straightforward to calculate. For simulations in full Liouville spaces, which were performed here with SPINEVOLUTION [141], it is first necessary to express the density matrix in an appropriate basis set; the method we used to perform this transformation is described in section 6.3.2.

Figure 6.5 shows the spin-order decomposition of the density matrix for a typical example of a 10-proton system under 10 kHz magic-angle spinning, for both exact and LCL simulations. After only 200 μs of evolution, it can be seen that the coherences that are excluded from the reduced Liouville space make a large contribution in the exact dynamics to $\|\sigma(t)\|^2$. In addition, there is a large discrepancy between the contribution made by the low-order coherences in the reduced and full Liouville spaces. The latter observation is a direct consequence of the former, since $\|\sigma(t)\|^2 \equiv 1$ under both the full Liouvillian and the reduced Liouvillian. However, we note that the values of the polarisations are correct, and this holds throughout the simulation.

Figure 6.5 highlights the fact that the accuracy of LCL simulations is not achieved by excluding coherences that are unimportant for the exact dynamics of the density matrix σ; rather, the excluded coherences make a large contribution to the evolution of σ but a neg-

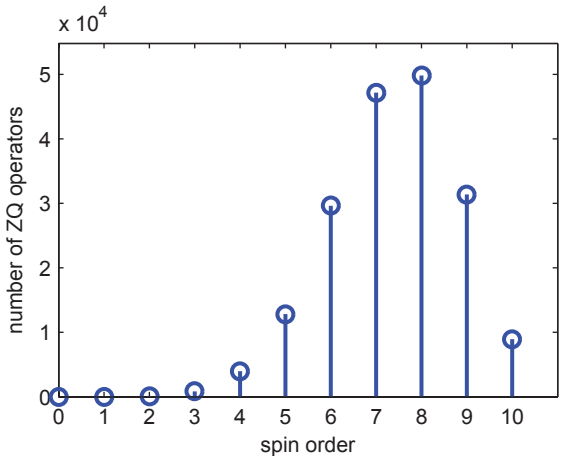

Figure 6.6: Number N_p of product operators of a given spin order in the zero-quantum subspace of a system of 10 spins $I = 1/2$.

ligible net contribution to the evolution of the experimental observable being simulated. The mechanism of LCL thus contrasts with the use of spin-space reduction in solution-state magnetic resonance, where analytical and numerical schemes have been designed to identify coherences that make a negligible contribution to $\|\sigma(t)\|^2$ [160–162].

It can be noted that after a sufficiently long period of evolution the distribution of coefficients I_p for the spin-order decomposition is found to be qualitatively similar to the distribution of integers N_p, where N_p is defined for a given system of spins $I = 1/2$ as the number of operators of spin order p. The distribution of N_p can be calculated as described in section 6.3.3, and the rough similarity between $\{I_p\}$ and $\{N_p\}$ can be seen by comparing figures 6.5 and 6.6. A similar phenomenon has been observed in multiple-quantum NMR, where statistical models can often be used to describe the excitation of multiple-quantum coherences [151, 171].

6.3.2 Change of basis set

NMR simulation programs, such as SPINEVOLUTION [141], often represent the density matrix σ for a system of N spins $I = 1/2$ as an operator in Hilbert space, using a basis set consisting of Zeeman product states. The matrix elements of σ in this Hilbert-space basis can be identified with the coefficients c_s obtained by expanding σ as a vector in Liouville space:

$$\sigma = \sum c_s C_s, \tag{6.2}$$

where the Liouville-space basis elements C_s are product operators of the form

$$C_s = \prod_{i=1}^{N} I_{i,s}, \tag{6.3}$$

with $I_{i,s} \in \{I_{i+}, I_{i-}, I_{i\alpha}, I_{i\beta}\}$, and with the α and β single-spin operator defined by

$$\begin{aligned} I_{i\alpha} &= \frac{1}{2}E_i + I_{iz}, \\ I_{i\beta} &= \frac{1}{2}E_i - I_{iz}. \end{aligned} \tag{6.4}$$

Using Eq. 6.4, the elements of the change-of-basis matrix from the basis set $\{C_s\}$ to the basis set $\{B_r\}$ described in section 5.2 can be calculated. This change-of-basis matrix can be calculated once and for all for a given N, and the density matrix in the basis set $\{B_r\}$ can then be obtained by using an NMR simulation program to write the elements of σ in the $\{C_s\}$ basis and then multiplying by the change-of-basis matrix.

In order to write the change-of-basis matrix explicitly and to use it to perform matrix-vector multiplication in Liouville space, a scheme is required to index the basis sets. For vectors in Hilbert space, Zeeman product states can be conveniently indexed by identifying the state of each spin with a bit. Here, the product operators can be indexed with a similar approach, using 2 bits for each single-spin operator and the convention:

$$E_i \leftrightarrow 00 \quad I_{iz} \leftrightarrow 11 \quad I_{i+} \leftrightarrow 01 \quad I_{i-} \leftrightarrow 10, \tag{6.5}$$

for the basis set $\{B_r\}$ used in Tourbillon, and

$$I_{i\alpha} \leftrightarrow 00 \quad I_{i\beta} \leftrightarrow 11 \quad I_{i+} \leftrightarrow 01 \quad I_{i-} \leftrightarrow 10, \tag{6.6}$$

for the basis set $\{C_s\}$ used in SPINEVOLUTION.

6.3.3 Dimension of the spin-order subspaces

In the basis set introduced in section 5.2, the number of product operators having a spin order of zero, i.e., belonging to the zero-quantum subspace, is $\binom{2N}{N}$ [54]. Within the zero-quantum subspace, the number of product operators that have spin order q and include exactly c raising operators in the product is

$$s(q,c) = \binom{N}{c}\binom{N-c}{c}\binom{N-2c}{q-2c}, \tag{6.7}$$

i.e., the number of ways to choose c distinct spins for which the product will include the raising operator I_{i+}; multiplied by the number of ways to choose c distinct spins for which the product will include the lowering operator I_{i-}, with these c spins chosen from the $N-c$ spins not already associated with a raising operator; multiplied by the number of ways to choose $q-2c$ distinct spins among the remaining $N-2c$ spins, to be represented in the product by an operator I_{iz}. For a given q, the total number $S(q)$ of zero-quantum operators of spin order q can be found by summing $s(q,c)$ over the integers $c \geq 0$ such that $q-2c \geq 0$:

$$\begin{aligned} S(q) &= \sum_{c,q-2c\geq 0} s(q,c) \\ &= \sum_{c,q-2c\geq 0} \binom{N}{c}\binom{N-c}{c}\binom{N-2c}{q-2c}. \end{aligned} \tag{6.8}$$

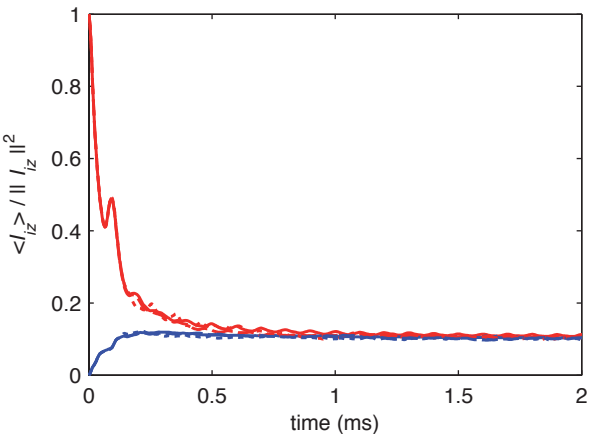

Figure 6.7: Long-term behaviour of a powder-averaged simulation of polarisation transfer for a 10-spin system consisting of the protons in a single molecule of L-serylglycine under 10 kHz MAS. Simulations are performed in the full Liouville space (solid), and in reduced Liouville spaces where all coherences involving more than $q_{\max} = 4$ (dotted) or $q_{\max} = 5$ (dashed) spins are excluded. The initial density matrix, observables, atomic coordinates, timestep and set of orientations are the same as in Fig. 6.2.

6.4 Quasi-equilibria in full and reduced Liouville spaces

6.4.1 Calculation in the time domain

We have observed, by studying a large number of polarisation-transfer curves for a selection of organic solids, that a quasi-equilibrium is in general reached on the experimental timescale, i.e., within about a millisecond for protons and a hundred milliseconds for carbons. In such a quasi-equilibrium, although the state of the system is still time-dependent, the single-spin polarisations no longer evolve. A quasi-equilibrium can result from the fully coherent evolution of a closed system, and is distinct from the equilibrium that can be reached through the interaction of the system with a bath.

For polarisation transfer among homonuclear spins I under magic-angle spinning, the quasi-equilibrium observed in exact numerical simulations in general corresponds to a uniform distribution of the initial polarisation over the spins in the system. LCL simulations adequately reproduce this aspect, as illustrated in Fig. 6.7, which shows the quasi-equilibria of two polarisation-transfer curves in an LCL simulation of a 10-spin system consisting of the protons in a single molecule of L-serylglycine.

In contrast, polarisation transfer among S spins, in the presence of surrounding I spins, leads for small spin systems to a quasi-equilibrium where the S spins have unequal polarisations [3]. Such quasi-equilibria are in general not correctly reproduced by LCL simulations. For example, in a system consisting of two carbons and several protons, the difference polarisation reaches a quasi-equilibrium value which is not zero in the exact dynamics, while in LCL simulations performed with $q_{\mathrm{H,max}} = 4$, the difference polarisation reaches a quasi-equilibrium value of zero. Fig. 6.8 illustrates this discrepancy for

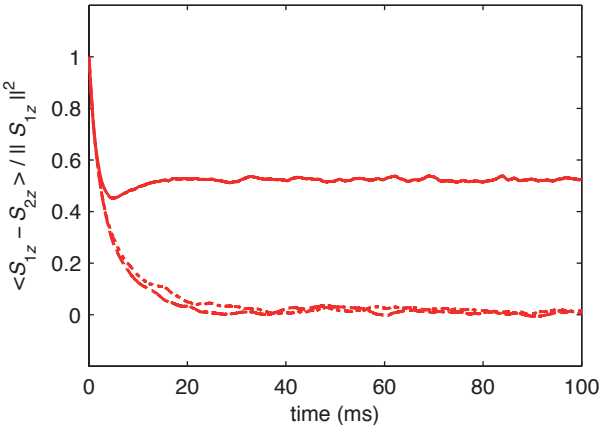

Figure 6.8: Long-term behaviour of a powder-averaged simulation of polarisation transfer for a spin system consisting of the C_α and C_β carbons (labelled 1 and 2, respectively) and the seven protons of a molecule of L-alanine under 10 kHz MAS. Simulations are performed in the full Liouville space (solid), and in reduced Liouville spaces where all coherences involving more than $q_{\mathrm{H,max}} = 4$ (dotted) or $q_{\mathrm{H,max}} = 5$ (dashed) spins are excluded. The initial density matrix is $\sigma(0) = S_{1z}$, and the observable is $\langle S_{1z} - S_{2z} \rangle$. Atomic coordinates for a single molecule are taken from a crystal structure (CSD entry: lalnin12). The timestep in the simulation is 0.5 μs, and a ZCW set of 50 orientations is used for powder averaging.

a system consisting of the C_α and C_β carbons and the seven protons of a molecule of L-alanine.

It should be noted that LCL simulations of polarisation transfer among carbons in the presence of protons nevertheless share certain features of LCL simulations of polarisation transfer among protons. In particular, magic-angle spinning is observed to increase the time during which LCL simulations reproduce the exact dynamics, and powder averaging improves the accuracy of the LCL curves, as illustrated later in Fig. 6.9.

6.4.2 Prediction of quasi-equilibrium expectation values

6.4.2.1 Numerical spin thermodynamics in Liouville space

The results obtained with "direct" time-domain simulations of polarisation transfer can be analysed in more detail with a numerical study of the operator that governs the time-evolution. The theory for the prediction of quasi-equilibria in the frequency domain is well-known (see for example Ref. [40, 41]). It is in general, however, explained with a formalism where the density matrix is considered as an operator in Hilbert space. Such a description is not applicable as such to simulations in reduced Liouville space, and we thus describe here an approach adapted to a Liouville-space formalism.

As will be seen below, predicting numerically the quasi-equilibrium value of an observable requires an explicit representation of the operator that governs the time evolution. One of the central features of the Tourbillon implementation of LCL is that it only ever

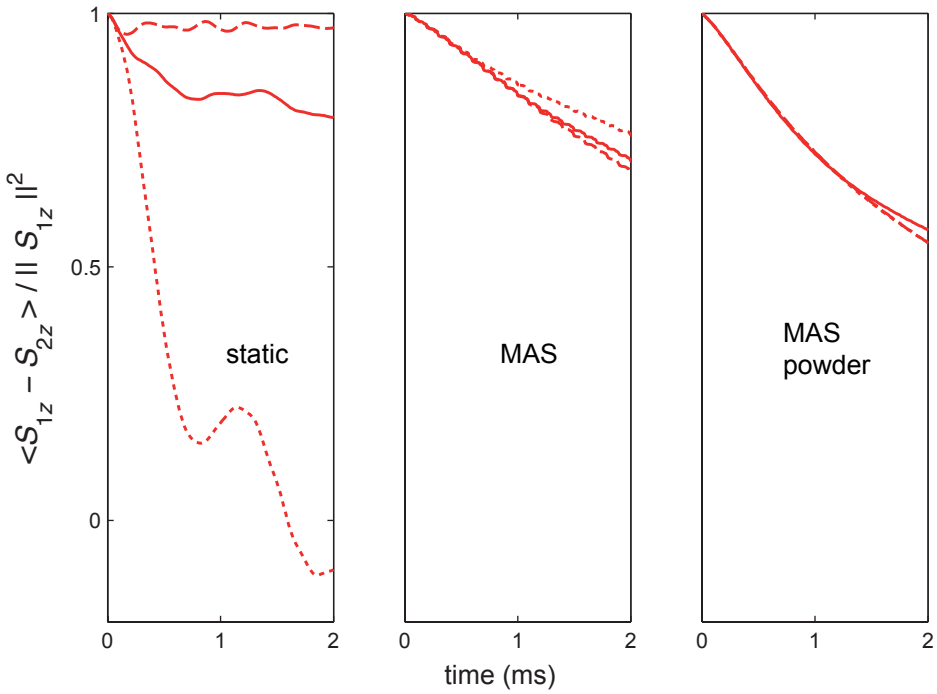

Figure 6.9: Short-term behaviour of a simulation of polarisation transfer for a spin system consisting of the C_α and C_β carbons (labelled 1 and 2, respectively) and the seven protons of a molecule of L-alanine. Simulations are performed in the full Liouville space (solid), and in reduced Liouville spaces where all coherences involving more than $q_{\mathrm{H,max}} = 4$ (dotted) or $q_{\mathrm{H,max}} = 5$ (dashed) spins are excluded. The initial density matrix, observables, atomic coordinates, and set of orientations are the same as in Fig. 6.8, and the timestep is 1 μs.

stores a single copy of the density matrix and no operator that acts on that matrix. Therefore, it is not well-suited to predicting quasi-equilibria in the frequency domain.

A method has been designed and implemented by Meghan Halse to calculate an explicit representation of the Liouvillian using the basis set described in section 5.2.2 and an arbitrary value of the maximum spin order $q_{\max}$ [196]. While the matrix elements of the Liouvillian can be calculated using the rules for evolution given in Tables 5.1 and 5.2, the main difficulty is the design of an indexing scheme that makes it possible to order the basis elements. Notably, the intuitive scheme used for example in the change-of-basis scheme described in section 5.2 is not compatible as such with a Liouville-space reduction performed according to spin order.

It can be noted that in the absence of Liouville-space reduction, quasi-equilibria can be equivalently studied with explicit representations of operators in Hilbert space. Such representation can be printed by various simulation software, and further manipulated numerically. The figures shown in this section were obtained with this approach.

6.4.2.2 Static Liouvillian

The Liouvillian $\hat{L}$, either full or reduced, is an anti-Hermitian operator, and it can thus be diagonalised. Let $\{-i\omega_s, |s\rangle\}$ be a full set of eigenvalues and eigenvectors of the Liouvillian; any operator can be expanded in this eigenbasis, and in particular the density matrix at time zero, $\sigma_0 \equiv \sigma(0)$, can be written

$$|\sigma_0\rangle = \sum_{s=1}^{2^{2N}} \frac{\langle s|\sigma_0\rangle}{\|s\|^2}|s\rangle. \tag{6.9}$$

After an evolution during t under the action of $\hat{L}$, the density matrix becomes

$$|\sigma(t)\rangle = \sum_{s=1}^{2^{2N}} \exp(-i\omega_s t)\frac{\langle s|\sigma_0\rangle}{\|s\|^2}|s\rangle, \tag{6.10}$$

and the expectation value of an observable Q is

$$\langle Q\rangle(t) = \sum_{s=1}^{2^{2N}} \exp(-i\omega_s t)\frac{\langle s|\sigma_0\rangle}{\|s\|^2}\langle Q|s\rangle. \tag{6.11}$$

The notion of "quasi-equilibrium" arises from the fact that, after a sufficiently long evolution time, the time-dependent coefficients $\exp(-i\omega_s t)$ will be entirely out of phase, and the contribution to the expectation value of Q of the projections of σ_0 on the eigenvectors with non-zero eigenvalues will cancel out. The expectation value of Q thus has a long-term, time-independent value $\langle Q\rangle_{\text{qe}}$. Introducing the set of eigenvectors A_m with eigenvalue zero, that is, the constants of motion for an evolution governed by $\hat{L}$, the quasi-equilibrium value of Q takes the form

$$\langle Q\rangle_{\text{qe}} = \sum_{m=1}^{M} \frac{\langle A_m|\sigma_0\rangle}{\|A_m\|^2}\langle Q|A_m\rangle, \tag{6.12}$$

where M is the total number of constants of motion.

Equation 6.12 suggests a definition for a quasi-equilibrium density matrix

$$|\sigma_{\mathrm{qe}}\rangle = \sum_{m=1}^{M} \frac{\langle A_m|\sigma_0\rangle}{\|A_m\|^2}|A_m\rangle, \tag{6.13}$$

such that

$$\langle Q\rangle_{\mathrm{qe}} = \langle Q|\sigma_{\mathrm{qe}}\rangle. \tag{6.14}$$

The quasi-equilibrium density matrix σ_{qe} is the projection of the initial density matrix on the constants of motion of the Liouvillian. As explained by Waugh, the notion of quasi-equilibrium is only really meaningful for the expectation value of observables, as the density matrix keeps on evolving even after a very long time [40, 41].

Eq. 6.13 and 6.14 provide a recipe to calculate numerically the quasi-equilibrium expectation value of an observable for a given Liouvillian. First, the Liouvillian is diagonalised. Then, the density matrix is written in an eigenbasis, and projected onto the constants of motion to yield the quasi-equilibrium density matrix. Finally, the expectation value of the observable of interest is calculated for the quasi-equilibrium density matrix. An example of such a calculation is shown in Fig. 6.10 for a simulation of polarisation transfer in a system of seven protons. In this example, the time-dependent contributions to the expectation value of the polarisation do not entirely cancel out, and there are thus residual oscillations around the quasi-equilibrium value.

It can be noted that in a full Liouville space, the eigenvalues of the Liouvillian correspond to differences of eigenvalues of the Hamiltonian. In the absence of accidental degeneracies, the constants of motion of a full Liouvillian are thus the projectors in Hilbert space on the eigenvectors of the Hamiltonian. This structure is lost in general for a reduced Liouvillian, a fact which might contribute to explain the differences in quasi-equilibria between full and reduced Liouville spaces. In contrast to a calculation based on the matrix representation of the Hamiltonian in Hilbert space, the approach described here applies to both full and to reduced Liouville spaces.

6.4.2.3 Periodic Liouvillian: stroboscopic observation

For solid-state NMR experiments performed with magic-angle spinning, nuclear interactions vary periodically with time at a frequency $\omega_r/2\pi$. An effective Liouvillian $\hat{\bar{L}}$, which describes the time-evolution of the system over a rotor period, can be defined such that

$$\begin{aligned} \exp(\hat{\bar{L}}\tau_r) &= \hat{U}(\tau_r,0) \\ &= \hat{\bar{T}}\exp\left(\int_0^{\tau_r}\hat{L}(t)dt\right), \end{aligned} \tag{6.15}$$

where τ_r is the rotor-period, $\hat{U}(\tau_r,0)$ is the propagator over a rotor period, and $\hat{\bar{T}}$ is the time-ordering operator; the effective Liouvillian is not unique, and in particular its eigenvalues are defined modulo ω_r. In practice, an effective Liouvillian can be calculated

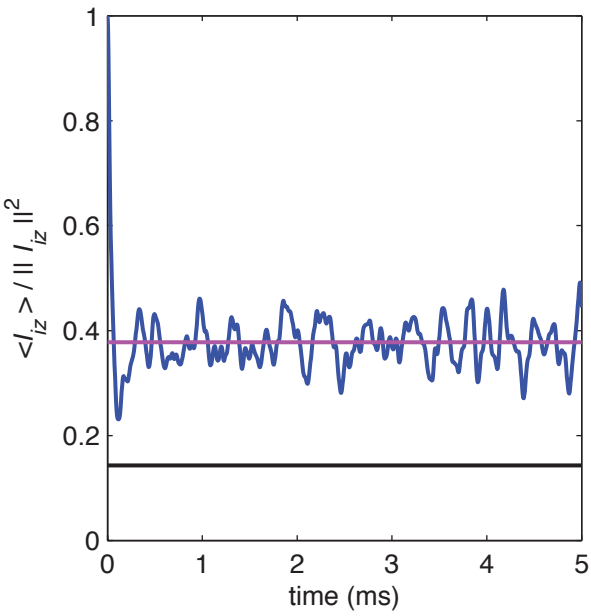

Figure 6.10: Long-term behaviour of a simulation of polarisation transfer in a static system of 7 protons. The system consists of the 7 protons in a molecule of L-alanine, and a single orientation is considered. The simulation is performed in a full Liouville space, and the quasi-equilibrium value, shown as a magenta line, is calculated using the approach described in section 6.4.2 for a static interaction. The black line corresponds to a value of the polarisation equal to 1/7th of its initial value. Atomic coordinates for a single molecule are taken from a crystal structure (CSD entry: lalnin12). The initial density matrix and the observable are $I_{CH_3a,z}$.

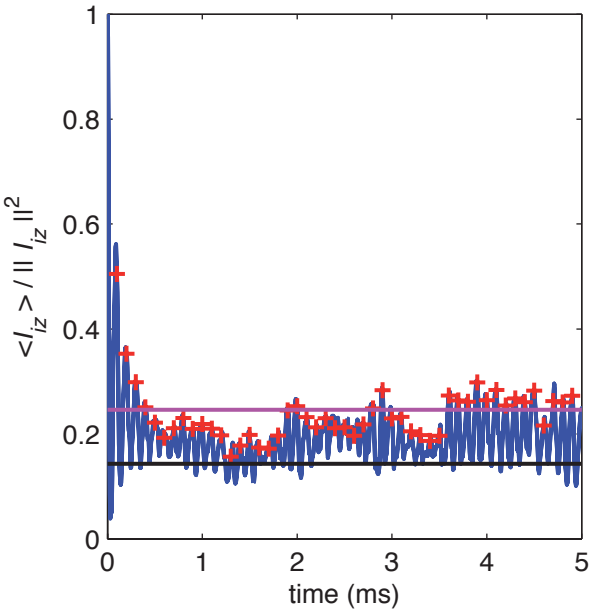

Figure 6.11: Long-term behaviour of a simulation of polarisation transfer in a system of 7 protons with 10 kHz MAS. The system consists of the 7 protons in a molecule of L-alanine, and a single orientation is considered. The simulation is performed in a full Liouville space, and the quasi-equilibrium value, shown as a magenta line, is calculated using the approach described in section 6.4.2 for a static interaction. The stroboscopically sampled polarisation curve is shown in red. The black line corresponds to a value of the polarisation equal to 1/7th of its initial value. The initial density matrix, atomic coordinates and observable are the same as in Fig. 6.10.

numerically by considering that $\hat{L}$ is piece-wise time-independent, calculating the propagator over a rotor period, and taking the logarithm of the effective propagator.

The approach considered in section 6.4.2.2 can be employed for an evolution governed by the effective Liouvillian $\hat{\bar{L}}$, to obtain a quasi-equilibrium density matrix $\bar{\sigma}_{\mathrm{qe}}$ and the corresponding expectation values $\langle \bar{Q} \rangle_{\mathrm{qe}} = \langle Q | \bar{\sigma}_{\mathrm{qe}} \rangle$. In the context of a system under MAS, these quantities provide a description for an observation every rotor period, i.e., the calculated quasi-equilibrium values correspond to a stroboscopically sampled signal. An example is shown in Fig. 6.11, for a simulation of polarisation transfer in a system of seven protons, specifically chosen such that the quasi-equilibrium values are distinct for the full polarisation curve and for the stroboscopically sampled polarisation curve.

6.4.2.4 Periodic Liouvillian: general case

Maricq has developed an approach to study quasi-equilibria for time-periodic interactions [197–199], which can be adapted to a Liouville-space formalism. To derive a practical formula, it is here convenient to start from a formal expression of the quasi-equilibrium

expectation value of an observable:

$$\begin{aligned}\langle Q\rangle_{\mathrm{qe}} &= \lim_{t\to\infty}\frac{1}{t}\int_0^t \langle Q\rangle(t')dt' \\ &= \lim_{t\to\infty}\frac{1}{t}\int_0^t \langle Q|\hat{U}(t',0)|\sigma_0\rangle dt'. \end{aligned} \tag{6.16}$$

According to Floquet's theorem [200], the propagator $\hat{U}(t,0)$ can be written as the product of a time-periodic operator $\hat{P}(t)$ and of a propagator for a time-independent, effective Liouvillian $\hat{\bar{U}}(0,t) = \exp(\hat{\bar{L}}t)$:

$$\hat{U}(t) = \hat{P}(t)\exp(\hat{\bar{L}}t). \tag{6.17}$$

Equation 6.16 can thus be written

$$\langle Q\rangle_{\mathrm{qe}} = \lim_{t\to\infty}\frac{1}{t}\int_0^t \langle \tilde{Q}(t')|\hat{\bar{U}}(t',0)|\sigma_0\rangle dt', \tag{6.18}$$

with

$$\tilde{Q}(t) = \hat{P}^{\dagger}(t)Q. \tag{6.19}$$

The vector $\tilde{Q}(t)$ is time-periodic and can thus be expressed as a Fourier series $\tilde{Q}(t) = \sum_m \tilde{Q}_m \exp(i\omega_r t)$. If $\bar{L}$ is chosen such that its eigenvalues are folded in the interval $]-\omega_r/2, \omega_r/2]$, then only the time-independent component of $\tilde{Q}$ will contribute to the integral, which becomes

$$\langle Q\rangle_{\mathrm{qe}} = \lim_{t\to\infty}\frac{1}{t}\int_0^t \langle \tilde{Q}_0|\hat{\bar{U}}(t',0)|\sigma_0\rangle(t')dt'. \tag{6.20}$$

The effective Liouvillian $\hat{\bar{L}}$ is a time-independent operator, and it is possible to define a quasi-equilibrium density matrix with respect to $\hat{\bar{L}}$ as explained in section 6.4.2.2. The quasi-equilibrium expectation value for Q is then the expectation value of the zero-frequency component of the time-periodic observable $\tilde{Q}$ for the quasi-equilibrium density matrix defined with respect to $\hat{\bar{L}}$:

$$\langle Q\rangle_{\mathrm{qe}} = \langle \tilde{Q}_0|\bar{\sigma}_{\mathrm{qe}}\rangle. \tag{6.21}$$

The zero-frequency component of the time-periodic vector $\tilde{Q}$ can also be calculated numerically if the interactions are considered as piece-wise time independent, and Eq. 6.21 thus provides a practical recipe to calculate the quasi-equilibrium value of Q. As an example, Fig. 6.12 shows the calculated quasi-equilibrium for a simulation of polarisation transfer in a 7-spin system with magic-angle spinning.

An alternative approach has been used by Sakellariou *et al.* to predict quasi-equilibria for systems under magic-angle spinning [156, 180]. The method, also based on Floquet's theorem, consists of using an explicit representation of a Floquet Hamiltonian, truncated to some finite dimension. Equivalent results can be obtained with the two approaches, provided that convergence is ensured with respect to the number of steps in the discretisation of the time-dependent interaction in one case, and to the size of the Floquet Hamiltonian in the other case.

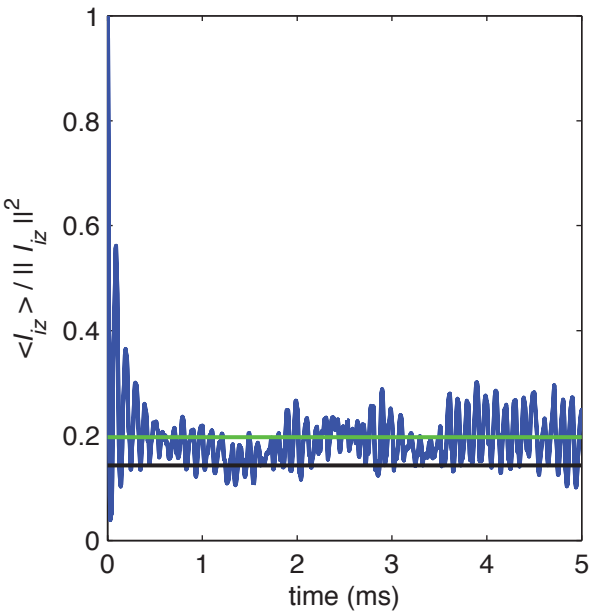

Figure 6.12: Long-term behaviour of a simulation of polarisation transfer in a system of 7 protons with 10 kHz MAS. The system consists of the 7 protons in a molecule of L-alanine, and a single orientation is considered. The simulation is performed in a full Liouville space, and the quasi-equilibrium value, shown as a green line, is calculated using the approach described in section 6.4.2 for a time-periodic interaction. The black line corresponds to a value of the polarisation equal to 1/7th of its initial value. The initial density matrix, atomic coordinates and observable are the same as in Fig. 6.10.

6.4.3 Calculation in the frequency domain

6.4.3.1 General expression of the quasi-equilibrium polarisations

The properties of LCL simulations described qualitatively in section 6.4.1 can be analysed in the frequency domain, with numerical calculations of the constants of motion. For a static system, the time-independent Liouvillian can be considered, while for a system under magic-angle spinning, constants of motion can be calculated with the effective Liouvillian. For an ensemble of N homonuclear spins, the total polarisation $F_z = \sum I_{iz}$ is always a constant of motion, which plays a particular role in the spin thermodynamics of the system. We will thus consider a full set of M constants of motion A_m, chosen to be orthogonal and such that $A_1 = F_z$.

Using Eq. 6.12, for an initial density matrix consisting of a single polarised spin i, the quasi-equilibrium value of the polarisation for spin j is

$$\frac{\langle I_{jz}\rangle_{\mathrm{qe}}}{\|I_{1z}\|^2} = \frac{1}{\|I_{1z}\|^2}\sum_{m=1}^{M}\frac{\langle A_m|I_{iz}\rangle}{\|A_m\|^2}\langle I_{jz}|A_m\rangle, \tag{6.22}$$

The contribution of the total polarisation can be calculated explicitly, and the expression then becomes

$$\frac{\langle I_{jz}\rangle_{\mathrm{qe}}}{\|I_{1z}\|^2} = \frac{1}{N} + \frac{1}{\|I_{1z}\|^2}\sum_{m=2}^{M}\frac{\langle A_m|I_{iz}\rangle}{\|A_m\|^2}\langle I_{jz}|A_m\rangle. \tag{6.23}$$

The long-term expectation value for a single-spin polarisation thus consists of the projection on the total polarisation, which corresponds to a uniform distribution of the polarisation among all the spins, and of the contribution of additional constants of motion. In particular, for spin i

$$\frac{\langle I_{iz}\rangle_{\mathrm{qe}}}{\|I_{1z}\|^2} = \frac{1}{N} + \frac{1}{\|I_{1z}\|^2}\sum_{m=2}^{M}\frac{|\langle A_m|I_{iz}\rangle|^2}{\|A_m\|^2}. \tag{6.24}$$

The quasi-equilibrium polarisation for the spin initially polarised is thus in general more than 1 Nth of the total polarisation, and equality is only obtained if the contribution of all the constants of motion with $m > 1$ constants is negligible compared to that of the total polarisation.

6.4.3.2 Ergodicity in reduced Liouville spaces

A system for which the total polarisation is the only "relevant" constant of motion, i.e., the only constant of motion that makes a significant contribution to the quasi-equilibrium value of experimental observables, is said to be ergodic. Numerical simulations of polarisation transfer for small spin systems are not expected to be ergodic in that sense, as illustrated for example in the case of static systems [38, 40, 41]. Non-ergodic behaviour is also the norm for simulations of polarisation transfer in small systems with magic-angle spinning, although the degree of departure from a uniform distribution of the total polarisation is in general very small for homonuclear spin systems.

Table 6.1: Quasi-equilibrium expectation values for the single-spin polarisations in a system of 5 protons, in full and reduced Liouville spaces. The system consists of the 5 protons in a molecule of glycine, and a single orientation is considered. The calculations are performed in a full Liouville space and in a reduced Liouville space that excludes coherences involving more that $q_{\max} = 4$ spins. Quasi-equilibrium values are calculated using the approach described in section 6.4.2 for a time-periodic interaction. The value given in row i and column j corresponds to an initial density matrix $\sigma(0) = I_{i,z}$ and an observable $\langle I_{j,z} \rangle$. Atomic coordinates for a single molecule are taken from a crystal structure (CSD entry: glycin05).

	full					reduced				
	1	2	3	4	5	1	2	3	4	5
1	0.38	0.22	0.20	0.11	0.09	0.20	0.20	0.20	0.20	0.20
2	0.15	0.28	0.28	0.15	0.15	0.20	0.20	0.20	0.20	0.20
3	0.28	0.25	0.25	0.11	0.11	0.20	0.20	0.20	0.20	0.20
4	0.11	0.12	0.13	0.45	0.18	0.20	0.20	0.20	0.20	0.20
5	0.09	0.12	0.14	0.18	0.47	0.20	0.20	0.20	0.20	0.20

Extensive numerical studies have shown, however, that for systems under magic-angle spinning described in reduced Liouville spaces, the total polarisation is the only relevant constant of motion for polarisation transfer [196]. More precisely, the quasi-equilibrium value for the single-spin polarisations seems to be analytically 1 Nth of the total polarisation. In consequence, the polarisation curves obtained show an apparently ergodic behaviour. A formal expression of this property is that for a Liouvillian $\hat{L}$, the effective reduced Liouvillian $\hat{\tilde{L}}_X$ has constants of motion A_m that verify

$$\langle A_m | I_{iz} \rangle = 0 \quad \text{for} \quad m > 1, \tag{6.25}$$

where

$$\hat{\tilde{L}}_X A_m = 0 \quad \text{and} \quad \langle A_m | F_z \rangle = 0 \quad \text{for} \quad m > 1. \tag{6.26}$$

An example of this behaviour is given in table 6.1, where the quasi-equilibrium polarisations are compared, for a 5-spin system, for simulations in full and reduced Liouville spaces. Although its validity has been verified with a large set of calculations, no derivation of Eq. 6.25 has been found so far. It should be noted that Eq. 6.25 is in general not verified for a static system.

The effectively ergodic behaviour of systems under MAS described in reduced Liouville spaces contributes to the ability of LCL simulations to reproduce or not exact simulations for systems of a dozen spins of less. For exact simulations of polarisation transfer in a purely homonuclear spin system under MAS, the quasi-equilibrium polarisations approach 1 Nth of the total polarisation rapidly when the size of the system is increased, as illustrated in Fig. 6.7. In contrast, for polarisation transfer in a system of S spins in the presence of heteronuclear I spins, non-ergodic behaviour is in general observed, as illustrated in Fig. 6.8, and LCL simulations thus fail to reproduce exact simulations. As explained in section 6.4.2, the analysis outlined here is applicable, for systems under MAS, to an observation every rotor period. Additional calculations also suggest,

however, that $\langle Q \rangle_{\mathrm{qe}} = \langle \bar{Q} \rangle_{\mathrm{qe}}$, i.e., the apparently ergodic behaviour does not seem to be related to stroboscopic sampling.

It should be noted that the simulations analysed here did not include any chemical-shift difference. Taking such differences into account will add a layer of complexity to the spin dynamics and thermodynamics, in both full and reduced Liouville spaces. Results obtained in the absence of chemical-shift differences are nevertheless useful to characterise LCL simulation.

6.5 Conclusions

Some properties of Liouville-space reduction in solids have been illustrated with numerical simulation in both the time and the frequency domain. It has been observed that accurate LCL simulation of polarisation transfer relies on the exclusion of coherences that make a large contribution to the exact density matrix but a negligible net contribution to the evolution of experimental observables. It has also been shown that the spin thermodymanics of polarisation transfer are modified in reduced Liouville spaces, and in particular that spin systems described with the LCL approach show an effectively ergodic behaviour. In spite of an imperfect understanding of Liouville-space reduction in solids, the current LCL approach provides a way to describe polarisation transfer in an experimentally relevant regime.

Chapter 7

Ab initio simulation of spin diffusion

7.1 Introduction

The study of spin diffusion has led to a great variety of applications, such as the determination of atomic-resolution structures of proteins [201] and the measurement of domain sizes in polymer blends [4]. Experimentally, fully quantitative methods have been developed to detect spin diffusion between spins with resolvable resonance frequencies, using 2D correlation NMR techniques [54]. As spin diffusion is driven by dipolar couplings between spins, which depend directly on molecular geometry, it can in principle be exploited to determine structures. In practice, however, modelling spin diffusion is anything but simple and is now one of the key barriers to accurate NMR-driven structure determination of solid materials.

As discussed in chapter 2, spin diffusion is usually described approximately using a diffusion equation or a kinetic model, with expressions for the rate constants either obtained from simplified models or chosen empirically [4, 16]. These approaches all involve some level of approximation, however, and notably all the models used today overlook to some extent the coherent nature of the spin diffusion process, and are thus unable to describe many experimental features influencing the transfer. While it is in principle possible to compute spin diffusion *ab initio*, by numerically solving the Liouville-von Neumann equation for a system of strongly coupled nuclear spins, this approach quickly hits the "exponential wall" preventing simulation of large quantum mechanical systems, and the number of spins that can be simulated exactly is largely insufficient to capture the spin diffusion process. This constitutes not only a fundamental limitation of the understanding of spin diffusion dynamics, but also of its usefulness for structural studies.

In this chapter, we show that *ab initio* simulation in reduced Liouville spaces can quantitatively reproduce experimental multi-spin polarisation transfer curves measured from spin diffusion experiments among protons (PSD) and among carbons (PDSD) in powdered organic solids under magic-angle spinning, using a network of dipolar couplings derived only from geometry, and with no adjustable parameters aside from renormalisation. These simulations are shown to capture the full dynamics observed experimentally, and thus provide a way to predict spin diffusion for a given structure.

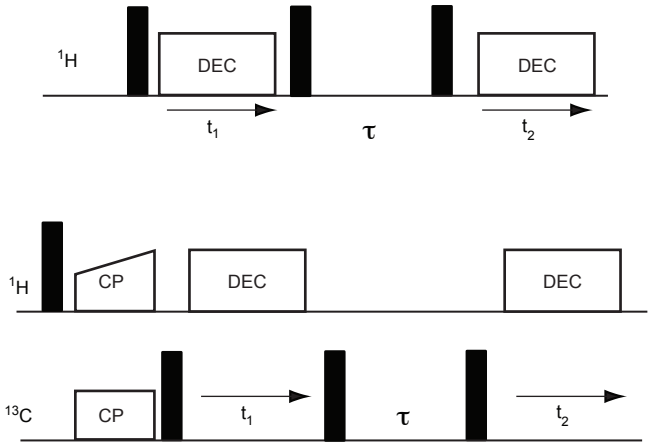

Figure 7.1: Pulse sequences for the 2D ^{1}H (top) and ^{13}C (bottom) spin exchange experiments.

7.2 Comparing simulation and experiment

7.2.1 Initial density matrix and observables

As explained in section 2.3.2, spin diffusion can be observed experimentally using the 2D pulse sequences shown in Fig. 7.1 for a set of mixing times $\{\tau\}$. In the 2D spectrum, a transfer of polarisation during the mixing time τ from spins observed at frequency ν_1 to spins observed at frequency ν_2 results in a cross peak at frequency coordinates (ν_1, ν_2). The peak volumes as a function of the mixing time τ, $P_{exp}(\nu_1, \nu_2, \tau)$, can be conveniently arranged in a $M \times M$ matrix, where M is the number of resolved peaks in the 1D spectrum, and are usually plotted as a $M \times M$ matrix of build-up curves.

The simulations performed here did not consider the effect of the full spin-exchange pulse sequence on an equilibrium initial state. Instead, only the mixing period was considered, and simulations were performed for a series of non-equilibrium initial states. The appropriate choice of initial density matrices and observables, in order to make a comparison with experimental build-up curves, can be understood from an analysis of the 2D spin exchange pulse sequence. In the absence of experimental imperfections, the volume of the (ν_1, ν_2) peak for a mixing time τ can be written formally [54]:

$$P_{\text{sim}}(\nu_1, \nu_2, \tau) = \sum_{j=1}^{N_2} \langle I_{b_j z} | \hat{U}(\tau, 0) | \sum_{i=1}^{N_1} I_{a_i z} \rangle, \tag{7.1}$$

where the first and second summations are over groups of spins $\{a_i\}_{i=1,N_1}$ and $\{b_j\}_{j=1,N_2}$ that are observed at frequency ν_1 and ν_2 respectively, $\hat{U}(\tau, 0)$ is the time-evolution superoperator for a mixing time τ. In the absence of unresolved or accidentally isochronous chemical sites, the spins observed at frequency ν_1 are equivalent; the notion of equivalence will be analysed more precisely in section 7.2.3. The expression for the peak volume can then be simplified to:

$$P_{\text{sim}}(\nu_1, \nu_2, \tau) = N_1 \sum_{j=1}^{N_2} \langle I_{b_j z} | \hat{U}(\tau, 0) | I_{a_1 z}, \rangle \tag{7.2}$$

where a_1 is any spin belonging to the group of equivalent spins observed at frequency ν_1. In consequence, the build-up curves can be simulated by performing one independent calculation for each group of equivalent spins, with an initial density matrix that corresponds to a single polarised spin $\sigma(0) = I_{a_1 z}$, and observables that consist of the summed polarisations for groups of equivalent spins $\sum_j \langle I_{b_j z} \rangle$. The resulting curves can be processed to take into account accidentally isochronous chemical sites and unresolved peaks, by simply summing over groups that correspond to a given peak in the 2D NMR spectra.

The experimental and simulated spin diffusion build-up curves are related by an overall normalisation factor

$$P_{\text{exp}}(\nu_1, \nu_2, \tau) = \xi P_{\text{sim}}(\nu_1, \nu_2, \tau), \tag{7.3}$$

where ξ depends on many experimental contributions that are not measured. In order to compare simulated and experimental data, ξ was determined here from a least-squares fit between the calculated and experimental peak volumes. Separate values were obtained for each initial density matrix, i.e., for each line in the $M \times M$ matrix of build-up curves; these additional degrees of freedom make it possible to account for some effects that are not included in the simulation, such as the non-ideality of the experimental pulse sequence.

In order to simulate spin diffusion 2D spectra instead of build-up curves, the effect of the full spin exchange pulse sequence would have to be considered, for large spin systems. This has recently been shown to be practical for experiments where ^{13}C is observed in both dimensions [202], as the ^{13}C single-quantum dynamics of the evolution and detection periods can be simulated to a large extent with clusters consisting of a single carbon surrounded by a few protons. In the current implementation of this mixed approach, a master-equation approach is used to describe the mixing period, but LCL could be used in a similar way [202].

7.2.2 Extended periodic systems

In organic solids, intermolecular ^{1}H-^{1}H couplings can contribute as much as intramolecular couplings to the dynamics of spin diffusion among protons. Not only is the ^{1}H-^{1}H dipolar interaction very intense, but in addition in a typical geometry protons are the most external nuclei in a molecule. Consequently, in the absence of experimental isotopic dilution, accurate modelling of spin diffusion among protons in organic solids requires a system that includes more than an isolated molecule.

Using reduced spin spaces, spin diffusion can be simulated from first principles among more than 100 protons, and such a system size allows both the extended nature of a solid and precise structural information to be included in the simulation. Most importantly, the system size accessible with LCL is larger than the number of protons in a primitive unit cell for a large range of organic solids. As a result, a simulation cell consisting of one or more primitive unit cells can be used; this then allows the use of periodic boundary conditions, which can be applied using the minimum image convention [179] so as to decrease the unrealistically high proportion of spins located at the edges of the system that

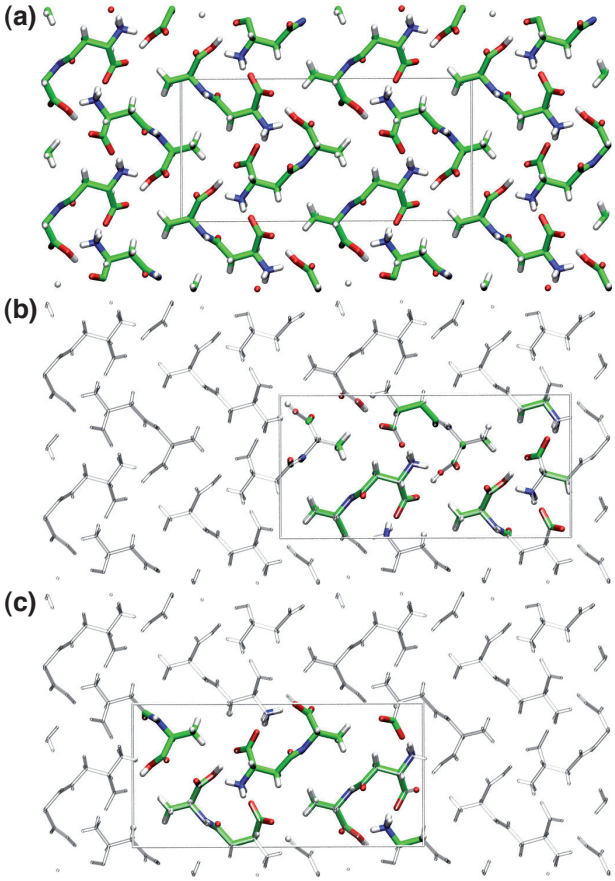

Figure 7.2: Application of periodic boundary conditions to a simulation cell, using the minimum image convention, illustrated for a single primitive unit cell of β-L-aspartyl-L-alanine. The spin system consists of the protons contained in a simulation cell (a), and each proton i interacts with the protons located in a simulation cell centred on i, as illustrated for an NH_3 (b) and a CH_2 (c) proton.

would be present in the case of an isolated cluster of spins. This approach is illustrated in Fig. 7.2, by the application of the minimum image convention to the simulation of an entire unit cell of the crystal formed by β-L-aspartyl-L-alanine. In order to obtain meaningful results, the convergence of simulated curves with respect to the number of unit cells included in the system has to be assessed, and for the systems studied here we have found that a single primitive unit cell is satisfactory.

For spin diffusion among carbons in fully ^{13}C-enriched systems, the inclusion of intermolecular ^{13}C-^{13}C couplings is expected to be less mandatory to obtain a fair description of the experimentally observed spin dynamics, even for relatively small molecules. Simulations performed with small spin systems can nevertheless suffer from pathological behaviours for subtle spin dynamical reasons, as discussed in section 7.4.

7.2.3 Symmetry and equivalence

In the discussion above, the notion of "equivalence" has been employed somewhat loosely, and a clearer meaning should be given to this term. For extended periodic systems, Haeberlen has introduced the notions of magnetic equivalence and crystallographic equivalence [127]. By definition, two spins are crystallographically equivalent if they are related by any symmetry operation of the crystal, and magnetically equivalent if they are related by translation or inversion. Two properties are of particular interest for studies of spin diffusion. Anisotropic spin interactions, such as the secular dipolar Hamiltonian, are left unchanged by a translation or inversion of the system, while they are in general modified by other symmetry operations. In contrast, isotropic interactions are left unchanged by any symmetry operation. It should be noted that the definitions introduced by Haeberlen are distinct from the definitions of chemical and magnetic equivalence used in solution-state NMR, and from the notion of total magnetic equivalence introduced by Levitt and coworkers [203].

For the analysis of spin-diffusion build-up curves experiments, two spins a_i and $a_{i'}$ can be regarded as equivalent if the initial states $\sigma(0) = I_{a_i z}$ and $\sigma'(0) = I_{a_{i'} z}$ yield the same set of polarisation transfer curves $\{\sum_j < I_{b_j z} >\}$. For a single orientation, magnetic equivalence is in general necessary for two spins to be equivalent according to that criterion. For a polycrystalline system, however, the expression of the peak volumes given in Eq. 7.1 becomes

$$P_{\text{sim}}(\nu_1, \nu_2, \tau) = \overline{\sum_j^{N_2} \langle I_{b_j z} | \hat{U}(\tau, 0) | \sum_{i=1}^{N_1} I_{a_i z} \rangle}, \tag{7.4}$$

where the bar denotes an average over all orientations. Equation 7.4 can be rearranged as

$$P_{\text{sim}}(\nu_1, \nu_2, \tau) = \sum_{i=1}^{N_1} \sum_{j=1}^{N_2} \overline{\langle I_{b_j z} | \hat{U}(\tau, 0) | I_{a_i z} \rangle}. \tag{7.5}$$

For two nuclei a_i and $a_{i'}$ that are crystallographically equivalent but magnetically inequivalent, the sums of powder-averaged curves $\sum_j \overline{\langle I_{b_j z} | \hat{U}(\tau, 0) | I_{a_i z} \rangle}$ and $\sum_j \overline{\langle I_{b_j z} | \hat{U}(\tau, 0) | I_{a_{i'} z} \rangle}$, where j runs over an ensemble of crystallographically equivalent nuclei, are equal, although the sums $\sum_j \langle I_{b_j z} | \hat{U}(\tau, 0) | I_{a_i z} \rangle$ and $\sum_j \langle I_{b_j z} | \hat{U}(\tau, 0) | I_{a_{i'} z} \rangle$ are not. The equality can be understood by noting that the set of crystallites where a_i is polarised and the set of crystallites where $a_{i'}$ is polarised are identical if a_i and $a_{i'}$ are related by a rotation or a screw rotation, and related by an inversion if a_i and $a_{i'}$ are related by a reflection or a glide reflection. In consequence, the peak volumes for a polycrystalline sample can be written

$$P_{\text{sim}}(\nu_1, \nu_2, \tau) = N_1 \overline{\langle \sum_{j=1}^{N_2} I_{b_j z} | \hat{U}(\tau, 0) | I_{a_1 z} \rangle} \tag{7.6}$$

for groups of N_1 and N_2 crystallographically equivalent spins.

In conclusion, simulating spin diffusion build-up curves for an extended periodic system requires one simulation for each group of magnetically equivalent spins in the case

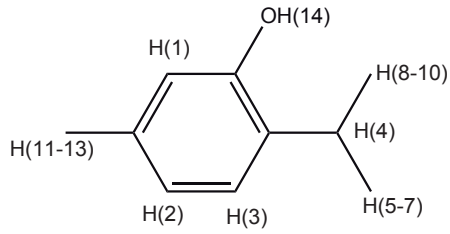

3

Figure 7.3: Chemical structure of thymol.

of a single orientation, and one powder-averaged simulation for each group of crystallographically equivalent spins in the case of a polycrystalline sample. It should be noted that, in addition to reducing the influence of edge effects, the use of a unit cell under periodic boundary conditions makes it possible to preserve, for a finite spin system, the symmetry properties of a periodic extended system. In the absence of periodic boundary conditions, a system consisting of more than one asymmetric unit would not in general have the same symmetry properties as the extended system from which it is extracted.

7.3 Proton spin diffusion

7.3.1 Accurate simulation from crystal geometry

We have shown that LCL simulations are able to reproduce the exact dynamics of a system of strongly coupled protons for powdered samples under magic-angle spinning, and that the use of reduced spin spaces makes it possible to simulate large systems of homonuclear spins. We can thus make a comparison between experimental proton spin diffusion build-up curves and simulations performed for a known crystal structure, using a primitive unit cell under periodic boundary conditions.

Figures 7.4 and 7.5 show the comparison between experimental measurements and LCL simulations for two organic solids, β-L-aspartyl-L-alanine (**2**, see Fig. 5.4) and thymol (**3**, see Fig. 7.3); a good agreement is obtained between experimental and simulated build-up curves for both systems. In particular, simulations do in most cases reproduce both the short-term variations of the polarisations, which depend on the local environment of the spins, and the longer-term "quasi-equilibrium" values, which result from the extended nature of the system. This agreement is particularly impressive if we consider that there are no adjustable parameters in this simulation: the spin diffusion behaviour is derived directly from the atomic coordinates.

The experimental proton spin diffusion build-up curves were recorded by Bénédicte Elena and Elodie Salager, as described in Ref. [84, 86]. β-L-aspartyl-L-alanine was studied at a MAS frequency of 6.25 kHz and a ^{1}H Larmor frequency of 500 MHz, and thymol was studied at a MAS frequency of 6.6 kHz and a ^{1}H Larmor frequency of 700 MHz. For both systems, only one crystal structure is known, and is available from the Cambridge Structural Database [133] (entry code FUMTEM for β-L-aspartyl-L-alanine and IPMEPL

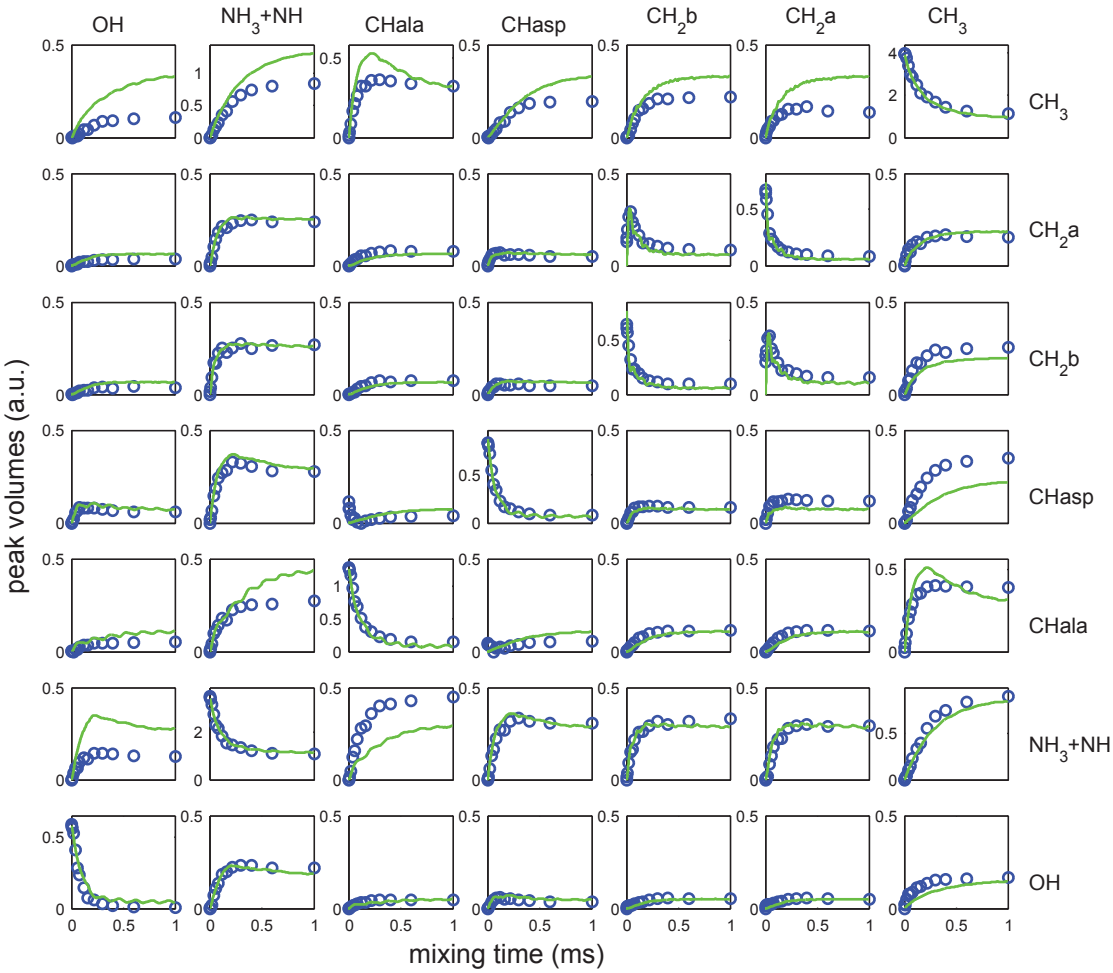

Figure 7.4: Comparison between experimental (blue) and simulated (green) proton spin diffusion build-up curves for a powdered sample of β-L-aspartyl-L-alanine under 6.25 kHz MAS. The simulated curves were obtained from LCL simulations of a system consisting of the 48 protons in a primitive unit cell under periodic boundary conditions. Atomic coordinates are taken from a crystal structure (CSD entry: fumtem). The time step in the simulation is 1 μs, and a ZCW set of 50 orientations is used for the powder average. Experimental details are given in Ref. [84].

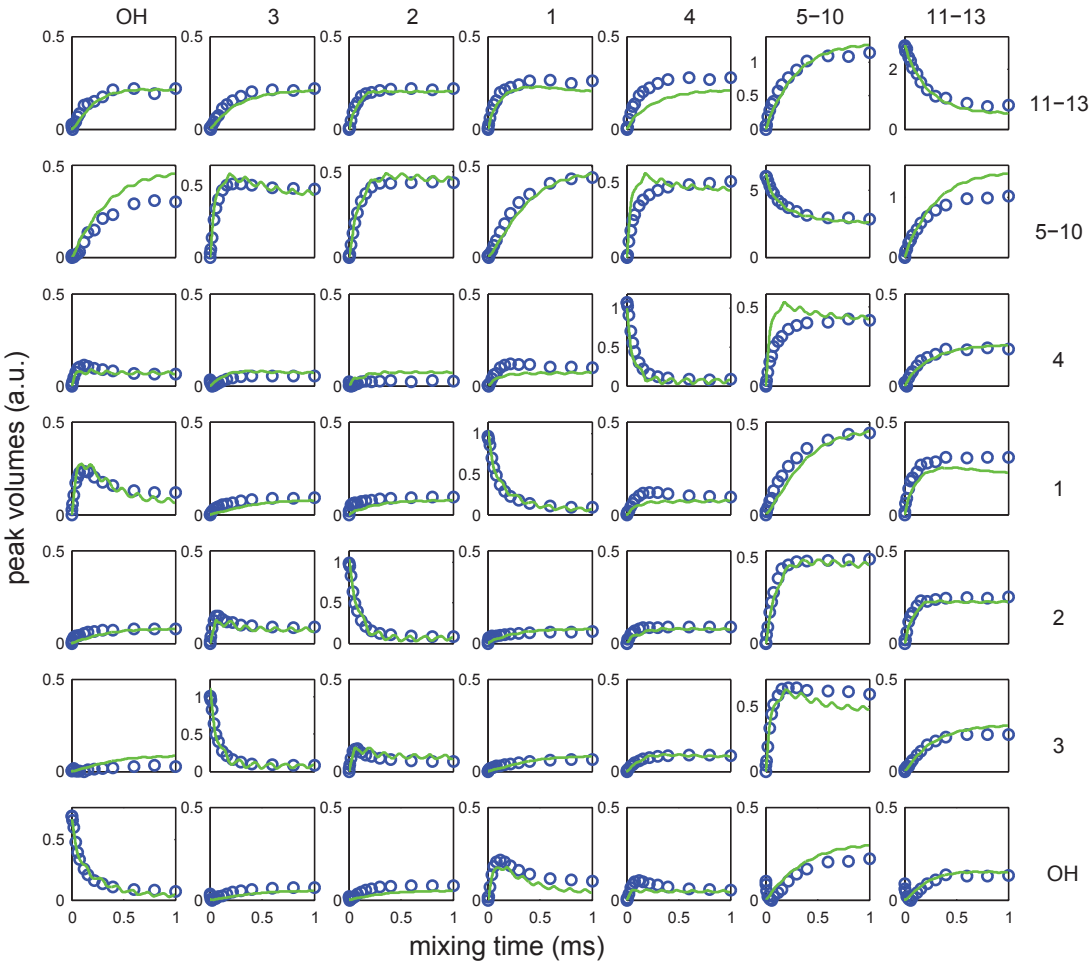

Figure 7.5: Comparison between experimental (blue) and simulated (green) proton spin diffusion build-up curves for a powdered sample of thymol under 6.6 kHz MAS. The simulated curves were obtained from LCL simulations of a system consisting of the 84 protons in a primitive unit cell under periodic boundary conditions. Atomic coordinates are taken from a crystal structure (CSD entry: ipmepl). The time step in the simulation is 1 μs, and a ZCW set of 50 orientations is used for the powder average. Experimental details are given in Ref. [86].

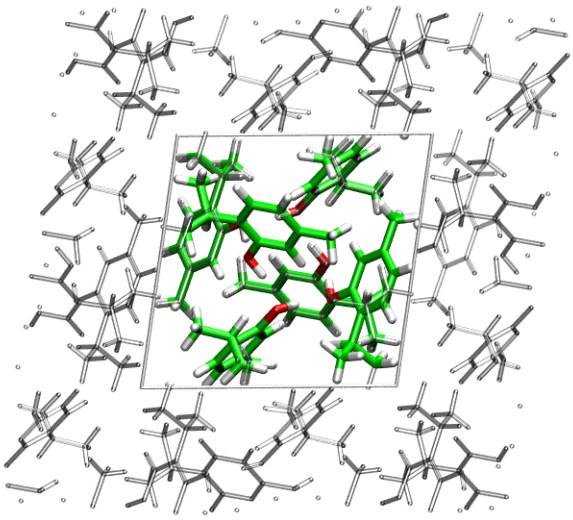

Figure 7.6: Crystal structure of thymol. The content of a primitive unit cell is shown in colour.

for thymol). LCL simulations were performed with proton positions taken from the single crystal X-ray diffraction data, shown in Fig. 7.6 and 7.2, where in each case the content of a primitive unit cell is highlighted.

As explained in section 7.2.1, while simulated build-up curves can be obtained from crystal geometry, a renormalisation is necessary to calibrate the scales of the experimental and simulated observables, which are both initially arbitrary. Such a renormalisation was performed for the comparison shown in Figs 7.4 and 7.5.

7.3.2 Role of intermolecular couplings

The fact that large dipolar-coupled networks are required to accurately simulate spin diffusion among protons can be further illustrated by comparing experimental data and data simulated for an isolated molecule. It can be seen in Fig. 7.7, where a single molecule of thymol is considered, that the discrepancies between experimental and simulated data are much more significant than for the curves obtained with a full primitive unit cell under periodic boundary conditions. As highlighted by the expanded plots in Fig. 7.7, in particular, simulations for isolated molecules often fail to reproduce the initial variations due to the local environment, which can involve close intermolecular contacts. In addition, the curves obtained with a small spin system in many cases do not reach the correct quasi-equilibrium value after 1 ms. These observations further highlight the fact that PSD build-up curves contain information about the full crystal structure, not just the molecular conformation.

It can be noted that the simulations shown in Fig. 7.7 were also performed with the LCL approach. No significant difference would be expected between an LCL and an exact simulation of a system of 14 protons, but the exact simulation cannot be performed with available software. This highlights the simple fact that even intramolecular polarisation transfer cannot be addressed with exact simulations when the number of protons in a

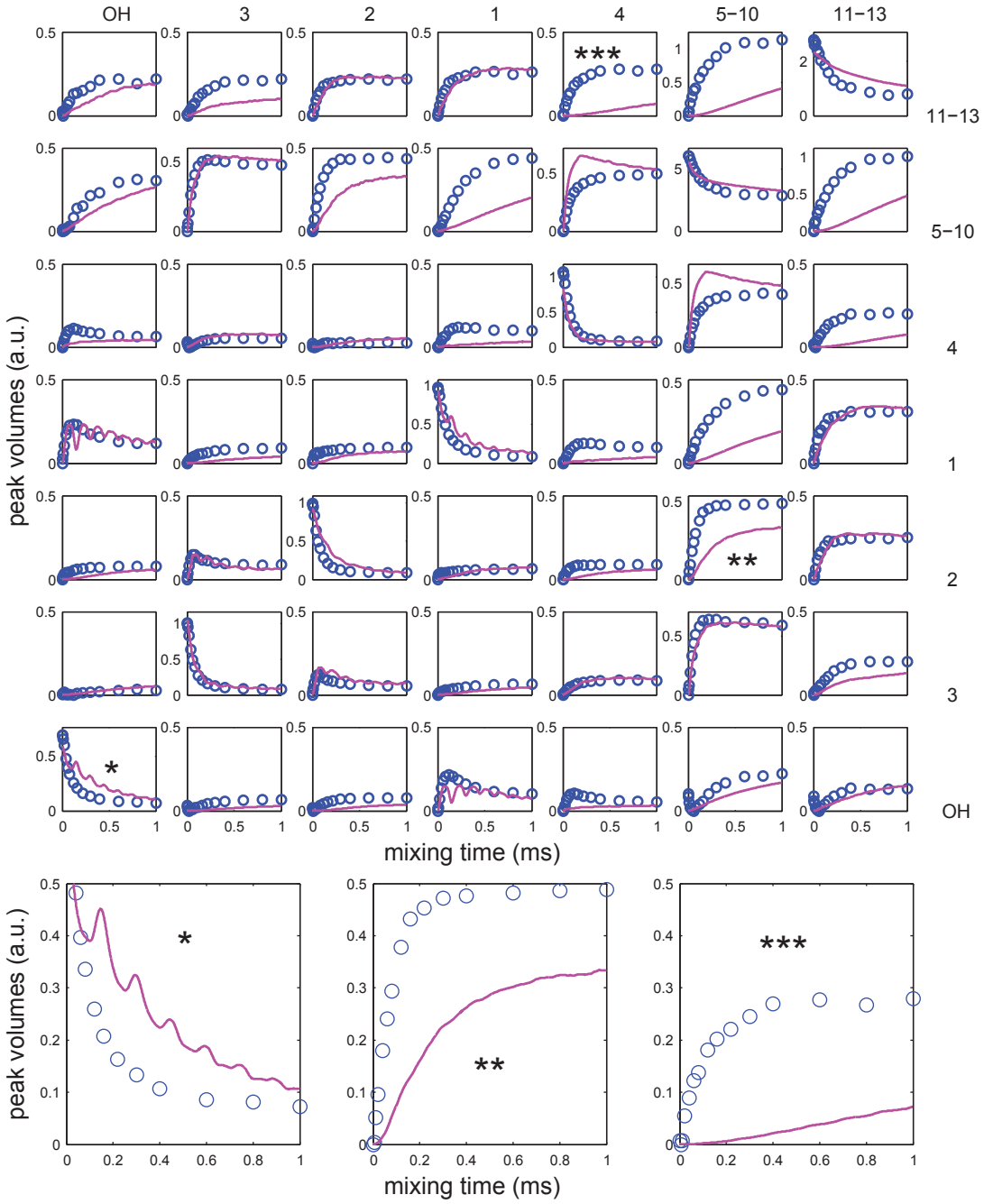

Figure 7.7: Comparison between experimental (blue) and simulated (magenta) proton spin diffusion build-up curves for a powdered sample of thymol under 6.6 kHz MAS. The simulated curves were obtained from LCL simulations of a 14-proton system consisting of the protons in a single molecule of thymol. Atomic coordinates are taken from a crystal structure (CSD entry: ipmepl), and a ZCW set of 50 orientations is used for the powder average. Experimental details are given in Ref. [86]. Full set of build-up curves (top); Enlarged views of three selected curves (bottom).

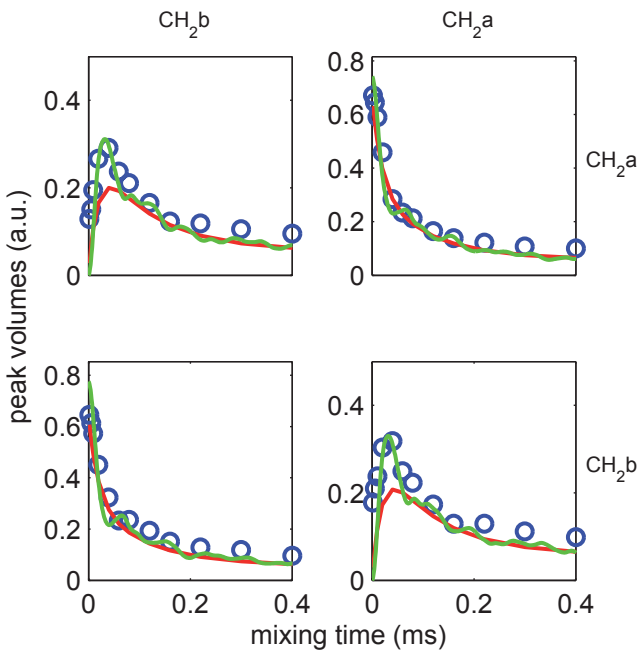

Figure 7.8: Comparison between experimental measurements (blue), LCL simulation (green), and an empirical rate-matrix modelling (red) of proton spin diffusion build-up curves for a powdered sample of β-L-aspartyl-L-alanine under 6.25 kHz MAS. LCL simulations were performed using a 48-proton system consisting of the protons in a primitive unit cell of β-L-aspartyl-L-alanine under periodic boundary conditions, and the results of the rate-matrix analysis are taken from Ref. [84]. A zoom on the portion of the matrix of build-up curves corresponding to the CH_2 group of β-L-aspartyl-L-alanine is shown.

single molecule is too large.

7.3.3 Coherent features of the observed spin dynamics

It has previously been shown that a master-equation for the polarisations, which is in this case largely empirical, can be used to model spin diffusion among protons with a good accuracy [84, 86]. For the two systems studied here, an overall similar agreement with experiments is obtained for the empirical master-equation approach and for LCL simulations. Some features of the experimental curves, however, cannot be captured by the empirical model, as they arise from the coherent nature of the underlying spin dynamics. This is particularly well illustrated for the case of the CH_2 protons of β-L-aspartyl-L-alanine shown in Fig. 7.8, where the initial strong variations of the build-up curves are more accurately predicted by the *ab initio* method.

The rate-matrix approach has been used to drive a structure search [85, 86], and in such a context the fact that some strong-coupling dynamics are not present can be a limitation. Fitting the curves with a kinetic model will lead to a systematic distortion of the crystal geometry to try to compensate for the erroneous spin dynamics. The LCL simulation accurately captures the relevant dynamics, without any need for adjustment, and could

thus be used to refine a structure.

The relevance of an *ab initio* approach to the simulation of spin diffusion is further reinforced by the fact that it provides a straightforward way to account for experimentally relevant parameters such as the magic-angle spinning frequency. When a master-equation approach is used to describe of proton spin diffusion, the dependence of the rate constants on these parameters is difficult to include in a first-principles derivation, and leads to a case-by-case empirical fitting.

7.4 Proton-driven carbon-13 spin diffusion

7.4.1 Thermodynamic wall of exact simulations

In relatively small systems of carbons and protons, spin diffusion among carbons in general does not lead to a uniform distribution of the total carbon polarisation, even after an infinitely long time. Instead, the single-carbon polarisations reach subtle quasi-equilibrium values, which depend on the detailed form of the dipolar interaction. Quasi-equilibrium in polarisation transfer have been discussed in section 6.4. Such quasi-equilibria can be observed numerically even in the absence of ^{13}C chemical-shift differences. When chemical-shift differences are taken into account, the departure of the quasi-equilibrium polarisations from a uniform distribution is expected to be even more significant. In part for that reason, exact simulations of proton-driven carbon-13 spin diffusion are not expected to bear much resemblance to experimental measurements.

Build-up curves acquired for ^{13}C-labelled samples can be used to assess the possibility to perform direct simulations of proton-driven carbon-13 spin diffusion. Figure 7.9 shows a comparison between experimental and simulated build-up curves for a polycrystalline sample of L-histidine.H_2O.HCl with 15 kHz MAS. The experimental build-up curves have already been analysed with a master-equation approach in chapter 3, and here we consider numerical simulation of the density matrix. As the maximum number of spins that can be simulated with SPINEVOLUTION is 13, and as a single molecule of histidine comprises 6 carbons, a system of 6 carbons and 7 protons was used, with the protons chosen according to their effective dipolar couplings to the 6 carbons. It can be seen in Fig. 7.9 that only the first few milliseconds of the spin diffusion process observed experimentally are reasonably captured by exact simulations. The simulated curves rapidly depart from the experimental ones, and entirely stop to evolve, so that the experimental build-up curves are overall not well reproduced. It can be noted that for spin diffusion among carbons, chemical-shift differences play a key role in the mechanism for polarisation transfer, and cannot simply be removed from the description of the spin dynamics. The dramatic effect of chemical-shift differences has already been observed by Grommek *et al.*, who then used a ^{1}H relaxation superoperator to facilitate polarisation transfer among carbons [43]. They did not report, however, a comparison between experimental and simulated data.

In striking contrast to the behaviour obtained for exact simulations, experimental spin diffusion build-up curves in general display a full equilibration of the carbon polarisations. In consequence, the fact that simulations of polarisation transfer in reduced Liouville

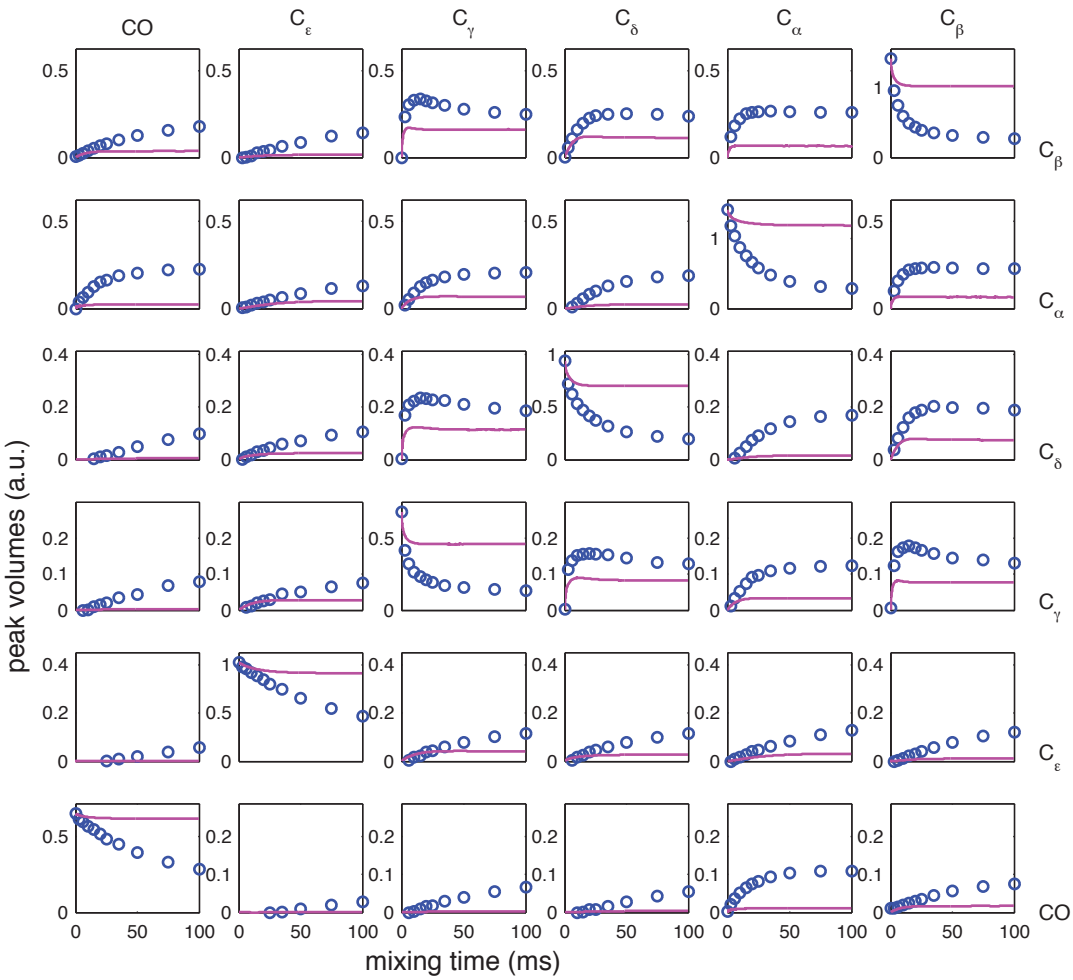

Figure 7.9: Comparison between experimental (blue) and simulated (magenta) proton-driven spin diffusion build-up curves for a powdered sample of L-histidine.H_2O.HCl under 15 kHz MAS. The simulated curves were obtained from exact simulations of a system of 6 carbons and 7 protons, consisting of all the carbons of a molecule of L-histidine.H_2O.HCl and of the 7 protons that are the most strongly coupled to these carbons. Atomic coordinates are taken from a crystal structure (CSD entry: histcm12), and a ZCW set of 50 orientations is used for the powder average. Experimental details are given in Fig. 3.1. Here the normalisation for each row was performed so that the calculated and experimental initial volumes of the diagonal peaks are identical.

spaces display an effectively ergodic behaviour, which can be seen as a deleterious artefact when comparisons with exact simulations are made for small spin systems, turns out to be an efficient way to bypass a thermodynamic wall for the prediction of experimental spin diffusion build-up curves.

7.4.2 Accurate simulation from crystal geometry

The observations collected so far suggest that LCL simulation could be used to simulate spin diffusion among carbons, with an appropriately designed reduced Liouville space. First, the notion of a separation of time-scales, illustrated in the discussion of the master-equation approach, between the slow transfer of polarisation between carbon pairs and the fast decoherence of carbon-carbon correlations under the action of surrounding protons, suggests that coherences involving more than 2 carbons can be excluded from the reduced Liouville space. Then, the results obtained with LCL simulations performed with a maximum proton spin order of 4, which reproduce both exactly simulated and experimental proton spin dynamics, suggest that a similar reduction should be appropriate to capture the effect of the proton bath on the carbon spin dynamics of interest. Finally, the ergodic behaviour forced upon experimental observables by Liouville-space reduction could compensate for the high significance of constants of motion other than the total polarisation, which is apparent in exact simulations but absent from experimental measurements.

Figure 7.10 shows a comparison between experimental PDSD build-up curves and LCL simulations performed directly from crystal geometry, for a polycrystalline sample of L-histidine.H_2O.HCl under 15 kHz MAS; comparisons were also made for curves at 10 and 20 kHz MAS. Excellent agreement is obtained, on the full time scale and for the three spinning frequencies. Importantly, the simulated build-up curves shown in Fig. 7.10 are obtained without any adjustable parameters, and a comparison of the 3 sets of curves shows that the influence of the spinning frequency is correctly described.

Simulations were performed with a system consisting of the 6 carbons and 10 protons of a single molecule of histidine, in a reduced Liouville space that excludes coherences involving more than 2 carbons or 4 protons. A series of additional simulations were also performed to assess the influence of the number of protons on the simulated curves. Simulated build-up curves obtained with 13 protons do not show significant changes, and thus suggest that the curves obtained with 10 protons are reasonably converged. Simulations performed with 7 protons, however, show clear discrepancies with the experimental data, and thus reveal that the drastic differences between Fig. 7.9 and 7.10 result from two complementary contributions. First, the modified spin thermodynamics in reduced Liouville spaces make it possible to obtain a full equilibration of the polarisations. Second, the larger number of protons that can be taken into account yields a more accurate value of the intantaneous rates of transfer.

The simulations shown here were obtained with a single molecule of histidine. Although intermolecular couplings are not expected to be as significant as for spin diffusion among protons, they contribute to some extent to the observed spin dynamics. In particular, the most noticeable discrepancies between experiment and LCL simulation are ob-

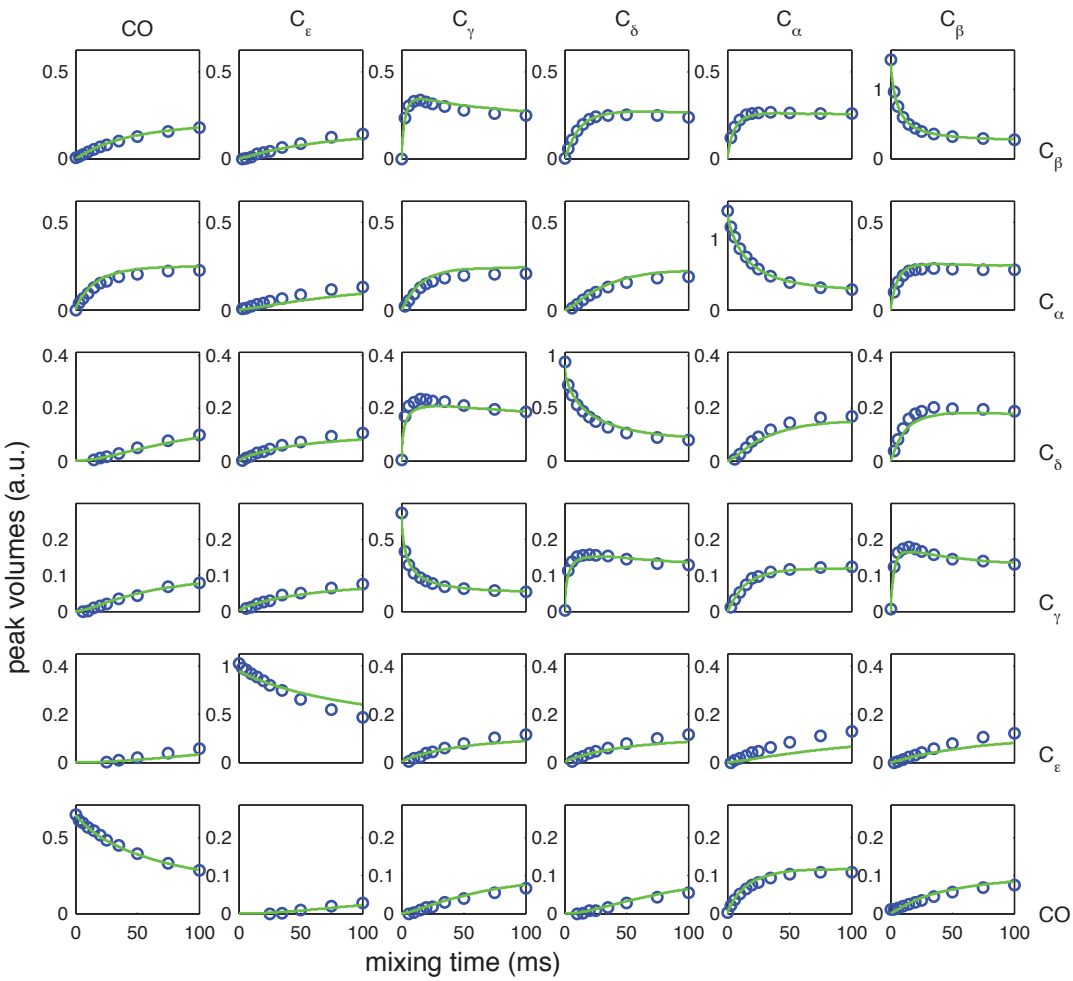

Figure 7.10: Comparison between experimental (blue) and simulated (green) proton driven spin diffusion build-up curves for a powdered sample of L-histidine.H_2O.HCl under 15 kHz MAS. The simulated curves were obtained from LCL simulations of a system of 6 carbons and 10 protons, consisting of a single molecule of L-histidine.H_2O.HCl. Atomic coordinates are taken from a crystal structure (CSD entry: histcm12). The time step in the simulation is 0.5 μs, and a ZCW set of 50 orientations is used for the powder average. Experimental details are given in Fig. 3.1

tained for the polarisation curves of C_ε, for which the ratios between intramolecular and intermolecular couplings are the largest. Improved results could be obtained by taking into account several molecules in the simulation. The current implementation of LCL, however, cannot conveniently be used to simulate proton-driven spin diffusion for very large systems. As explained in section 5.3, memory requirements are not a limitation, as they are kept to a minimum by the use of an algorithm that only requires a single copy of the density matrix. Simulation times, however, can become excessively long. Simulations are performed in the time domain, with a time step determined by the fast dynamics of the protons, while the phenomenon of interest occurs on a much longer time scale. Several approaches could be used to address this deficiency, such as the use of multiple time steps in the simulation.

It can finally be noted that polarisation transfer is equally well reproduced for all the carbon pairs, including those with a very strong ^{13}C-^{13}C dipolar coupling. These pairs are not correctly described in the master-equation approach using simulated zero-quantum lineshape, a fact that, although it is not a limitation for structural studies, prevents the accurate prediction of build-up curves from crystal geometry. The comparison shown in Fig. 7.10 is thus, to the best of our knowledge, the first accurate simulation of proton-driven carbon-13 simulation in a fully ^{13}C-labelled systems, directly from crystal geometry and without any adjustable parameters.

7.5 Conclusions

Simulations in reduced Liouville spaces have been shown to provide an accurate description of spin diffusion for polycrystalline solids under magic-angle spinning. For polarisation transfer both among carbons and among protons, the ability of the LCL model to describe fast proton dynamics is an essential ingredient of the simulation. For proton spin diffusion, the use of large spin systems then makes it possible to include most of the interactions that contribute to the experimental dynamics. For proton-driven carbon-13 spin diffusion, the long-term behaviour of the single-spin polarisations in reduced Liouville spaces, combined with the correctly described effect of surrounding protons, also leads to an accurate description over the full experimental time scale. The ability to predict spin diffusion from crystal geometry is a key ingredient to extract detailed structural information from experimental NMR measurements, and the parameter-free approach introduced here could thus contribute to future structural studies.

Chapter 8

Conclusions

As illustrated throughout this thesis, spin diffusion plays a central role in nuclear magnetism and its description from first principles is, to some extent, an open problem, largely because of the many-body nature of the underlying spin dynamics. Progress in this respect has been reported here, for high-resolution solid-state NMR studies of polycrystalline organic solids under magic-angle spinning. The approaches developed during this thesis could contribute to the improvement of applications that exploit spin diffusion, and could also turn out to be pertinent for the description of other processes.

For spin diffusion among carbons facilitated by surrounding protons, the possibility to simulate numerically the fast decoherence of carbon correlations has proved useful, in the context of a master-equation approach, to link experimentally measurable rate constants with structural information. The parameter-free analysis introduced here could be exploited to improve the interpretation of experimental data that are commonly acquired for structural studies.

Although the master-equation approach to the description of proton-driven carbon-13 spin diffusion has been shown to be very effective in practice, it does not fully capture the dynamics of this process, as the assumptions on which the model relies are in some cases not justified. The obstacles met by simplified descriptions are even more acute for spin diffusion among protons, as in most cases no approximation is applicable *a priori*. Notably, under magic-angle spinning both the internal multi-body dynamics and the external modulation occur on a comparable time scale. Alternative approaches are thus necessary.

We have observed that the time evolution of experimental observables can in some cases be described accurately in reduced Liouville spaces that include only low-order correlations. A model based on this finding, which we call LCL, has been developed to describe the spin dynamics of large systems of strongly coupled nuclear spins. The LCL approach has empirically been found to be applicable for the experimentally relevant case of powdered systems under magic-angle spinning, through a comparison with simulations performed in full Liouville spaces. However, Liouville-space reduction in solids remains imperfectly understood, and requires further study to increase its full range of potential applications.

Using LCL, we have performed simulations of spin diffusion among protons, and showed that experimental measurements could be reproduced with good accuracy using

information about the crystal geometry only and no adjustable parameter. An appropriate choice of spin system is required to capture the experimentally observed behaviour, and the large systems accessible with LCL make it possible to simulate primitive unit cells under periodic boundary conditions, and thus to simultaneously capture the extended nature of a solid and include detailed structural information.

The concepts on which the master-equation approach relies and the ability of LCL to describe the fast dynamics of proton spin diffusion have been brought together to perform simulations of proton-driven carbon-13 spin diffusion in reduced spin spaces, which show an excellent agreement with experimental measurements. Additional investigation is required to further validate and better understand the methods introduced here, but these methods appear to capture to a large extent the many-body dynamics of nuclear spin diffusion for polycrystalline organic solids under magic-angle spinning.

LCL could be exploited to describe other phenomena, especially if a more comprehensive understanding of Liouville-space reduction in solids emerges. Improved implementations of existing schemes could also be designed; LCL has been implemented in the independent Tourbillon program, and it could be interfaced with existing software for practical applications. Finally, although it has turned out to be negligible in the case of polycrystalline solids under magic-angle spinning, the effect of excluded variables on the dynamics of experimental observables could be taken into account in an effective way, to broaden the applicability of Liouville-space reduction in solids.

Afterword

The work reported in this thesis has raised several questions that have yet to be addressed. Perhaps the most intriguing of these questions relate to the unusual spin dynamics observed in the reduced Liouville spaces utilised in the LCL method. For example, the effect of multi-spin correlations on the time evolution of single-spin observables has been observed to differ dramatically between the cases of a static and of a periodic time-dependent interaction. No analysis has been proposed, however, to account rigourously and quantitatively for the effect of magic-angle spinning on the short and medium-term spin dynamics in full and reduced Liouville spaces. The validation of the LCL model for polycrystalline systems under magic-angle spinning presented in this thesis remains largely empirical. In addition, no derivation has been found to explain the intriguing long-term behaviour of LCL simulations. The apparently ergodic behaviour observed for systems under magic-angle spinning described in reduced Liouville spaces, which is a key feature of the LCL approach for the accurate simulation of experimental measurements of spin diffusion, is well characterised numerically, but not well understood analytically. Progress with respect to one or both of these questions would make it possible to better understand and eventually predict the validity of Liouville-space reduction for a broader range of interactions in nuclear magnetic resonance.

At the time of writing, several hypotheses are being explored to develop a general criterion for the validity of Liouville-space reduction in spin simulations. A strong motivation is provided by the goal of developing a microscopic, quantum-mechanical description of dynamic nuclear polarisation.[1,2] Large ensembles of nuclear spins are involved in the DNP process, in which nuclear spin diffusion is expected to play an important role. It has been recently hypothesised that the fast relaxation of high-order correlations could lead to unpopulated states that can safely be removed from the description of the system,[2] although no experimental validation has yet been proposed. It is also conceivable that a simplified description could be found to account for the effect of multi-spin correlations that are actually populated, and thus to remove them from the explicit description of the system.

Aside from the more theoretical aspects of the simulation schemes presented in this thesis, there is room also for improvement in the practical implementation of Liouville-space reduction. The Tourbillon scheme has very favourable memory requirements, but it involves a case-by-case implementation of the operators and interactions of interest. Other implementations are far more flexible, at the cost of more significant memory requirements. Towards the goal of a highly optimised but also flexible implementation of

Liouville-space reduction, there remains much to be learned from the approximations and numerical methods employed in related fields, such as quantum information processing.

With significant progress in both the theoretical understanding as well as the practical implementation of Liouville-space reduction, polynomially-scaling simulations of large spin systems could become routine in NMR spectroscopy for solving a range of problems related to interactions between large groups of spins.

Lyon, the 4th of May 2011

[1] Y. Hovav, A. Feintuch, and S. Vega. Dynamic nuclear polarization assisted spin diffusion for the solid effect case. J. Chem. Phys., 134:074509, 2011.

[2] A. Van Der Drift, A. Karabanov, I. Kuprov and W. Köckenberger. Liouville space caculations of solid effect dynamic nuclear polarisation using state space restriction methods. The 52nd ENC, Asilomar, 2011.

References

[1] N. Bloembergen. On the interaction of nuclear spins in a crystalline lattice. *Physica*, 15:386, 1949. 5, 8, 16

[2] M. Ernst and B. H. Meier. Spin diffusion in solids. In I. Ando and T. Asakura, editors, *Solid State NMR of Polymers*, volume 84. Elsevier, Amsterdam, 1998. 5, 23, 26

[3] B. H. Meier. Polarization transfer and spin diffusion in solid-state NMR. *Adv. Opt. Magn. Reson.*, 18:1, 1994. 78

[4] K. Schmidt-Rohr and H. W. Spiess. *Multidimensional Solid-State NMR and Polymers*. Academic Press, New York, 1994. 16, 23, 49, 91

[5] C. Ramanathan. Dynamic nuclear polarization and spin diffusion in nonconducting solids. *App. Magn. Reson.*, 34:409, 2008. 5

[6] S. Zhang, B. H. Meier, and R. R. Ernst. Polarization echoes in NMR. *Phys. Rev. Lett.*, 69:2149, 1992. 6

[7] T. Karlsson, M. Helmle, N. D. Kurur, and M. H. Levitt. Rotational resonance echoes in the nuclear magnetic resonance of spinning solids. *Chem. Phys. Lett.*, 247:534, 1995.

[8] M. Tomaselli, S. Hediger, D. Suter, and R. R. Ernst. Nuclear magnetic resonance polarization and coherence echoes in static and rotating solids. *J. Chem. Phys.*, 105:10672, 1996.

[9] T. Karlsson and M. H. Levitt. Longitudinal rotational resonance echoes in solid state nuclear magnetic resonance: Investigation of zero quantum spin dynamics. *J. Chem. Phys.*, 109:5493, 1998. 6

[10] M. G. Colombo, B. H. Meier, and R. R. Ernst. Rotor-driven spin diffusion in natural-abundance ^{13}C spin systems. *Chem. Phys. Lett.*, 146:189, 1988. 8, 33

[11] D. P. Raleigh, M. H. Levitt, and R. G. Griffin. Rotational resonance in solid-state NMR. *Chem. Phys. Lett.*, 146:71, 1988. 33

[12] M. H. Levitt, D. P. Raleigh, F. Creuzet, and R. G. Griffin. Theory and simulations of homonuclear spin pair systems in rotating solids. *J. Chem. Phys.*, 92:6347, 1990. 8, 43

[13] G. R. Khutsishvili. Nuclear magnetic relaxation in ionic crystals. *Sov. Phys. Jetp-Ussr*, 4:382, 1957. 8

[14] P. G. de Gennes. Sur la relaxation nucleaire dans les cristaux ioniques. *J. Phys. Chem. Solids*, 7:345, 1958. 8

[15] J. Pescia. La diffusion de spins. *J. Phys-Paris*, 25:1041, 1964. 8

[16] A. Abragam. *Principles of Nuclear Magnetism*. Oxford University Press, Oxford, 1983. 8, 23, 39, 91

[17] A. G. Redfield. Spatial diffusion of spin energy. *Phys. Rev.*, 116:315, 1959. 8

[18] I. J. Lowe and S. Gade. Density-matrix derivation of spin-diffusion equation. *Phys. Rev.*, 156:817, 1967.

[19] P. Borckman and D. Walgraef. Irreversibility in paramagnetic spin systems - free induction decay and spin diffusion. *Phys. Rev.*, 167:282, 1968.

[20] A. G. Redfield and W. N. Yu. Moment-method calculation of magnetization and interspin-energy diffusion. *Phys. Rev.*, 169:443, 1968.

[21] J. I. Kaplan. Modified linear-response method for obtaining the spin-diffusion constant of a rigid dipole system. *Phys. Rev. B*, 2:4578, 1970.

[22] T. T. P. Cheung. Spin diffusion in NMR in solids. *Phys. Rev. B*, 23:1404, 1981. 16

[23] D. Greenbaum, M. Kindermann, C. Ramanathan, and D. G. Cory. Hydrodynamic approach to coherent nuclear-spin transport. *Phys. Rev. B*, 71:054403, 2005.

[24] A. L. Kuzemsky. Statistical theory of spin relaxation and diffusion in solids. *J. Low Temp. Phys.*, 143:213, 2006. 8

[25] W. P. Aue, E. Bartholdi, and R. R. Ernst. 2-dimensional spectroscopy - application to nuclear magnetic-resonance. *J. Chem. Phys.*, 64:2229, 1976. 9

[26] J. Jeener, B. H. Meier, P. Bachmann, and R. R. Ernst. Investigation of exchange processes by 2-dimensional NMR-spectroscopy. *J. Chem. Phys.*, 71:4546, 1979. 9

[27] A. Pines, M. G. Gibby, and J. S. Waugh. Proton-enhanced NMR of dilute spins in solids. *J. Chem. Phys.*, 59:569, 1973. 9, 12

[28] J. Schaefer and E. O. Stejskal. ^{13}C nuclear magnetic-resonance of polymers spinning at magic angle. *J. Am. Chem. Soc.*, 98:1031, 1976. 9, 12

[29] D. Suter and R. R. Ernst. Spectral spin diffusion in the presence of an extraneous dipolar reservoir. *Phys. Rev. B*, 25:6038, 1982. 9

[30] D. Suter and R. R. Ernst. Spin diffusion in resolved solid-state NMR-spectra. *Phys. Rev. B*, 32:5608, 1985. 9, 10, 23, 25, 39, 45, 49

[31] P. M. Henrichs, M. Linder, and J. M. Hewitt. Dynamics of the ^{13}C spin-exchange process in solids - a theoretical and experimental-study. *J. Chem. Phys.*, 85:7077, 1986. 9, 45

[32] A. Kubo and C. A. Mcdowell. ^{31}P spectral spin diffusion in crystalline solids. *J. Chem. Phys.*, 89:63, 1988. 9, 26, 39, 45

[33] A. Kubo and C. A. Mcdowell. Spectral spin diffusion in polycrystalline solids under magic-angle spinning. *J. Chem. Soc. Faraday T.*, 84:3713, 1988. 9, 23, 25, 33, 46

[34] H. M. Pastawski, P. R. Levstein, and G. Usaj. Quantum dynamical echoes in the spin-diffusion in mesoscopic systems. *Phys. Rev. Lett.*, 75:4310, 1995. 10

[35] P. R. Levstein, G. Usaj, and H. M. Pastawski. Attenuation of polarization echoes in nuclear magnetic resonance: A study of the emergence of dynamical irreversibility in many-body quantum systems. *J. Chem. Phys.*, 108:2718, 1998. 10

[36] A. K. Khitrin and B. M. Fung. Proton polarization transfer in a ring system. *J. Chem. Phys.*, 111:7480, 1999. 10

[37] M. Aluas, C. Tripon, J. M. Griffin, X. Filip, V. Ladizhansky, R. G. Griffin, S. P. Brown, and C. Filip. CHHC and ^{1}H-^{1}H magnetization exchange: Analysis by experimental solid-state NMR and 11-spin density-matrix simulations. *J. Magn. Reson.*, 199:173, 2009. 10, 50

[38] R. Brüschweiler and R. R. Ernst. Non-ergodic quasi-equilibria in short linear spin 1/2 chains. *Chem. Phys. Lett.*, 264:393, 1997. 11, 70, 87

[39] Y. Hovav, A. Feintuch, and S. Vega. Dynamic nuclear polarization assisted spin diffusion for the solid effect case. *J. Chem. Phys.*, 134:074509, 2011. 11

[40] J. S. Waugh. Equilibrium and ergodicity in small spin systems. *Mol. Phys.*, 95:731, 1998. 11, 70, 79, 82, 87

[41] J. S. Waugh. Thermodynamic equilibrium in isolated spin systems. *App. Magn. Reson.*, 27:165, 2004. 11, 70, 79, 82, 87

[42] L. Müller, A. Kumar, T. Baumann, and R. R. Ernst. Transient oscillations in NMR cross-polarization experiments in solids. *Phys. Rev. Lett.*, 32:1402, 1974. 11

[43] A. Grommek, B. H. Meier, and M. Ernst. Distance information from proton-driven spin diffusion under MAS. *Chem. Phys. Lett.*, 427:404, 2006. 11, 20, 23, 102

[44] A. Verhoeven, P. T. F. Williamson, H. Zimmermann, M. Ernst, and B. H. Meier. Rotational-resonance distance measurements in multi-spin systems. *J. Magn. Reson.*, 168:314, 2004. 11

[45] P. T. F. Williamson, A. Verhoeven, M. Ernst, and B. H. Meier. Determination of internuclear distances in uniformly labeled molecules by rotational-resonance solid-state NMR. *J. Am. Chem. Soc.*, 125:2718, 2003. 11

[46] D. K. Sodickson and J. S. Waugh. Spin-diffusion on a lattice - classical simulations and spin coherent states. *Phys. Rev. B*, 52:6467, 1995. 12

[47] C. G. Tang and J. S. Waugh. Dynamics of classical spins on a lattice - spin diffusion. *Phys. Rev. B*, 45:748, 1992. 12, 49

[48] M. C. Butler, J.-N. Dumez, and L. Emsley. Dynamics of large nuclear-spin systems from low-order correlations in liouville space. *Chem. Phys. Lett.*, 477:377, 2009. 12, 63

[49] J.-N. Dumez, M. C. Butler, and L. Emsley. Numerical simulation of free evolution in solid-state nuclear magnetic resonance using low-order correlations in liouville space. *J. Chem. Phys.*, 133:224501, 2010. 12

[50] J.-N. Dumez, M. C. Butler, E. Salager, B. Elena-Herrmann, and L. Emsley. *Ab initio* simulation of proton spin diffusion. *Phys. Chem. Chem. Phys.*, 12:9172, 2010. 12

[51] J.-N. Dumez and L. Emsley. A master-equation approach to the description of proton-driven spin diffusion from crystal geometry using simulated zero-quantum lineshapes. *Phys. Chem. Chem. Phys.*, 13:7363, 2011. 12

[52] N. M. Szeverenyi, M. J. Sullivan, and G. E. Maciel. Observation of spin exchange by two-dimensional fourier-transform ^{13}C cross polarization-magic-angle spinning. *J. Magn. Reson.*, 47:462, 1982. 12, 13, 16

[53] P. Caravatti, P. Neuenschwander, and R. R. Ernst. Characterization of heterogeneous polymer blends by 2-dimensional proton spin diffusion spectroscopy. *Macromolecules*, 18:119, 1985. 12, 13

[54] R. R. Ernst, G. Bodenhausen, and A. Wokaun. *Principles of Nuclear Magnetic Resonance in One and Two Dimensions*. Oxford University Press, Oxford, 1990. 12, 23, 39, 49, 51, 53, 77, 91, 92

[55] E. R. Andrew, A. Bradbury, and R. G. Eades. Nuclear magnetic resonance spectra from a crystal rotated at high speed. *Nature*, 182:1659, 1958. 12

[56] E. R. Andrew, A. Bradbury, and R. G. Eades. Removal of dipolar broadening of nuclear magnetic resonance spectra of solids by specimen rotation. *Nature*, 183:1802, 1959.

[57] I. J. Lowe. Free induction decays of rotating solids. *Phys. Rev. Lett.*, 2:285, 1959. 12

[58] P. Hodgkinson. Heteronuclear decoupling in the NMR of solids. *Prog. Nucl. Magn. Reson. Spectrosc.*, 46:197, 2005. 12

[59] S. R. Hartmann and E. L. Hahn. Nuclear double resonance in rotating frame. *Phys. Rev.*, 128:2042, 1962. 12

[60] P. K. Madhu. High-resolution solid-state NMR spectroscopy of protons with homonuclear dipolar decoupling schemes under magic-angle spinning. *Solid State Nucl. Mag.*, 35:2, 2009. 15

[61] S. Zhang, B. H. Meier, and R. R. Ernst. Local monitoring of proton spin diffusion in static and rotating samples via spy detection. *Solid State Nucl. Mag.*, 1:313, 1992. 15

[62] M. Wilhelm, H. Feng, U. Tracht, and H. W. Spiess. 2D CP/MAS ^{13}C isotropic chemical shift correlation established by ^{1}H spin diffusion. *J. Magn. Reson.*, 134:255, 1998. 15

[63] F. M. Mulder, W. Heinen, M. van Duin, J. Lugtenburg, and H. J. M. de Groot. Spin diffusion with ^{13}C selection and detection for the characterization of morphology in labeled polymer blends with MAS NMR. *J. Am. Chem. Soc.*, 120:12891, 1998. 15

[64] I. Scholz, B. H. Meier, and M. Ernst. MIRROR-CP: A proton-only experiment for the measurement of ^{13}C spin diffusion. *Chem. Phys. Lett.*, 479:296, 2009. 15

[65] M. Goldman and L. Shen. Spin-spin relaxation in LaF_3. *Phys. Rev.*, 144:321, 1966. 15

[66] J. Clauss, K. Schmidt-Rohr, and H. W. Spiess. Determination of domain sizes in heterogeneous polymers by solid-state NMR. *Acta Polym.*, 44:1, 1993. 15, 16

[67] D. E. Demco, A. Johansson, and J. Tegenfeldt. Proton spin-diffusion for spatial heterogeneity and morphology investigations of polymers. *Solid State Nucl. Mag.*, 4:13, 1995. 15

[68] W. R. Zhang and D. G. Cory. First direct measurement of the spin diffusion rate in a homogenous solid. *Phys. Rev. Lett.*, 80:1324–1327, 1998. 15

[69] K. W. Eberhardt, S. Mouaziz, G. Boero, J. Brugger, and B. H. Meier. Direct observation of nuclear spin diffusion in real space. *Phys. Rev. Lett.*, 99:227603, 2007. 15

[70] M. Linder, P. M. Henrichs, J. M. Hewitt, and D. J. Massa. Use of carbon carbon nuclear-spin diffusion for the study of the miscibility of polymer blends. *J. Chem. Phys.*, 82:1585, 1985. 16, 23

[71] D. L. Vanderhart. Natural-abundance ^{13}C-^{13}C spin exchange in rigid crystalline organic-solids. *J. Magn. Reson.*, 72:13, 1987. 16

[72] C. E. Bronniman, N. M. Szeverenyi, and G. E. Maciel. ^{13}C spin diffusion of adamantane. *J. Chem. Phys.*, 79:3694, 1983. 23

[73] M. H. Frey and S. J. Opella. ^{13}C spin exchange in amino-acids and peptides. *J. Am. Chem. Soc.*, 106:4942, 1984. 16

[74] D. L. VanderHart and G. B. McFadden. Some perspectives on the interpretation of proton NMR spin diffusion data in terms of polymer morphologies. *Solid State Nucl. Mag.*, 7:45, 1996. 16

[75] D. Massiot, B. Alonso, F. Fayon, F. Fredoueil, and B. Bujoli. New NMR developments for structural investigation of proton-bearing materials at different length scales. *Solid State Sci.*, 3:11, 2001. 16

[76] B. Alonso and D. Massiot. Multi-scale NMR characterisation of mesostructured materials using ^{1}H -> ^{13}C through-bond polarisation transfer, fast MAS, and ^{1}H spin diffusion. *J. Magn. Reson.*, 163:347, 2003. 16

[77] S. P. Brown. Probing proton-proton proximities in the solid state. *Prog. Nucl. Magn. Reson. Spectrosc.*, 50:199, 2007. 16

[78] A. Lange, S. Luca, and M. Baldus. Structural constraints from proton-mediated rare-spin correlation spectroscopy in rotating solids. *J. Am. Chem. Soc.*, 124:9704, 2002. 16, 20

[79] A. Lange, K. Seidel, L. Verdier, S. Luca, and M. Baldus. Analysis of proton-proton transfer dynamics in rotating solids and their use for 3D structure determination. *J. Am. Chem. Soc.*, 125:12640, 2003. 17, 23

[80] K. Seidel, M. Etzkorn, L. Sonnenberg, C. Griesinger, A. Sebald, and M. Baldus. Studying molecular 3D structure and dynamics by high-resolution solid-state NMR: Application to L-tyrosine-ethylester. *J. Phys. Chem. A*, 109:2436, 2005. 17, 23

[81] A. Lange, T. Schupp, F. Petersen, T. Carlomagno, and M. Baldus. High-resolution solid-state NMR structure of an anticancer agent. *Chemmedchem*, 2:522, 2007. 17, 18

[82] J. Brus, H. Petrickova, and J. Dybal. Potential and limitations of 2D ^{1}H-^{1}H spin-exchange CRAMPS experiments to characterize structures of organic solids. *Monatsh. Chem.*, 133:1587, 2002. 17

[83] J. Brus, H. Petrickova, and J. Dybal. Influence of local molecular motions on the determination of ^{1}H-^{1}H internuclear distances measured by 2D ^{1}H spin-exchange experiments. *Solid State Nucl. Mag.*, 23:183, 2003. 17

[84] B. Elena and L. Emsley. Powder crystallography by proton solid-state NMR spectroscopy. *J. Am. Chem. Soc.*, 127:9140, 2005. 17, 19, 23, 96, 97, 101

[85] B. Elena, G. Pintacuda, N. Mifsud, and L. Emsley. Molecular structure determination in powders by NMR crystallography from proton spin diffusion. *J. Am. Chem. Soc.*, 128:9555, 2006. 17, 19, 101

[86] E. Salager, R. S. Stein, C. J. Pickard, B. Elena, and L. Emsley. Powder NMR crystallography of thymol. *Phys. Chem. Chem. Phys.*, 11:2610, 2009. 17, 23, 96, 98, 100, 101

[87] H. Takahashi, M. Kainosho, H. Akutsu, and T. Fujiwara. ^{1}H-detected ^{1}H-^{1}H correlation spectroscopy of a stereo-array isotope labeled amino acid under fast magic-angle spinning. *J. Magn. Reson.*, 203:253, 2010. 17

[88] H. Takahashi, H. Akutsu, and T. Fujiwara. A magic-angle-spinning NMR method for ^{1}H-^{1}H distance measurement using coherent polarization transfer in ^{13}C-labeled organic solids. *J. Chem. Phys.*, 129:154504, 2008. 17, 50

[89] Z. Olender, D. Reichert, A. Muller, H. Zimmermann, R. Poupko, and Z. Luz. Carbon-13 chemical-shift correlation, spin diffusion and self diffusion in isotopically enriched tropolone. *J. Magn. Reson. A*, 120:31, 1996. 17, 23

[90] D. Reichert, G. Hempel, R. Poupko, Z. Luz, Z. Olejniczak, and P. Tekely. MAS NMR studies of carbon-13 spin exchange in durene. *Solid State Nucl. Mag.*, 13:137, 1998. 17

[91] P. Tekely, M. J. Potrzebowski, Y. Dusausoy, and Z. Luz. Measurement of spin diffusion and intermolecular distances between chemically equivalent nuclei in rotating solids. *Chem. Phys. Lett.*, 291:471, 1998. 17

[92] P. Tekely, C. Gardiennet, M. J. Potrzebowski, A. Sebald, D. Reichert, and Z. Luz. Probing molecular geometry of solids by nuclear magnetic resonance spin exchange at the $n = 0$ rotational-resonance condition. *J. Chem. Phys.*, 116:7607, 2002. 17, 23

[93] P. M. Henrichs and M. Linder. ^{13}C spin diffusion in the determination of intermolecular structure in solids. *J. Magn. Reson.*, 58:458, 1984. 17

[94] P. Robyr, B. H. Meier, and R. R. Ernst. Tensor correlation by 2D spin-diffusion powder NMR-spectroscopy - determination of the asymmetry of the hydrogen-bond potential in benzoic-acid. *Chem. Phys. Lett.*, 187:471, 1991. 17

[95] P. Robyr, B. H. Meier, P. Fischer, and R. R. Ernst. A combined structural study using NMR chemical-shielding-tensor correlation and neutron-diffraction in polycrystalline methanol. *J. Am. Chem. Soc.*, 116:5315, 1994. 17

[96] R. Tycko and G. Dabbagh. Nuclear-magnetic-resonance crystallography - molecular orientational ordering in 3 forms of solid methanol. *J. Am. Chem. Soc.*, 113:3592, 1991. 17

[97] R. Tycko, D. P. Weliky, and A. E. Berger. Investigation of molecular structure in solids by two-dimensional NMR exchange spectroscopy with magic angle spinning. *J. Chem. Phys.*, 105:7915, 1996. 17

[98] F. Castellani, B. van Rossum, A. Diehl, M. Schubert, K. Rehbein, and H. Oschkinat. Structure of a protein determined by solid-state magic-angle-spinning NMR spectroscopy. *Nature*, 420:98, 2002. 17, 20

[99] A. Lange, S. Becker, K. Seidel, K. Giller, O. Pongs, and M. Baldus. A concept for rapid protein-structure determination by solid-state NMR spectroscopy. *Angew. Chem. Int. Ed.*, 44:2089, 2005. 20

[100] K. Seidel, M. Etzkorn, H. Heise, S. Becker, and M. Baldus. High-resolution solid-state NMR studies on uniformly ^{13}C,^{15}N -labeled ubiquitin. *Chembiochem*, 6:1638, 2005.

[101] T. Manolikas, T. Herrmann, and B. H. Meier. Protein structure determination from ^{13}C spin-diffusion solid-state NMR spectroscopy. *J. Am. Chem. Soc.*, 130:3959, 2008. 20, 23, 38

[102] A. Loquet, B. Bardiaux, C. Gardiennet, C. Blanchet, M. Baldus, M. Nilges, T. Malliavin, and A. Bockmann. 3D structure determination of the Crh protein from highly ambiguous solid-state NMR restraints. *J. Am. Chem. Soc.*, 130:3579, 2008.

[103] J. Korukottu, R. Schneider, V. Vijayan, A. Lange, O. Pongs, S. Becker, M. Baldus, and M. Zweckstetter. High-resolution 3D structure determination of kaliotoxin by solid-state NMR spectroscopy. *Plos One*, 3:e2359, 2008.

[104] X. H. Peng, D. Libich, R. Janik, G. Harauz, and V. Ladizhansky. Dipolar chemical shift correlation spectroscopy for homonuclear carbon distance measurements in proteins in the solid state: Application to structure determination and refinement. *J. Am. Chem. Soc.*, 130:359, 2008. 23

[105] C. Wasmer, A. Lange, H. Van Melckebeke, A. B. Siemer, R. Riek, and B. H. Meier. Amyloid fibrils of the HET-s(218-289) prion form a beta solenoid with a triangular hydrophobic core. *Science*, 319:1523, 2008.

[106] I. Bertini, A. Bhaumik, G. De Paepe, R. G. Griffin, M. Lelli, J. R. Lewandowski, and C. Luchinat. High-resolution solid-state NMR structure of a 17.6 kDa protein. *J. Am. Chem. Soc.*, 132:1032, 2010.

[107] H. Van Melckebeke, C. Wasmer, A. Lange, A. B. Eiso, A. Loquet, A. Bockmann, and B. H. Meier. Atomic-resolution three-dimensional structure of HET-s(218-289) amyloid fibrils by solid-state NMR spectroscopy. *J. Am. Chem. Soc.*, 132:13765, 2010. 20, 23

[108] I. de Boer, L. Bosman, J. Raap, H. Oschkinat, and H. J. M. de Groot. 2D ^{13}C-^{13}C MAS NMR correlation spectroscopy with mixing by true ^{1}H spin diffusion reveals long-range intermolecular distance restraints in ultra high magnetic field. *J. Magn. Reson.*, 157:286, 2002. 20

[109] V. Ladizhansky. Homonuclear dipolar recoupling techniques for structure determination in uniformly ^{13}C-labeled proteins. *Solid State Nucl. Mag.*, 36:119, 2009. 20

[110] A. Egawa, T. Fujiwara, T. Mizoguchi, Y. Kakitani, Y. Koyama, and H. Akutsu. Structure of the light-harvesting bacteriochlorophyll *c* assembly in chlorosomes from *Chlorobium limicola* determined by solid-state NMR. *P. Natl. Acad. Sci.*, 104:790, 2007. 21, 23, 31

[111] J. J. Buffy, A. J. Waring, and M. Hong. Determination of peptide oligomerization in lipid bilayers using ^{19}F spin diffusion NMR. *J. Am. Chem. Soc.*, 127:4477, 2005. 21

[112] W. Luo and M. Hong. Determination of the oligomeric number and intermolecular distances of membrane protein assemblies by anisotropic ^{1}H-driven spin diffusion NMR spectroscopy. *J. Am. Chem. Soc.*, 128:7242, 2006. 21, 23, 31

[113] S. Sharif, M. Singh, S. J. Kim, and J. Schaefer. Staphylococcus aureus peptidoglycan tertiary structure from carbon-13 spin diffusion. *J. Am. Chem. Soc.*, 131:7023, 2009. 21

[114] D. Huster, X. L. Yao, and M. Hong. Membrane protein topology probed by ^{1}H spin diffusion from lipids using solid-state NMR spectroscopy. *J. Am. Chem. Soc.*, 124:874, 2002. 21

[115] C. Ader, R. Schneider, K. Seidel, M. Etzkorn, S. Becker, and M. Baldus. Structural rearrangements of membrane proteins probed by water-edited solid-state NMR spectroscopy. *J. Am. Chem. Soc.*, 131:170, 2009.

[116] M. Etzkorn, S. Martell, O. C. Andronesi, K. Seidel, M. Engelhard, and M. Baldus. Secondary structure, dynamics, and topology of a seven-helix receptor in native membranes, studied by solid-state NMR spectroscopy. *Angew. Chem. Int. Ed.*, 46:459, 2007. 21

[117] P. Hodgkinson and L. Emsley. The accuracy of distance measurements in solid-state NMR. *J. Magn. Reson.*, 139:46, 1999. 23

[118] H. H. Limbach, B. Wehrle, M. Schlabach, R. Kendrick, and C. S. Yannoni. CPMAS polarization transfer methods for superposed chemical-exchange and spin diffusion in organic-solids. *J. Chem. Phys.*, 77:84, 1988. 23

[119] P. Robyr, M. Tomaselli, J. Straka, C. Grobpisano, U. W. Suter, B. H. Meier, and R. R. Ernst. Rf-driven and proton-driven NMR polarization transfer for investigating local order - an application to solid polymers. *Mol. Phys.*, 84:995, 1995. 24

[120] J. Virlet and D. Ghesquieres. NMR longitudinal cross relaxation induced by natural abundance ^{13}C-^{13}C dipolar interaction in organic-solids - hexamethylethane. *Chem. Phys. Lett.*, 73:323, 1980. 23

[121] S. Dusold, J. Kummerlen, T. Schaller, A. Sebald, and W. A. Dollase. A ^{31}P spin diffusion and ^{31}P-^{113}Cd CP/MAS NMR study of polycrystalline $Cd_3(PO_4)_2$. *J. Phys. Chem. B*, 101:6359, 1997. 23

[122] X. Helluy, C. Marichal, and A. Sebald. Through-bond indirect and through-space direct dipolar coupling ^{31}P MAS NMR constraints for spectral assignment in the cubic 3 x 3 x 3 superstructure of Ti_2O_7. *J. Phys. Chem. B*, 104:2836, 2000.

[123] X. Helluy and A. Sebald. Structure and dynamic properties of solid L-tyrosine-ethylester as seen by ^{13}C MAS NMR. *J. Phys. Chem. B*, 107:3290, 2003.

[124] H. Nakamura, D. Kuwahara, and T. Mochida. High-resolution solid-state NMR investigation of the phase transition in decamethylferrocene-acenaphthenequinone charge-transfer complex. *J. Phys. Chem. A*, 113:13601, 2009.

[125] R. Ohashi and K. Takegoshi. Asymmetric ^{13}C-^{13}C polarization transfer under dipolar-assisted rotational resonance in magic-angle spinning NMR. *J. Chem. Phys.*, 125:214503, 2006.

[126] J. Xu, J. Struppe, and A. Ramamoorthy. Two-dimensional homonuclear chemical shift correlation established by the cross-relaxation driven spin diffusion in solids. *J. Chem. Phys.*, 128:052308, 2008. 23

[127] U. Haeberlen. *High resolution NMR in solids: selective averaging*. Academic Press, New York, 1976. 25, 95

[128] T. Karlsson, A. Brinkmann, P. J. E. Verdegem, J. Lugtenburg, and M. H. Levitt. Multiple-quantum relaxation in the magic-angle-spinning NMR of ^{13}C spin pairs. *Solid State Nucl. Mag.*, 14:43, 1999. 26, 30

[129] V. E. Zorin, S. P. Brown, and P. Hodgkinson. Quantification of homonuclear dipolar coupling networks from magic-angle spinning ^{1}H NMR. *Mol. Phys.*, 104:293, 2006. 26, 31

[130] B. M. Fung, A. K. Khitrin, and K. Ermolaev. An improved broadband decoupling sequence for liquid crystals and solids. *J. Magn. Reson.*, 142:97, 2000. 27

[131] D. J. States, R. A. Haberkorn, and D. J. Ruben. A two-dimensional nuclear overhauser experiment with pure absorption phase in 4 quadrants. *J. Magn. Reson.*, 48:286, 1982. 27

[132] J. R. Lewandowski, J. Sein, H. J. Sass, S. Grzesiek, M. Blackledge, and L. Emsley. Measurement of site-specific ^{13}C spin-lattice relaxation in a crystalline protein. *J. Am. Chem. Soc.*, 132:8252, 2010. 26

[133] F. H. Allen. The cambridge structural database: a quarter of a million crystal structures and rising. *Acta Crystallogr. B*, 58:380, 2002. 29, 63, 96

[134] S. Macura and R. R. Ernst. Elucidation of cross relaxation in liquids by two-dimensional NMR-spectroscopy. *Mol. Phys.*, 41:95, 1980. 29

[135] E. W. Abel, T. P. J. Coston, K. G. Orrell, V. Sik, and D. Stephenson. Two-dimensional NMR exchange spectroscopy - quantitative treatment of multisite exchanging systems. *J. Magn. Reson.*, 70:34, 1986. 29

[136] J. D. Gehman, E. K. Paulson, and K. W. Zilm. The influence of internuclear spatial distribution and instrument noise on the precision of distances determined by solid state NMR of isotopically enriched proteins. *J. Biomol. NMR*, 27:235, 2003. 29

[137] Z. Zolnai, N. Juranic, and S. Macura. Least-squares method for quantitative determination of chemical exchange and cross-relaxation rate constants from a series of two-dimensional exchange NMR spectra. *J. Phys. Chem. A*, 101:3707, 1997. 29, 30

[138] S. Caldarelli and L. Emsley. Intrinsic asymmetry in multidimensional solid-state NMR correlation spectra. *J. Magn. Reson.*, 130:233, 1998. 30

[139] M. Bak, J. T. Rasmussen, and N. C. Nielsen. SIMPSON: A general simulation program for solid-state NMR spectroscopy. *J. Magn. Reson.*, 147:296, 2000. 31, 49, 50, 69

[140] P. Hodgkinson and L. Emsley. Numerical simulation of solid-state NMR experiments. *Prog. Nucl. Magn. Reson. Spectrosc.*, 36:201, 2000. 61

[141] M. Veshtort and R. G. Griffin. SPINEVOLUTION: A powerful tool for the simulation of solid and liquid state NMR experiments. *J. Magn. Reson.*, 178:248, 2006. 31, 49, 50, 58, 62, 69, 75, 76

[142] V. E. Zorin, S. P. Brown, and P. Hodgkinson. Origins of linewidth in ^{1}H magic-angle spinning NMR. *J. Chem. Phys.*, 125:144508, 2006. 31, 49

[143] A. Abragam and M. Goldman. *Nuclear Magnetism: Order and Disorder*. Oxford University Press, Oxford, 1982. 39, 41, 42

[144] M. Mehring. *Principles of High Resolution NMR in Solids*. Springer-Verlag, Berlin, 1983. 39, 41, 42

[145] F. S. Debouregas and J. S. Waugh. Antiope, a program for computer experiments on spin dynamics. *J. Magn. Reson.*, 96:280, 1992. 49, 69

[146] S. A. Smith, T. O. Levante, B. H. Meier, and R. R. Ernst. Computer-simulations in magnetic-resonance - an object-oriented programming approach. *J. Magn. Reson. A.*, 106:75, 1994. 49, 69

[147] V. E. Zorin, M. Ernst, S. P. Brown, and P. Hodgkinson. Insights into homonuclear decoupling from efficient numerical simulation: Techniques and examples. *J. Magn. Reson.*, 192:183, 2008. 49, 50

[148] P. Hodgkinson, D. Sakellariou, and L. Emsley. Simulation of extended periodic systems of nuclear spins. *Chem. Phys. Lett.*, 326:515, 2000. 49, 50

[149] H. Geen, J. J. Titman, J. Gottwald, and H. W. Spiess. Solid-state proton multiple-quantum NMR-spectroscopy with fast magic-angle-spinning. *Chem. Phys. Lett.*, 227:79, 1994. 49

[150] Y. S. Yen and A. Pines. Multiple-quantum NMR in solids. *J. Chem. Phys.*, 78:3579, 1983. 51

[151] M. Munowitz and A. Pines. Principles and applications of multiple-quantum NMR. *Adv. in Chem. Phys.*, 66:1, 1987. 51, 76

[152] H. G. Krojanski and D. Suter. Scaling of decoherence in wide NMR quantum registers. *Phys. Rev. Lett.*, 93:090501, 2004. 49

[153] D. A. McArthur, E. L. Hahn, and R. E. Walstedt. Rotating-frame nuclear-double-resonance dynamics. Dipolar fluctuation spectrum in CaF_2. *Phys. Rev.*, 188:609, 1969. 49

[154] M. H. Levitt, D. Suter, and R. R. Ernst. Spin dynamics and thermodynamics in solid-state NMR cross polarization. *J. Chem. Phys.*, 84:4243, 1986. 70

[155] M. Ernst, A. Verhoeven, and B. H. Meier. High-speed magic-angle spinning ^{13}C MAS NMR spectra of adamantane: Self-decoupling of the heteronuclear scalar interaction and proton spin diffusion. *J. Magn. Reson.*, 130:176, 1998. 49

[156] D. Sakellariou, P. Hodgkinson, and L. Emsley. Quasi equilibria in solid-state NMR. *Chem. Phys. Lett.*, 293:110, 1998. 70, 85

[157] A. Ajoy, G. A. Alvarez, and D. Suter. Optimal pulse spacing for dynamical decoupling in the presence of a purely dephasing spin bath. *Phys. Rev. A*, 83:032303, 2011. 49

[158] J. P. Bradley, C. Tripon, C. Filip, and S. P. Brown. Determining relative proton-proton proximities from the build-up of two-dimensional correlation peaks in ^{1}H double-quantum MAS NMR: insight from multi-spin density-matrix simulations. *Phys. Chem. Chem. Phys.*, 11:6941, 2009. 50

[159] R. Brüschweiler and R. R. Ernst. A cog-wheel model for nuclear-spin propagation in solids. *J. Magn. Reson.*, 124:122, 1997. 50, 53, 58, 61, 62, 69

[160] H. J. Hogben, P. J. Hore, and I. Kuprov. Strategies for state space restriction in densely coupled spin systems with applications to spin chemistry. *J. Chem. Phys.*, 132:174101, 2010. 50, 69, 76

[161] I. Kuprov. Polynomially scaling spin dynamics II: Further state-space compression using Krylov subspace techniques and zero track elimination. *J. Magn. Reson.*, 195:45, 2008.

[162] I. Kuprov, N. Wagner-Rundell, and P. J. Hore. Polynomially scaling spin dynamics simulation algorithm based on adaptive state-space restriction. *J. Magn. Reson.*, 189:241, 2007. 76

[163] H. J. Hogben, M. Krzystyniak, G. T. P. Charnock, P. J. Hore, and I. Kuprov. Spinach - a software library for simulation of spin dynamics in large spin systems. *J. Magn. Reson.*, 208:179, 2011. 69

[164] M. Krzystyniak, L. J. Edwards, and I. Kuprov. Destination state screening of active spaces in spin dynamics simulations. *J. Magn. Reson.*, 210:228, 2011. 50

[165] R. R. P. Senthamarai, I. Kuprov, and K. Pervushin. Benchmarking NMR experiments: A relational database of protein pulse sequences. *J. Magn. Reson.*, 203:129, 2010. 50

[166] H. De Raedt and K. Michielsen. Computational methods for simulating quantum computers. In M. Rieth and W Schommers, editors, *Handbook of Theoretical and Computational Nanotechnology*. American Scientific Publishers, 2006. 50, 58, 59

[167] W. X. Zhang, N. Konstantinidis, K. A. Al-Hassanieh, and V. V. Dobrovitski. Modelling decoherence in quantum spin systems. *J. Phys. Cond. Mat.*, 19:083202, 2007. 50, 58

[168] M. Suzuki, S. Miyashita, and A. Kuroda. Monte-carlo simulation of quantum spin systems .1. *Prog. Theor. Phys.*, 58:1377, 1977. 50, 58

[169] C. Filip, S. Hafner, I. Schnell, D. E. Demco, and H. W. Spiess. Solid-state nuclear magnetic resonance spectra of dipolar-coupled multi-spin systems under fast magic angle spinning. *J. Chem. Phys.*, 110:423, 1999. 51, 72

[170] O. W. Sorensen, G. W. Eich, M. H. Levitt, G. Bodenhausen, and R. R. Ernst. Product operator-formalism for the description of NMR pulse experiments. *Prog. Nucl. Magn. Reson. Spectrosc.*, 16:163, 1983. 52

[171] M. Munowitz, A. Pines, and M. Mehring. Multiple-quantum dynamics in NMR - a directed walk through Liouville space. *J. Chem. Phys.*, 86:3172, 1987. 53, 76

[172] H. Cho, T. D. Ladd, J. Baugh, D. G. Cory, and C. Ramanathan. Multispin dynamics of the solid-state NMR free induction decay. *Phys. Rev. B*, 72:054427, 2005. 53

[173] M. M. Maricq and J. S. Waugh. NMR in rotating solids. *J. Chem. Phys.*, 70:3300, 1979. 56

[174] M. Eden, Y. K. Lee, and M. H. Levitt. Efficient simulation of periodic problems in NMR. Application to decoupling and rotational resonance. *J. Magn. Reson. A*, 120:56, 1996. 58, 72

[175] M. Helmle, Y. K. Lee, P. J. E. Verdegem, X. Feng, T. Karlsson, J. Lugtenburg, H. J. M. de Groot, and M. H. Levitt. Anomalous rotational resonance spectra in magic-angle spinning NMR. *J. Magn. Reson.*, 140:379, 1999.

[176] M. Hohwy, H. Bildsoe, H. J. Jakobsen, and N. C. Nielsen. Efficient spectral simulations in NMR of rotating solids. the γ-COMPUTE algorithm. *J. Magn. Reson.*, 136:6, 1999. 58

[177] O. W. Sorensen. Polarization transfer experiments in high-resolution NMR-spectroscopy. *Prog. Nucl. Magn. Reson. Spectrosc.*, 21:503, 1989. 59, 70

[178] M. Eden. Computer simulations in solid-state NMR. II. implementations for static and rotating samples. *Concepts Mag. Reson. A*, 18:1, 2003. 61

[179] M. P. Allen and D. J. Tildesley. *Computer Simulation of Liquids*. Oxford Science, Oxford, 1987. 66, 93

[180] D. Sakellariou, P. Hodgkinson, S. Hediger, and L. Emsley. Experimental observation of periodic quasi-equilibria in solid-state NMR. *Chem. Phys. Lett.*, 308:381, 1999. 70, 85

[181] J. D. Walls and Y. Y. Lin. Constants of motion in NMR spectroscopy. *Solid State Nucl. Mag.*, 29:22, 2006.

[182] A. A. Nevzorov. Ergodicity and efficiency of cross-polarization in NMR of static solids. *J. Magn. Reson.*, 209:161, 2011. 70

[183] M. Goldman. *Spin Temperature and Nuclear Magnetic Resonance in Solids*. Oxford University Press, Oxford, 1970. 70

[184] M. H. Levitt. Unitary evolution, Liouville space, and local spin thermodynamics. *J. Magn. Reson.*, 99:1, 1992. 70

[185] O. W. Sorensen. A universal bound on spin dynamics. *J. Magn. Reson.*, 86:435, 1990.

[186] O. W. Sorensen. The entropy bound as a limiting case of the universal bound on spin dynamics - polarization transfer in $I_N S_M$ spin systems. *J. Magn. Reson.*, 93:648, 1991. 70

[187] M. C. Butler, J.-N. Dumez, and L. Emsley. work in progress. 72

[188] C. Filip, X. Filip, D. E. Demco, and S. Hafner. Spin dynamics under magic angle spinning by Floquet formalism. *Mol. Phys.*, 92:757, 1997. 72

[189] C. Filip, M. Bertmer, D. E. Demco, and B. Blumich. Application of the Floquet theory to multiple quantum NMR of dipolar-coupled multi-spin systems under magic angle spinning. *Mol. Phys.*, 99:1575, 2001. 72

[190] J. H. Shirley. Solution of Schrodinger equation with a Hamiltonian periodic in time. *Phys. Rev. B*, 138:979, 1965. 72

[191] T. Nakai and C. A. McDowell. Application of Floquet theory to the nuclear-magnetic-resonance spectra of homonuclear 2-spin systems in rotating solids. *J. Chem. Phys.*, 96:3452, 1992.

[192] A. Schmidt and S. Vega. The Floquet theory of nuclear-magnetic-resonance spectroscopy of single spins and dipolar coupled spin pairs in rotating solids. *J. Chem. Phys.*, 96:2655, 1992.

[193] M. Leskes, P. K. Madhu, and S. Vega. Floquet theory in solid-state nuclear magnetic resonance. *Prog. Nucl. Magn. Reson. Spectrosc.*, 57:345, 2010.

[194] I. Scholz, J. D. van Beek, and M. Ernst. Operator-based Floquet theory in solid-state NMR. *Solid State Nucl. Mag.*, 37:39, 2010. 72

[195] M. H. Levitt. Why do spinning sidebands have the same phase. *J. Magn. Reson.*, 82:427, 1989. 72

[196] M. E. Halse, J.-N. Dumez, and L. Emsley. work in progress. 81, 88

[197] M. M. Maricq. Thermodynamics for many-body systems evolving under a periodic time-dependent Hamiltonian - application to pulsed magnetic-resonance. *Phys. Rev. B*, 31:127, 1985. 84

[198] M. M. Maricq. Equilibrium in periodically time-dependent 2-level systems. *Phys. Rev. Lett.*, 56:1433, 1986.

[199] M. M. Maricq. Spin thermodynamics of periodically time-dependent systems - the quasi-stationary state and its decay. *Phys. Rev. B*, 36:516, 1987. 84

[200] G. Floquet. Sur les équations différentielles linéaires a coefficients périodiques. *Ann. Sci. Ecole Norm. S.*, 12:47, 1883. 85

[201] A. E. McDermott. Structural and dynamic studies of proteins by solid-state NMR spectroscopy: rapid movement forward. *Curr. Opin. Struc. Biol.*, 14:554, 2004. 91

[202] T. Vosegaard. Challenges in numerical simulations of solid-state NMR experiments: Spin exchange pulse sequences. *Solid State Nucl. Mag.*, 38:77, 2011. 93

[203] L. Duma, W. C. Lai, M. Carravetta, L. Emsley, S. P. Brown, and M. H. Levitt. Principles of spin-echo modulation by J-couplings in magic-angle-spinning solid-state NMR. *Chemphyschem*, 5:815, 2004. 95

Publications

Publications on spin diffusion

- M. C. Butler, J.-N. Dumez and L. Emsley. Dynamics of large nuclear-spin systems from low-order correlations in Liouville space. *Chem. Phys. Lett.*, 477:377, 2009.
- J.-N. Dumez, M. C. Butler, E. Salager, B. Elena-Herrmann and L. Emsley. *Ab initio* simulation of proton spin diffusion. *Phys. Chem. Chem. Phys.*, 12:9172, 2010.
- J.-N. Dumez, M. C. Butler and L. Emsley. Numerical simulation of free evolution in solid-state NMR using low-order correlations in Liouville space. *J. Chem. Phys.*, 133:224501, 2010.
- J.-N. Dumez and L. Emsley. A master-equation approach to the description of proton-driven carbon-13 spin diffusion from crystal geometry using zero-quantum lineshapes. *Phys. Chem. Chem. Phys.*, 13:7363, 2011.
- J.-N. Dumez, M. E. Halse, M. C. Butler and L. Emsley. A first-principles description of proton-driven spin diffusion. Manuscript in preparation.
- J.-N. Dumez and L. Emsley. Nuclear spin diffusion. Manuscript in preparation.

Other publications

- J.-N. Dumez and C. J. Pickard. Calculation of NMR chemical shifts in organic solids: accounting for motional effects. *J. Chem. Phys.*, 130:104701, 2009.
- E. Salager, J.-N. Dumez, R. S. Stein, S. Steuernagel, A. Lesage, B. Elena-Herrmann and L. Emsley. Homonuclear dipolar decoupling with very large scaling factors for high-resolution ultra-fast magic angle spinning ^{1}H solid-state NMR spectroscopy. *Chem. Phys. Lett.*, 498:214, 2010.
- J. Schlagnitweit, J.-N. Dumez, M. Nausner, A. Jerschow, B. Elena-Herrmann and N. Müller. Observation of NMR noise from solid samples. *J. Magn. Reson.*, 207:168, 2010.
- R. K. Harris, P. Hodgkinson, V. Zorin, J.-N. Dumez, B. Elena-Herrmann, L. Emsley, E. Salager and R. S. Stein. Computation and NMR crystallography of terbutaline sulfate. *Magn. Reson. Chem.*, 48:S103, 2010.
- E. Salager, J.-N. Dumez, M. H. Levitt and L. Emsley. A scaling factor theorem for homonuclear dipolar decoupling in solid-state NMR spectroscopy. In press.
- J. R. Lewandowski, J.-N. Dumez, U. Akbey, S. Lange, L. Emsley and H. Oschkinat. Enhanced resolution and coherence lifetimes in the solid-state NMR spectroscopy of perdeuterated proteins under ultra-fast magic-angle spinning. Submitted.